CHARACTERISATION OF BIOLOGICALLY FUNCTIONALISED SURFACES

A thesis for the degree of
Doctor of Philosophy
submitted to the Faculty of Engineering
University of Glasgow

by

Christopher Mark Cotton

October 1999

ProQuest Number: 10390879

ProQuest 10390879

ProQuest LLC.
789 East Eisenhower Parkway
P.O. Box 1346
Ann Arbor, MI 48106 – 1346

11909 (copy 2)

ABSTRACT

The work presented in this thesis investigates a number of the issues relating to biosensor technology, in particular the controlled design of bioelectronic interfaces.

Initially, the ability to produce mixed self-assembled monolayers (SAMs) of alkanethiols on gold is investigated. Using X-ray photoelectron spectroscopy (XPS) it is demonstrated, that through the displacement of a previously adsorbed monolayer by incubation in a secondary thiol (bearing an alternative headgroup) the degree of head-group functionality of a gold surface can be controlled. The interpretation of these XPS spectra also allows for the proposal of a mechanism by which this displacement may occur.

Having shown that the headgroup functionality of a gold surface can be controlled in this manner, these methods are used to manipulate molecular recognition at electrode surfaces in a variety of manners. Mixed monolayers are used to control electron transfer reactions between the redox protein cytochrome c, as well as controlling the immobilisation of a variety of proteins to the electrode surface. In this fashion the fabrication of protein gradients is demonstrated.

In addition to the use of SAMs protein gradients are also constructed by the manipulation of the competition of biotin and biotinylated proteins, for the biotin binding sites of immobilised avidin.

In the final chapter, both photolithographic and non-photolithographic methods are used to fabricate micro-electrodes and micro-electrode arrays, suitable for application to high through put micro-electrochemical assays, where the effective immobilisation of proteins could be used to increase sensitivity and improve detection limits.

ACKNOWLEDGEMENTS

GLOSSARY

BSA	Bovine serum albumin
CV	Cyclic voltammetry/voltammogram
DMSO	Dimethylsulphoxide
ELISA	Enzyme linked immunosorbent assay
FITC	Fluorescein isothio-cyanate
FMCA	Ferrocene monocarboxylic acid
FT-iR	Fourier transform infra-red spectroscopy
HRP	Horseradish peroxidase
HTS	High throughput screening
IgG	Immunoglobulin G
iR	Infra-red
NADH	Nicotinamide adenine dinucleotide
NSB	Non-specific binding
PBS	Phosphate buffered saline
PMMA	Poly-methylmethacrylate
pNPP	p-nitrophenylphosphate
RIE	Reactive ion etched
RO water	Reverse osmosis water
SAM	Self-assembled monolayer
STM	Scanning tunnelling microscopy
TMB	Tetramethyl-benzidine
TOA	Take off angle
XPS	X-ray photoelectron spectroscopy

CONTENTS

CHAPTER 1: INTRODUCTION

The interfaces that exist between biological media and man-made materials are important in many areas of science and technology, including implants and bio-compatibility[1,2]. One additional area, which has received particular attention over the past several years, involves those surfaces found in biosensors. This is not only as a consequence of the promising commercial opportunities that they offer, but also because of the unrivalled specificity and sensitivity shown by biomolecules and biological systems, and how, as a consequence such sensors can be used in research led projects[3].

A biosensor combines two functions: molecular recognition and signal transduction. This is achieved by the immobilisation of a biological sensing unit, such as an antibody or enzyme, in a close, and often functional, proximity to a transducer surface **Figure 1.1**[4-6]. The nature of the surface molecular environment in which the bio-molecule is immobilised, therefore, has considerable implications on the sensing properties of that surface. As a consequence, the control of the molecular immobilisation and the subsequent manipulation of the surface molecular architecture is of particular importance in the field of biosensors[7,8].

As well as there being an interest in controlling the surface molecular structure of sensing surfaces, there has been a concurrent desire to exploit the potential benefits offered by the microfabrication of these devices[9-12]. Miniaturisation offers a reduced assay cost, and as a result of their reduced geometries, enhanced analytical performance, for example, through a more efficient diffusion of analytes to the sensor[13]. These advantages are of particular interest in those applications where large numbers of assays are being performed, and as a consequence miniaturisation has shown promise in the area of high-throughput screening (HTS), where there have been intensive efforts to produce arrays of miniaturised sensing devices[14-16].
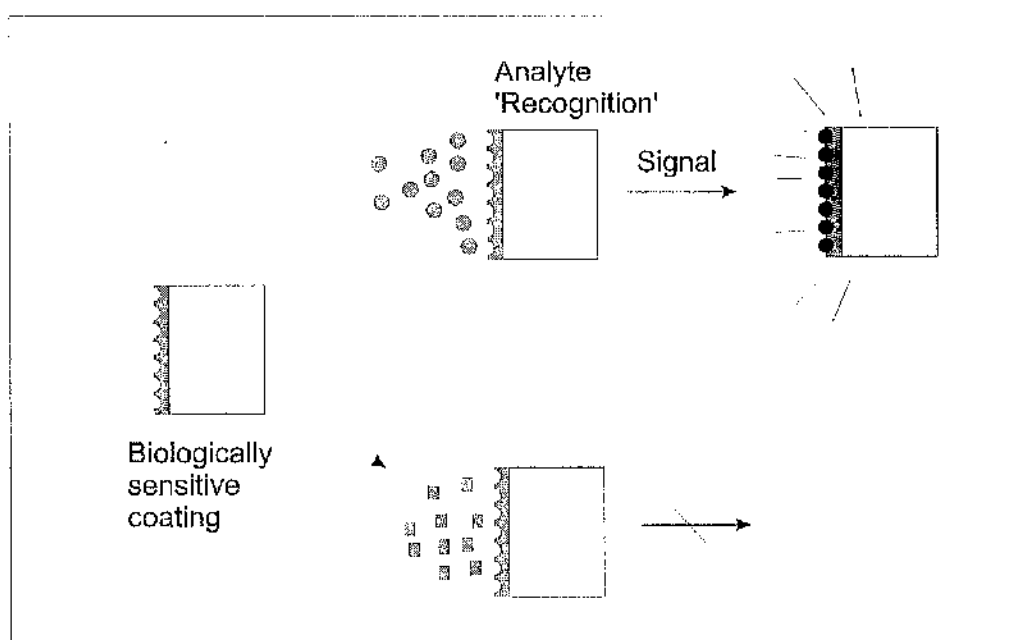
Figure 1.1 - The biosensor consists of a transducer modified with a biological sensing component. It is the specificity of the bio-recognition molecule for the target analyte which underlies the potential of biosensors as analytical tools.

With the decreasing geometries of the devices, optimisation of the analytical binding event and thus the surface molecular environment becomes more important. This thesis, therefore, investigates methods of controlling both the immobilisation of proteins and molecular recognition at gold surfaces, with particular application to the fabrication of arrays of miniaturised electrochemical sensors.

1.1 Protein Immobilisation

One of the most important factors in biosensor construction is the development of techniques for the stable immobilisation of biomolecules, especially proteins, in close proximity to a transducer surface. In the context of biosensing, the incorporation of biological components within membrane structures was first described by Clark and Lyons in 1962[17]. Since that pioneering work, various methods have been described for enzyme or protein immobilisation **Table 1.1**

Probably the simplest method of immobilisation, the adsorption of biomolecules from solution onto solid surfaces is facilitated via non-specific physical forces (e.g. van der Waals, ionic, or hydrophobic interactions). The adsorption of proteins has been shown as a simple method for constraining a number of different proteins on various surfaces[18-20]. Although it is generally regarded as a 'mild' coupling method that preserves protein activity, adsorption generally exhibits a high degree of reversibility and does not provide a high surface loading of proteins[21].

Although the adsorbed molecules can be stabilised to some extent through the use of cross-linking agents such as glutaraldehyde, an additional a loss of activity is believed to occur through the denaturation of proteins on adsorption through conformational changes, aggregation and multi-layering. Consequently biosensors employing adsorption as the immobilisation procedure often show reduced sensitivity and some degree of non-specificity[4].

Although the effective immobilisation of the sensing protein is paramount, this should be achieved whilst still maintaining free diffusion of substrates and products into and out of the immobilised layer. The occlusion of bio-molecules both behind membranes and in electrochemically formed polymers such as polypyrrole, are relatively simple techniques that have shown their potential in a number of situations[22,23]. However, they do have the potential disadvantage of creating a diffusional barrier between the electrode and the bulk solution through which only low molecular weight substrates can diffuse. Thus this method may be unsuitable for enzymes that act on macromolecules such as ribonuclease, trypsin or dextranase and are also unsuitable for antibodies specific to large antigens. N.b. The diffusional barriers that are created although often a disadvantage can be used in order to select analytes on the basis of charge or size and so exclude interferants or foulants.

Method	Advantages	Disadvantages
Adsorption on insoluble matrices (e.g. by van der Waals forces, ionic binding or hydrophobic forces).	Simple and mild conditions, which are less disruptive to the biological molecule	Linkages are highly dependent on pH, solvent used and reaction temperature. Resulting sensor often insensitive.
Entrapment in a polymer or gel / behind a semi-permeable membrane.	Universal procedure for any molecule; mild immobilisation procedure.	Large diffusional barriers, loss of enzyme activity by leakage, possible denaturation of the biomolecule as a result of the accumulation of free radicals.
Crosslinking by a multifunctional reagent.	Simple, strong chemical binding of biomolecules; widely used to stabilise physically adsorbed proteins or those covalently bound to a solid support.	Control of reaction difficult, large amount of protein required; low activity often associated with crosslinking.
Covalent bonding to solid support or membrane.	Probably most stable/irreversible method – desorption very unlikely, ideal for mass production and commercialisation, possibility of controlling protein orientation.	Complicated and time consuming; possible loss of activity due to reactions involving active site.

Table 1.1 – Summarising immobilisation procedures for biomolecules at transducer surfaces[24].

The most intensely studied of the immobilisation techniques is the formation of covalent bonds between the molecule and the solid support[24-26]. Chemical attachment involves more aggressive conditions and can lead to a significant loss of protein activity through inappropriate orientation and conformational changes on binding. In addition as with all immobilisation techniques there will be some non specific adsorption. As a consequence, there is generally a higher loss of activity through covalent immobilisation, but this loss does depend upon the protein[21], as well as the immobilisation chemistry and the substrate used[26].

4
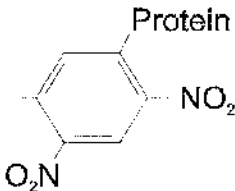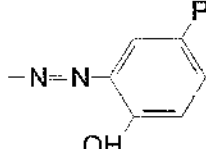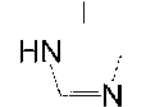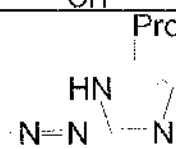
Amino Acid	Functional Group	Attachment Method	Reaction
ε - amino group of lysine and N - terminal amino group.	$-NH_2$	Diazotization	$--N-N--Protein$
		Peptide bond formation	$-\overset{\overset{O}{\|}}{C}-NH-Protein$
		Arylation	(structure with Protein, NO_2, O_2N)
		Alkylation	$-CH_2-NH--Protein$ $-CH=NH-Protein$
		Schiff-base formation	$\overset{NH_2^+}{\underset{\|}{-C}}-NH-Protein$
		Amidination	
Sulfhydryl of cysteine	$-SH$	Alkylation	$-CH_2-S-Protein$
		Thio-disulphide interchange	$-S-S-Protein$
		Mercury enzyme interaction	$-Hg-S-Protein$
Carboxyl group of aspartate and glutamate / C-terminus carboxyl group	$-COOH$	Peptide bond formation	$\overset{\overset{O}{\|\|}}{C}\ NH\ \ Protein$
Phenolic of tyrosine	(ring)$-OH$	Diazotization	$-N=N-$(ring with Protein, OH)
Imidazole of histidine	$\underset{\underset{N}{\|}}{HN}$ (imidazole)	Diazotization	(imidazole with Protein, HN, $N=N$, N)

Table 1.2 - Amino acids and functional groups involved in covalent immobilisation of proteins[27].

Although generally harsher than other immobilisation schemes, covalent binding can provide the highest irreversible surface loading[21], and research indicates that most

of the apparent loss of covalently bound protein activity is due to desorption of non-covalently bound protein to the solution[26]. As a result of the intense interest in immobilisation, several quite benign immobilisation procedures have been demonstrated and the range of functional groups on the amino acids of proteins which can be utilised is illustrated in **Table 1.2**. Lysine residues, are most commonly used for protein immobilisation, as they are typically present on the exterior of the protein due to their hydrophilic nature and are also good nucleophiles. In most proteins lysine residues abound on the external surfaces and attachment to the immobilisation support may occur through several groups.

Suitable functional groups must also be available for covalent attachment on the transducer surface. Of the materials widely used to serve as transducers, the noble metals gold, silver and platinum are probably most often used as surfaces in both electrochemical and optical systems such as those used in surface plasmon resonance[28]. These metals are unique in their ability to bind thiol groups with near covalent bond strength (188 kJ mol^{-1}), with many alkanethiols spontaneously forming so called self assembled monolayers (SAMs)[29-32]. It is the strength and spontaneity of the formation of such bonds which provides the basis for functionalisation of many gold, silver and platinum surfaces.

1.2 Self-Assembled Monolayers of Alkanethiols on Gold

Self assembled monolayers of alkanethiolates on gold, form spontaneously when a clean gold sample is exposed to a solution (or vapour) of an alkanethiol or dialkyldisulphide **Figure 1.2**[33]. Although other systems for the preparation of self assembled monolayers exist (silanes on silicon dioxide, fatty acids on metal oxide surfaces, phosphonates on phosphate surfaces and isocyanides on platinum)[34], the structural integrity and greater range of functionality produced accounts for the popularity that gold - sulphur systems have acquired in research[32].
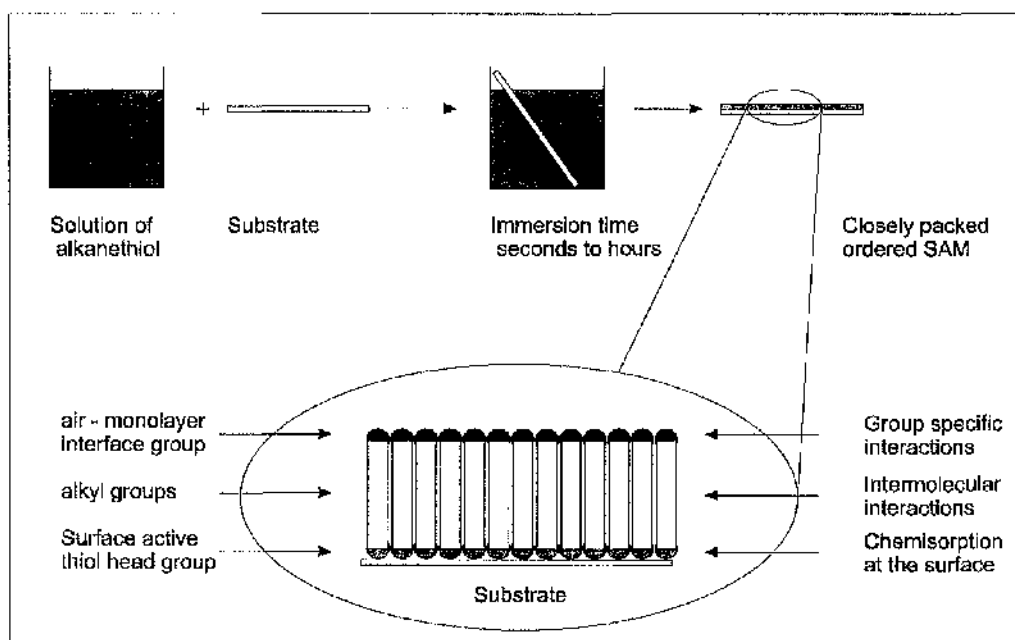
Figure 1.2 - Self-assembled monolayers of alkanethiols on gold are formed by simply immersing a gold covered substrate into a solution of the thiol. The driving force for the spontaneous formation of the 2D assembly includes chemical bond formation of molecules with the surface and intermolecular interactions.

The structure of these SAMs, for a range of alkanethiols, is now well established[35,36]. Characterised by a strong chemisorption bond to the surface through the thiol group, lateral interactions between the alkyl groups produce densely packed monolayers, with locally crystalline environments **Figure 1.3**. The stability of these monolayers is well documented, maintaining their integrity for a period of several months in air, or in both aqueous and ethanolic solutions[28].

It is the structural variety of alkane thiols available, particularly that of the end functional group (the tail), that makes the system of self-assembled monolayers of alkanethiols on gold probably the best for providing functionalised surfaces[28]. The convenience and flexibility of SAMs has, therefore, been exploited widely, especially for homogenous SAM surfaces[37-43].
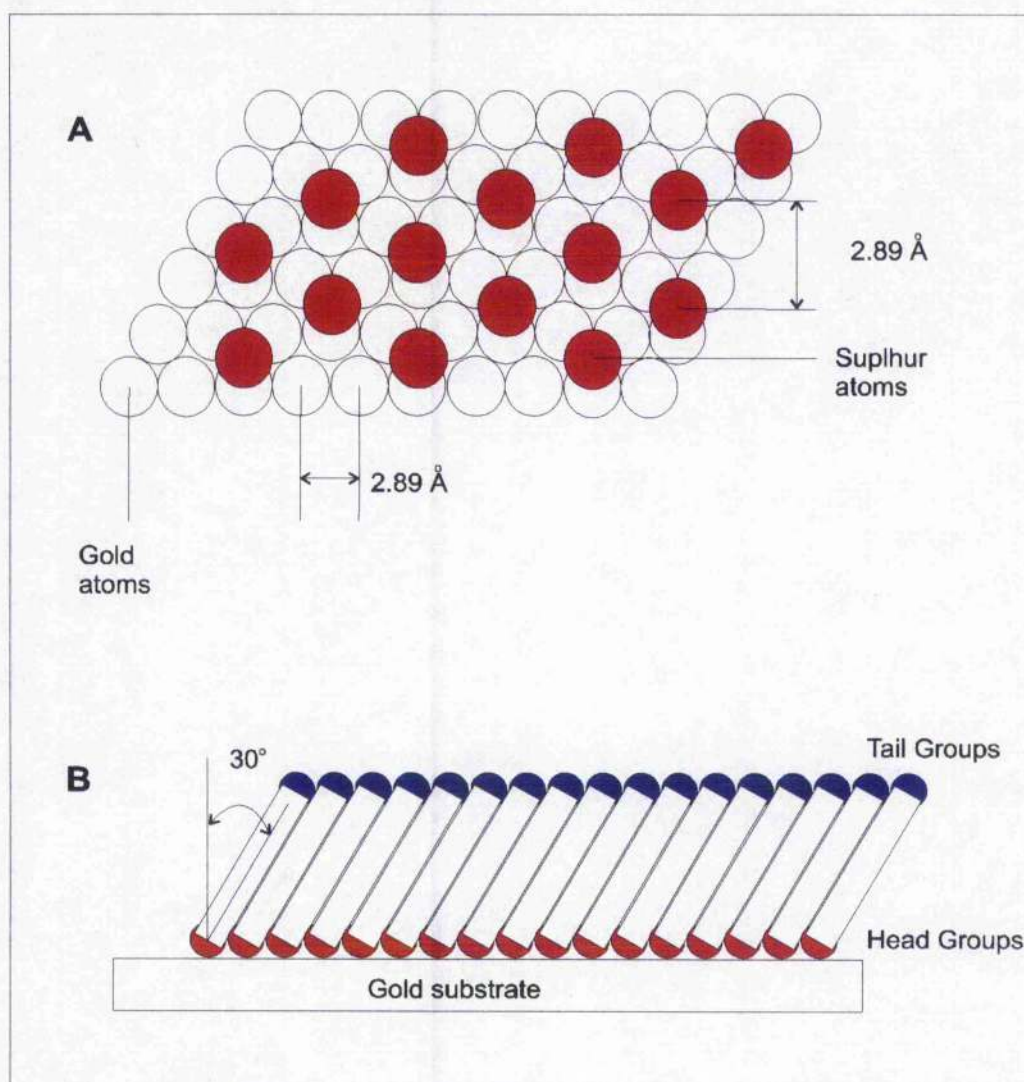
Figure 1.3 - The structure of an alkanethiol SAM on gold. The sulphur atoms of the alkanethiols co-ordinate to the hollow three fold sites of the gold surface **A**; the gold atoms are arranged in an hexagonal manner. The alkyl chains of the SAM are closely packed and tilted approximately 30° to the normal of the surface **B**.

More recently there has been an interest in the production of surfaces bearing mixed functionalities. The adsorption of a SAM from a mixture of two alkanethiols onto a gold surface allows the production of 'mixed' monolayers, mixed functionality being achieved if the constituents of the mixture have different tail functional groups. A number of research groups have thoroughly investigated mixed monolayers composed of terminally substituted alkanethiols; $X-(CH_2)_n-SH$ where n is typically 11 - 15 and the tail group X being either a methyl or hydroxyl group[44-57].

When Schlenoff *et al.* used ^{35}S labelled thiols to show that exchange between solution and surface bound phases occurs under ambient conditions, it became apparent that mixed monolayers could also be produced through the controlled displacement of an initial modifying thiol with a secondary thiol bearing an alternative tail group functionality[58].

1.3 Amperometric Sensors

The effective immobilisation of biomolecules at transducer surfaces is of paramount importance for the effective functioning of biosensors. Electrochemically based sensors are the most common form of biosensor[59]. Broadly speaking, electrochemical biosensors can be split into amperometric, conductimetric and potentiometric sensing systems. These systems differ in that an externally applied electrode potential is used to drive the electrode reaction in the case of amperometric sensors (where the current flow is measured), whereas in potentiometric sensing devices a local equilibrium is set up at the sensor interface and the electrode potential measured[60]. In a conductimetric sensor a potential (which may be alternating) is applied across the electrodes and changes in resitivity are measured.

Amperometric sensors have traditionally received attention through their high sensitivity and their wide linear range[61]. Elegant research on new sensing concepts, coupled with numerous technological innovations, have opened the door to the widespread biomedical use of amperometric devices[62,63]. In this thesis we will consider the use of amperometric sensors, consisting of planar arrays of two and three microelectrode sensors, structured within miniaturised high density microtitre plate formats.
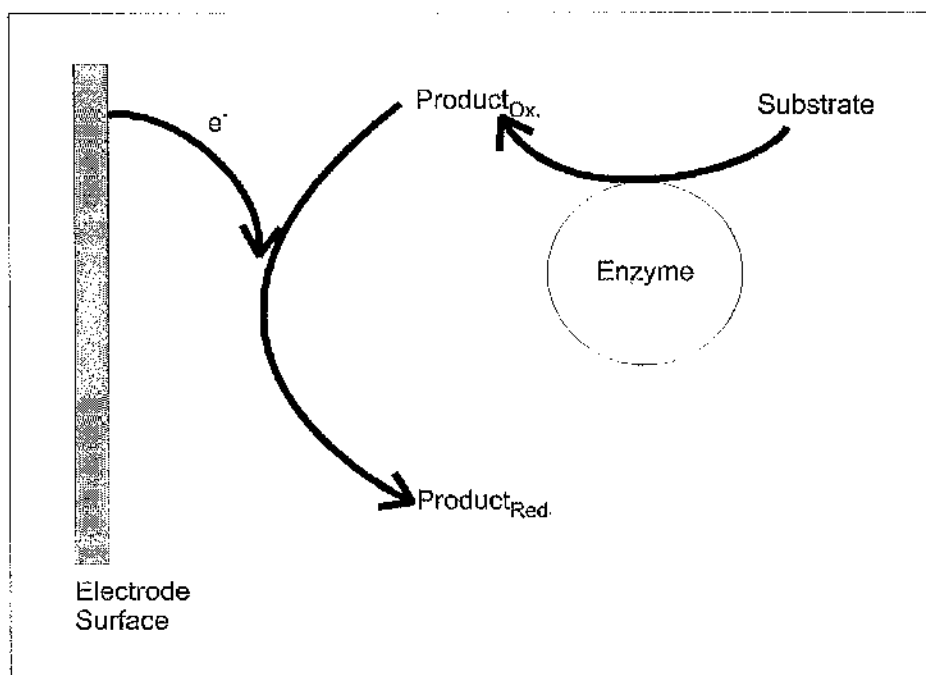
Figure 1.4 - Schematic representing the events occurring at a typical amperometric enzyme sensor. Often the enzyme is immobilised, but not always.

Those amperometric biosensors, which utilise enzymes, are often described as enzyme electrodes due to the fact that the enzyme is immobilised in close proximity to the transducer element[64,65]. It is the specificity of enzymes with regard to recognition and catalysis of substrates, which enables sensors incorporating enzymes to achieve a great selectivity for target analytes. Amperometric sensors measure the current that is produced when an electrode is held at a constant potential with respect to a reference electrode[61]. The current measured is as a result of the oxidation or reduction of an enzymatically produced electro-active species at the electrode surface. The current measured is a function of the concentration of that species at the electrode surface in those situations where mass transfer and enzyme kinetics are not limiting.

The enzyme or cascade of enzymes are chosen to catalyse a reaction which generates a product, or consumes a substrate which can be detected amperometrically **Figure 1.4**. Accordingly the most common enzymes utilised are redox enzymes, particularly

10

those belonging to either the oxidase, dehydrogenase or peroxidase sub-classes of oxido-reductases[66].

The enzymes generate, or consume, easily oxidisable hydrogen peroxide or reduced nicotinamide adenine dinucleotide (NADH). The hydrogen peroxide or NADH can be detected by poising a working (transducing) electrode at modest potentials to yield a current signal (+0.5V-+0.8V versus Ag|AgCl reference electrode)[67]. Probably the most widely quoted example of such a device is the glucose oxidase enzyme electrode used for the analysis of glucose, and based on the reaction scheme shown in illustrated in **Figure 1.5**[68-70].

Glucose
Oxidase

Glucose + O_2 $\longrightarrow$ Gluconolactone + H_2O_2
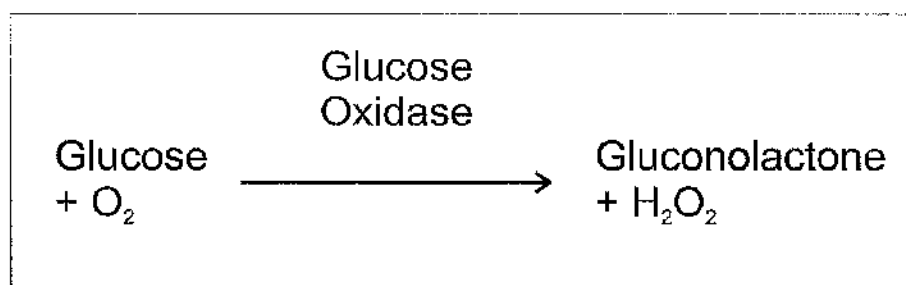
Figure 1.5 - The glucose oxidase reaction scheme most commonly utilised in glucose sensors, both the depletion of oxygen or the formation of hydrogen peroxidase can be followed amperometrically.

The various biomedical applications of oxidase electrodes, based on measurements of the liberated peroxide species, can be affected by fluctuations in the solution oxygen level or by interfering endogenous electroactive compounds (e.g. ascorbic or uric acids) that contribute to the signal[50,71]. Such problems have been alleviated using membranes to exclude potential interferents, as well as restricting the flux of the substrate, thereby improving the surface availability of oxygen[59,61]. However, an additional problem associated with dehydrogenase-based biosensors is that of gradual passivation due to the accumulation of reaction products[72].

The problems described above can be eliminated through direct electron transfer between the enzyme redox centre and the electrode surface. In practice, the thick protein shell surrounding the proteins electron transfer centre introduces a kinetic

11

barrier to electron transfer. The use of small-molecule electroactive, diffusional mediators, such as ferrocene deriveratives, ferrocyanide, conducting organic salts or quinone compounds, to enhance the rate of electron transfer has been extensively investigated[50,59,61,63]. The use of mediators enables reaction mechanisms to become insensitive to oxygen fluctuations, as the mediator replaces oxygen as the cofactor. In addition, amperometric experiments can be performed at lower potentials, thereby reducing the effect of interferents.

Probably the most widely investigated mediators are those derivatives of ferrocene which show stable, reversible, pH insensitive and rapid electron mediation of a number of flavoprotein enzymes[73]. Without a doubt the most successful application of ferrocene mediated amperometric detection is within commercial blood glucose self-testing meters[74].
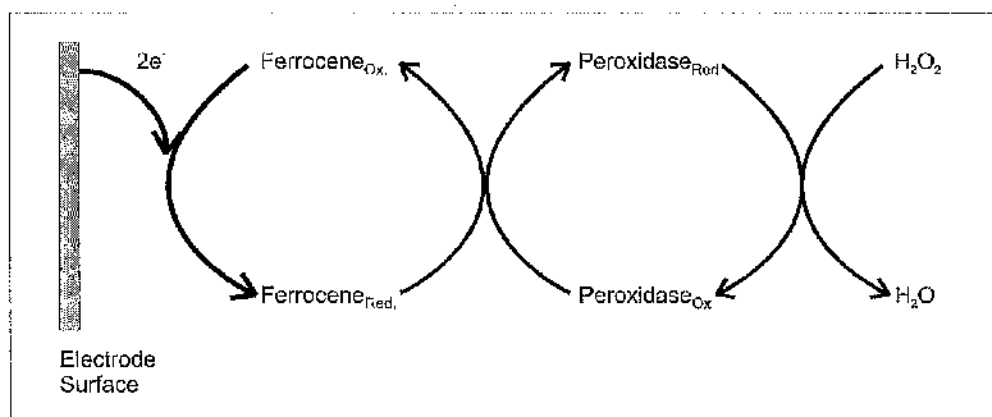
Figure 1.6 - The reaction process occurring at a ferrocene mediated peroxidase enzyme electrode, used for hydrogen peroxide sensing. The electrode is held at 0 mV with respect to a Ag|AgCl reference electrode.

Ferrocene mediators can be used in conjunction with a variety of oxidase enzymes, and their ability to act as an electron donor for peroxidases has also been exploited in an extremely sensitive assay for hydrogen peroxide following the reaction scheme illustrated in **Figure 1.6**[75]. Peroxidases are amongst the most widely used enzymes for the more traditional colourimetric detection, used in many assays (particularly immunoassay systems).

The excellent detection limits that can be achieved on small sample volumes with modern electrochemical techniques and microelectrodes[13] have stimulated the development of small volume electrochemical assay systems[76,77]. For example, nanomolar sensitivity in a nanolitre volume enables the detection of attomole amounts of analyte (ca. 1,000,000 molecules).

1.4 Microfabrication

Silicon-based microfabrication and micromachining processes have demonstrated their suitability for producing geometrically well-defined, highly reproducible micro-sized structures for the integrated circuit industry[78-81]. The same technology has recently found applications within the field of biotechnology[10,12,76,77,82-86]. In such instances, sensors realised with microelectronic production techniques have several advantages over traditional methods of microelectrode fabrication technologies namely "hand-crafted" or probe-type sensors. Bespoke solutions, such as the use of carbon fibres embedded in polyethylene tubes and gold wires sealed in glass[87,88] offer neither the reproducibility nor ease of production offered by photolithographical methods. In addition a major advantage conferred by photolithographic sensor production is that of cost[89]. After the initial design steps, the ease of automation of the fabrication process ensures that samples are cheap and easy to produce, if made in large numbers.

Additional advantages are also conferred by the high degree of reproducibility. The analytical benefits of microelectrodes are well understood and these benefits are largely as a consequence of the reduced geometries[13,90]. Theses advantages are characterised by lower capacitive current, smaller ohmic drop and faster mass transport in a stationary diffusion state, leading to a higher current density compared to electrodes of conventional size, with better signal:noise measurements.

The use of photolithography to define microelectrodes has enabled the reproducible fabrication of arrays of microelectrodes, previously unobtainable by other methods. As a result, interest in arrays of microelectrodes has increased dramatically in recent years[91-93]. The first attempts to employ such arrays were aimed at increasing the signal to noise ratio in liquid chromatography and flow injection devices by combining up to 100 electrodes[94,95]. The second stage in the development of microelectrode arrays began when specially constructed instruments allowed individual electrical access to each electrode within an array. With this approach each electrode could therefore be considered as an independent sensor producing a distinct response that is, in some way, a selective signal for an analyte present in the sample. Although much work has been focused on electrode arrays, the examples that predominate achieve selectivity by operating each electrode at a different potential, within the same sample solution[96-101]. Another approach to achieve the required selectivity involves the micropatterning of proteins on the electrodes, and much work has been reported, in the main part addressing each electrode using light activated covalent bonding techniques[102-105].

In addition some electrochemical microarray systems have been developed consisting of a microplate reader equipped with an single electrode probe, primarily utilising Enzyme Linked Immuno-Sorbent Assay(ELISA) systems[106]. The electrode visits each of the wells sequentially. However, the potential advantages of these assay systems have not yet been realised due to passivation of the working electrode surface[106]. Such passivation is caused by a combination of various factors, such as deposition of impurities and the formation of insoluble films, oxides, and protein adsorption, resulting in a short working lifetime of the electrode.

An alternative method would be the fabrication of individually addressable microelectrode arrays, where each electrode has its own sample applied to it. One industrial application which is fuelling the investigations into the effective miniaturisation of assay systems, is that of high-throughput screening within the pharmaceutical industry. In response to the cost of screening large numbers of compounds, several groups have begun to develop formats for very high density

screening using very small assay volumes[14-16]. One approach involves reducing the well size and increasing the density of the assay plate, whilst retaining the overall dimensions used in current 96-well based high throughput screening. Densities greater than 6500 assays in a standard 100cm^2 plate have been reported[107,108]. This approach significantly increases the number of assays per plate and the overall throughput of the screen, but is intrinsically limited by the constraint of detecting very small responses in a sensitive and timely manner.

Whilst the majority of assay systems used are based on light based sensing systems, we have chosen to investigate the use of photolithographically defined microelectrodes as a possible alternative, allowing for capitalisation of the analytical advantages offered through the miniaturisation of amperometric enzyme electrodes[13,90]. As the performance of such enzyme assay systems depends in part on the immobilisation of the enzyme layer, with miniaturisation the method of immobilisation used becomes a more pertinent issue

1.5 Outline of Thesis Structure

The work presented here, therefore, investigates the use of mixed monolayers of alkanethiols on gold to control the immobilisation of proteins at gold interfaces, with particular application to miniaturised high throughput assay systems utilising amperometric detection. Chapters 1 and 2 are introductory chapters, followed by four experimental chapters as follows:-

Chapter 3 describes the use of X-ray photoelectron spectroscopy to probe the composition of, as well as the mechanism of formation of mixed self assembled monolayers of short chain alkanethiols on gold.

Chapter 4 investigates the role SAMs play in moderating the molecular recognition of the redox enzyme cytochrome c at gold electrodes, and also uses FT-iR to

15

demonstrate one possible application of alkanethiol monolayers to prevent the non-specific absorption of proteins at electrodes.

Chapter 5 demonstrates the ability of mixed self-assembled monolayers on gold to act in conjunction with covalent cross-linking agents to provide a means of tethering proteins in close proximity to electrode surfaces. Controlling the composition of the monolayer we are able to illustrate the control by the formation of immobilised protein gradients. In addition avidin/biotin chemistry is also used to show an alternative method. By combining both self-assembled monolayer systems and avidn/biotin systems we demonstrate how the molecular architecture of electrodes could be controlled in a multi-layer fashion.

Finally Chapter 6 describes methods used to fabricate electrode arrays suitable for high throughput applications. Incorporating reference electrodes into the design of microelectrode arrays, we characterise devices made photolithographically and non-photolithographically using standard ferrocene electrochemical analysis, as well as amperometric enzyme assay based, systems.

Conclusions and recommendations for further work are found in Chapter 7, with references and a glossary appearing at the end of the thesis.

CHAPTER 2: ANALYTICAL TECHNIQUES.

2.1 Electrochemical Measurements

Methods of electrochemical characterisation that are used to measure electrode currents as a function of the voltage applied to the electrochemical cell are termed voltammetric techniques, and can be used to provide detailed information concerning the electrode processes occurring[64,109-112].
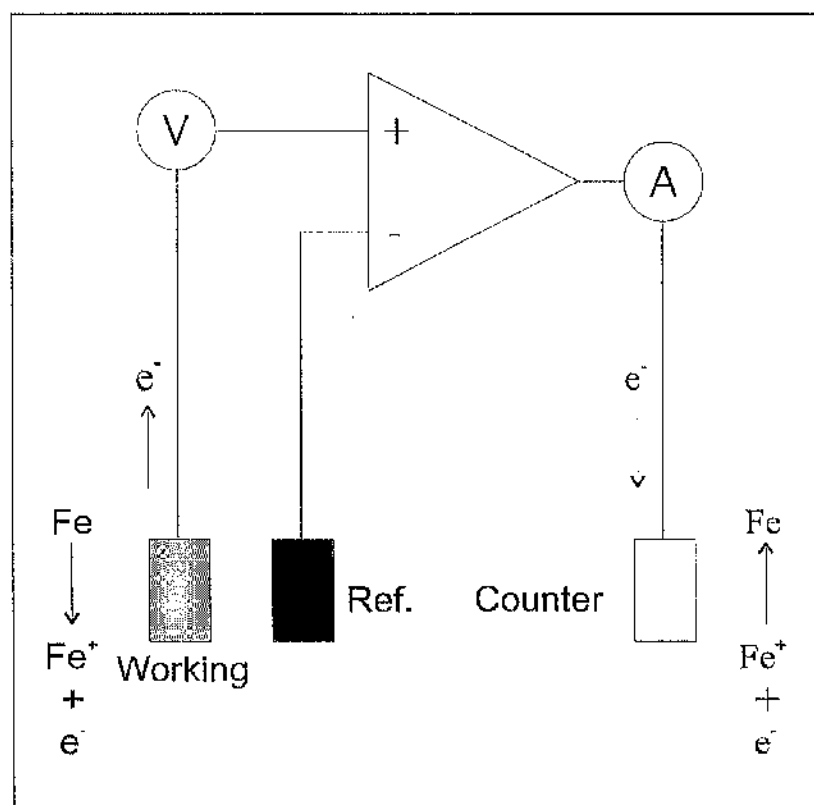
Figure 2.1 - A schematic illustration of the standard three electrode set up used for both cyclic voltammetric and chronoamperometric experiments, used throughout this thesis. The cell consists of three electrodes, a working electrode at which the electrode process under study occurs (in this case the oxidation of iron II), a counter electrode at which the reverse reaction occurs, and a reference electrode.

17

Two of the most commonly used voltammetric methods are cyclic voltammetry[111,113,114] and chronoamperommetry[111,112]. Both cyclic voltammetric and chronoamperometric experiments are performed using a standard three electrode set-up consisting of the working electrode (that at which measurements are taken), a reference electrode and a counter electrode[111], illustrated schematically in **Figure 2.1**.

2.1.1 Cyclic Voltammetry[111,113,114]

In cyclic voltammetry the potential of the working electrode, with respect to a reference electrode such as an Ag|AgCl electrode, is cycled through the potential range where an electrode reaction occurs. The change in potential is a linear function with a triangular waveform, **Figure 2.2.** The scan rate is reflected by the gradient of the 'saw-tooth'.
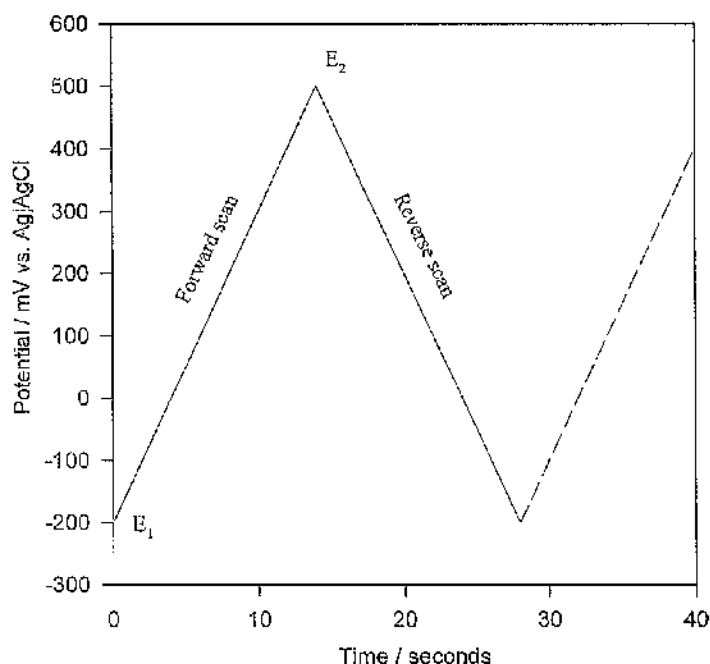
Figure 2.2 - The triangular waveform generated for cyclic voltammetry, in this case with switching potentials at -200 mV and +500 mV vs. Ag|AgCl (E_1 and E_2 respectively). Scan rate 50 mVs^{-1}.

A cyclic voltammogram is obtained by recording the current at the working electrode as a function of the potential, as illustrated for a fully reversible system in **Figure 2.3**. There are two components to the recorded current, a capacitive component resulting from the redistribution of charged and polar species at the electrode surface (termed non-Faradaic) and a component resulting from electron transfer reactions (termed Faradaic). As shown in the diagram, on the forward scan species in the vicinity of the electrode can be oxidised and on the reverse scan reduced, on both occasions resulting in Faradaic current.
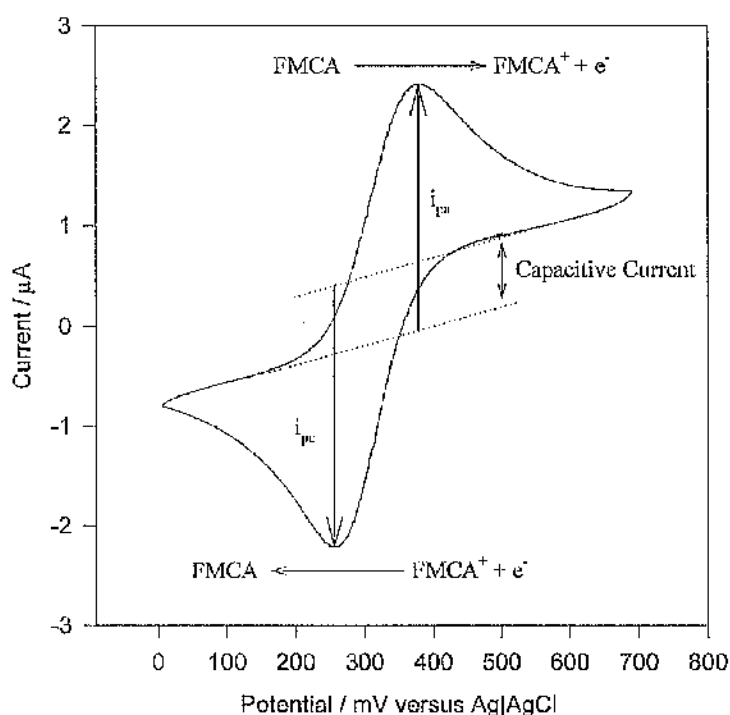
Figure 2.3 - A typical cyclic voltammogram obtained for a fully reversible, solution, redox chemical system. In this case, the voltammogram is of ferrocene monocarboxylic acid (FMCA) at a gold electrode with a psuedo- Ag|AgCl reference electrode. On the forward sweep, FMCA is oxidised, and on the reverse it is reduced. The anodic peak current (i_{pa}) is measured by extending a tangent from the capacitive component of the current and measuring the peak height. The reverse is true for the cathodic peak current (i_{pc}).

The form of the cyclic voltammogram is a consequence of the short time scale of the experiment, making the role of non steady state diffusion important. In a fully reversible system, as the potential is scanned through the range where oxidation of the analyte under study (in this case ferrocene) occurs, its surface concentration

decreases as it becomes oxidised. As a result a concentration gradient is formed between the electrode surface and the bulk solution. Initially the flux of unoxidised ferrocene to the surface also increases, the potential becomes more positive, until the surface concentration within the 'diffusion layer', becomes effectively zero. When the surface concentration approaches zero, the flux then decreases. This is because the oxidation of ferrocene occurs faster than it can be transferred from the bulk solution to the electrode. It is this decrease in flux (resulting from an increase in the thickness of the diffusion layer) that gives the corresponding peak in the voltammogram. During such experiments, the diffusion layer is thinner than in the steady state form, where the thickness is fixed by natural convection, giving linear concentration profiles, and as a consequence the concentration gradient is steeper, the flux greater and so the current also greater. This change in concentration gradient with increasing scan rate also accounts for the increased peak currents observed with increasing scan rates.

For a couple, $O + e^- \rightarrow R$ with a redox potential E^O the peak faradaic current i_p therefore depends upon the concentration gradient of O at the electrode surface as given by:

$$i_p = nFAD_O(\mathrm{d}[O]/\mathrm{d}x)_{x=0} \qquad \text{Equation 2.1}$$

where D_O is the diffusion coefficient of O, n the number of electrons transferred, F Faradays constant, and A the area of the electrode.

The concentration at the surface changes with potential according to the Nernst equation:

$$[O]/[R] = \exp[nF/RT(E - E^o)] \qquad \text{Equation 2.2}$$

Where E is the electrode potential, R is the gas constant and T the temperature in Kelvin. A redox couple which behaves according to **Equation 2.2** is termed Nerstian or reversible.

Although cyclic voltammetry is a powerful technique, which can be used to study complex electrochemical reactions such as enzyme coupled or irreversible reactions, for the purpose of the work presented here we will only be concerned with fully reversible reactions.

In a one electron reversible reaction the reduction and oxidation scans have the same shape. The peak current i_p for a reversible system is given by the Randles-Sevcik equation:

$$i_p = 0.4463 \, nFA(D_O a)^{1/2}[O] \qquad \qquad \textbf{Equation 2.3}$$

where [O] is the bulk concentration of O and $a = nFv/RT$. The peak occurs at potential $28.5/n$ mV cathodic of $E°$ at 298 K, and is independent of the potential scan rate. Hence for a reversible one-electron transfer reaction, voltammograms with a peak -to-peak separation of 57 mV will be obtained. In addition, the peak current, **Equation 2.3**, will be proportional to the square root of the potential sweep rate ($i_p/v^{1/2}$ is constant), and the ratio of the anodic to cathodic peak currents is equal to unity ($i_{pa}/i_{pc} = 1$). To measure the Faradaic peak currents from the voltammograms accurately it is necessary to subtract the non-Faradaic component by drawing a tangent to the initial slope as shown in **Figure 2.3**. At microelectrodes, as a consequence of the more efficient, hemispherical diffusion, mass transfer is not limiting, resulting in sigmoidal cyclic voltammograms, and i/V becomes constant.

2.1.2 Chronoamperometry

In contrast to cyclic voltammetry where the change in current is measured as a function of potential, chronoamperometric experiments are performed by applying a potential step to the working electrode, and monitoring the current response of the system as a function of time. The initial potential is chosen such that the electroactive species of interest is not oxidised or reduced, until the potential is stepped to that potential at which oxidation/reduction occurs. These potentials are

often identified using cyclic voltammetry. A current profile is recorded with respect to the electrode reaction **Figure 2.4**[50].
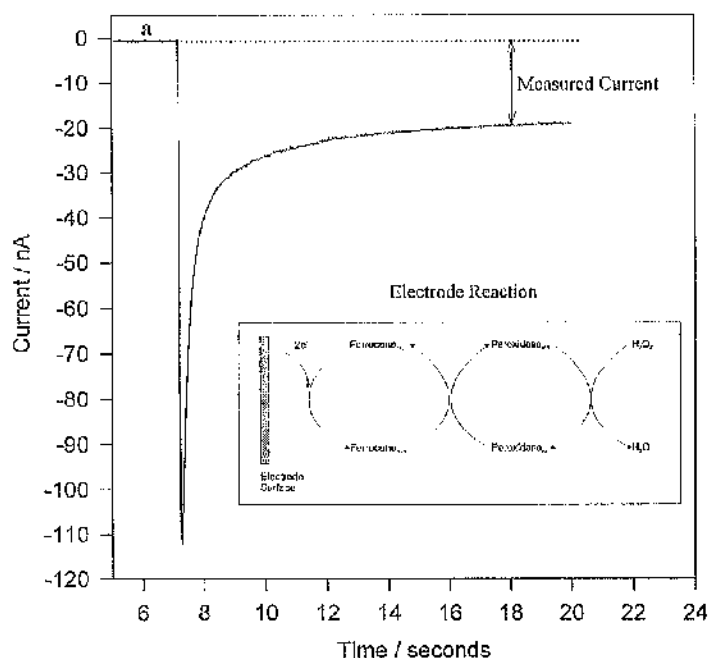
Figure 2.4 – A typical current time plot obtained in a chronoamperometric experiment for the electrode reaction shown. The working electrode was poised at 0 mV *vs.* Ag|AgCl in order to reduce the ferrocene , which in turn is recycled by the enzyme horseradish peroxidase.

Immediately following the potential step a rapid increase in current is observed as the species in close proximity to the electrode is oxidised/reduced. Over time this current falls to a steady state. The magnitude of the current is dependent upon the rate of diffusion to the electrode surface. As the species in close proximity becomes depleted, so the thickness of the diffusion layer grows, accounting for the fall off of the current. The current response i as a function of time t (and electrode area A) is described by the Cottrell equation, **Equation 2.4**.

$$i = nFAD^{1/2} \, c_R \, t^{1/2} \, (1/\pi^{1/2})$$ **Equation 2.4**

Where n is the number of electrons exchanged, F the Faraday's constant, D the diffusion coefficient of the electroactive species R, and c_R its bulk concentration as

before. Chronoamperommetry can thus be utilised to measure the concentration of an electroactive species in solution as well as the adsorbed species on the electrode.

As for cyclic voltammetry the measured current has two components; a non Faradaic capacitive component arising from the redistribution of charged species at the electrode surface, and a Faradaic current resulting from the exchange of electrons between the electrons between the electrode and species in solution. The capacitive component is rapid and contained within the initial spike of the current / time profile.

2.2 X-ray Photoelectron Spectroscopy

X-ray photoelectron spectroscopy[115-122] XPS (or electron spectroscopy for chemical analysis ESCA), is a commonly used method for surface analysis, due to its capability of determining the surface composition without, in many cases, altering the composition during analysis. Additionally, it can give information of the chemical environment of the surface components especially bond structure. The current application of XPS to surface characterisation results from the work of Kai Siegbahn and collaborators who developed the technique as it is known today[123].

In XPS monochromatic X-rays, which are incident on the surface under analysis, cause the emission of photoelectrons from the interfacial structure **Figure 2.5**. The X-ray photon of energy $h\nu$ directly ejects electrons from the core energy levels by the direct transfer of the energy to the core-level electron. The measured kinetic energy with which the photoelectron is emitted from the surface region can be described by **Equation 2.5**.

A

Electrostatic
hemispherical
electron analyser

Electrostatic
electron
lens

Large area
electron detector

Computer:
instrument control
and data analysis

Photo-
electrons

Monochromator
crystal

Sample
introduction
and preparation
chamber

hν

Sample

High vaccum
chamber

Vaccum
pump
(10⁻⁶ torr)

X-ray
anode

(10⁻¹⁰ torr)

Ultrahigh
vacuum
pumping
system

B

O1s photoelectron

X-ray
photon
hν

1s 2s 3s

Figure 2.5 - A a schematic of an XPS spectrometer. The key components of a state of the art spectrometer (X-ray anode, monochromator crystal, collection lens, hemispherical analyser and large area detector) are shown. **B** the X-ray photon transfers its energy to a core level electron leading to its photoemission.

$$E_K = hv - E_B - \phi$$ **Equation 2.5**

where E_K is the kinetic energy of the emitted electron (measured during the XPS experiment), hv is the energy of the X-ray source (a known value), E_B is the binding energy of the core electron (a function of the type of atom and its chemical environment from which the electron is ejected) and ϕ is the spectrometer work function (a constant for a given analyser). It is the ability to accurately measure the kinetic energies of the ejected photoelectrons which allows the determination of their binding energies and, thereby providing valuable information on the surface chemical environment.

It is convenient in XPS to plot the number of photoelectrons emitted with different binding energies, E_B, rather than the kinetic energies of the photoelectrons as shown in a typical XPS spectrum **Figure 2.6** (which are instrument dependent).
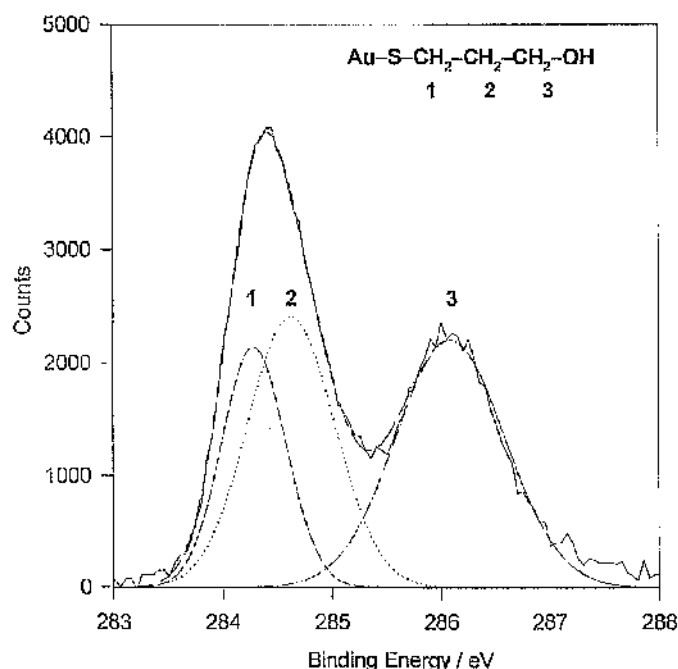
Figure 2.6 - A typical XPS spectra, in this instance recorded for the carbon C1s region of a mercaptopropanol substituent adsorbed as a SAM on gold.

It is the chemical bonds, both ionic and covalent, between atoms in a sample affect the electronic charge distribution and cause a shift in the electron energy levels in each atom, by comparison with a free neutral atom[115]. The size of this shift is dependant upon the functional group bound to that atom (i.e. its chemical environment), allowing identification of specific bond types. For example, in **Figure 2.6** this spectrum, obtained from a mercaptopropanol SAM chemisorbed on gold, shows the energy shifts observed for the C(1s) core electrons. Three peaks can be observed, showing different shifts, corresponding to different bonding by the three carbon atoms, C-S, C-C and C-OH respectively. An example of the range of binding energies observed for an atom is shown in **Table 2.1** where the typical C(1s) binding energies for a range of organic samples are shown. These energy shifts, as a result of chemical bonding, can be observed for every element of the periodic table, with the exception of hydrogen (as the binding energy for saturated carbon is taken as reference).

Functional Group		Binding Energy (eV)
hydrocarbon	C–H, C–C	285.0
amine	C–N	286.0
alcohol, ether	C–O–H,C–O–C	286.5
Cl bound to carbon	C–Cl	286.5
F bound to carbon	C–F	287.8
carbonyl	C=O	288.0
amide	N–C–O	288.2
acid, ester	O–C=O	289.0
urea	N–CO–N	289.0
carbamate	O–CO–N	289.6
carbonate	O–CO–O	290.3
2F bound to carbon	$-CH_2CF_2-$	290.6
carbon in PTFE	$-CF_2CF_2-$	292.0
3F bound to carbon	$-CF_3$	293-294

Table 2.1 - Typical C(1s) binding energies for organic samples. The observed binding energies will depend upon the specific environment where the functional groups are located. Most ranges are ±0.2 eV but some can be larger (e.g. fluorocarbon samples)[115].

Although the incident X-rays can penetrate relatively far into the sample, only electrons produced near the surface have any significant probability of escape without subsequent energy loss. Consequently, X-ray photoelectron spectra can only provide information on the atomic species that are present within approximately 10 nm of the sample surface. The technique is therefore highly surface sensitive and is ideal for surface characterisation. The fact that incident electrons do penetrate further, however, does have implications on the recorded spectra. Some core electrons deeper in the sample are ejected and move through the sample and are ejected with energy loss, it is these electrons which make up background counts recorded on XPS spectra. When characterising samples using XPS it is usual to collect a spectrum over a wide range of energies (a survey spectrum) prior to performing detailed analyses on particular areas of interest for the particular sample **Figure 2.7.**
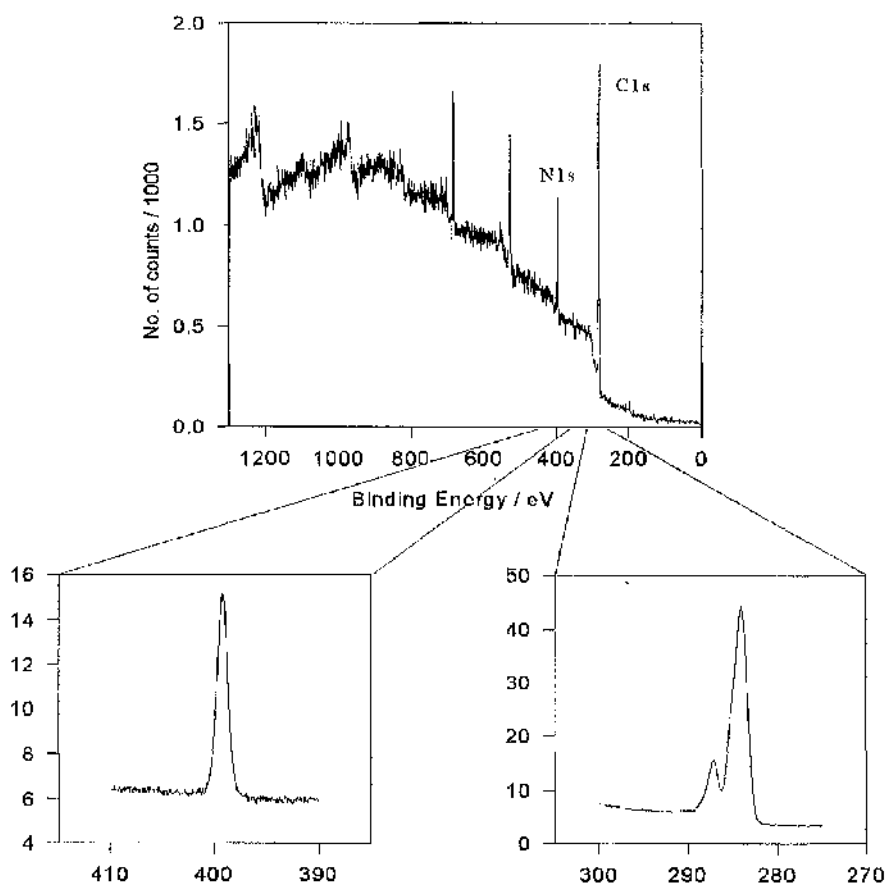
Figure 2.7 - A typical survey spectra shows the individual component peaks over a wide range of binding energies. Particular regions such as the carbon C(1s) and the nitrogen N(1s) regions can then be subjected to a more detailed analyses, as shown.

27

The XPS facility used for surface characterisation and analysis shown in this study was the SCIENTA ESCA300 X-ray photoelectron spectrometer (8 kW Al K(α) and Cr K(β) dual source) **Figure 2.8**, located in the Research Unit for Surfaces Transforms and Interfaces (RUSTI) , Daresbury Laboratories (Daresbury, UK). The combined features of high spectral intensity, high energy resolution (0.25 eV) and high spatial resolution (25 microns) of the machine enable detailed studies of structure, bonding, reactivity and dynamics of surfaces and interfaces.
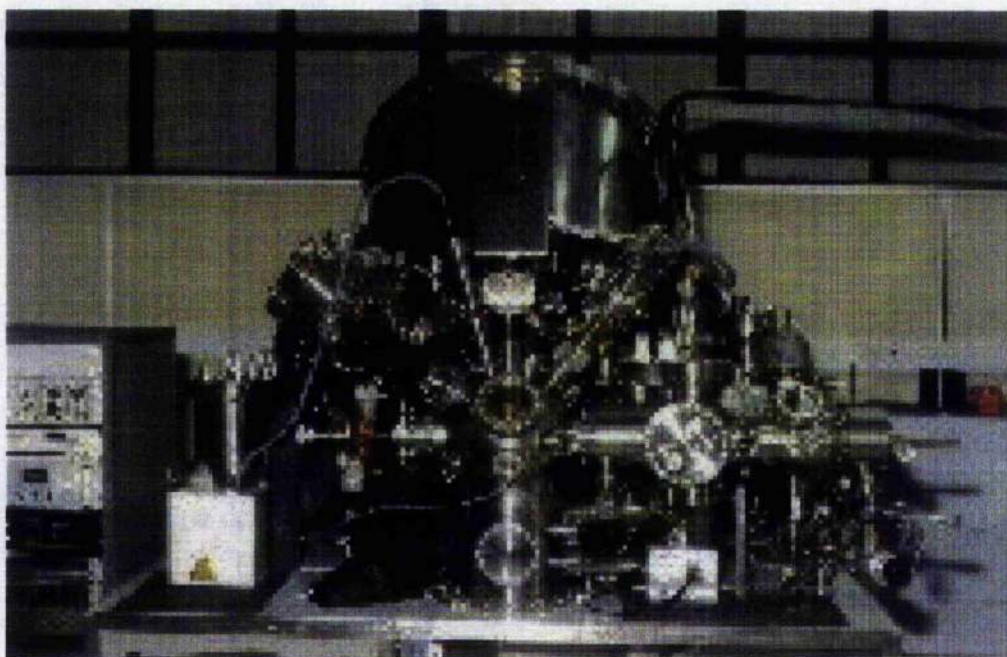
Figure 2.8 - Shows the Scienta ESCA300 X-ray photoelectron spectrometer facility at the Daresbury laboratory (Daresbury, U.K) used for the analysis of the SAMs used throughout this thesis.

2.3 Fourier Transform Infra-Red Spectroscopy (FT-iR)

Whereas XPS is a surface analysis technique providing data primarily on elemental composition, Fourier Transform Infra-Red Spectroscopy (FT-iR)[124-128], is a second surface analytical technique that can yield important information regarding

the composition of the bulk of the sample, primarily giving detail of the molecular bond composition.

Chemical bonds undergo a variety of fundamental perpetual movements including stretching, twisting and rotating. The energy of most these molecular vibrations corresponds to that of the infrared (iR) region of the electromagnetic spectrum. Infrared spectroscopy is sensitive to the vibrations that lead to changes of dipole moment within a molecule. Consequently when light from an infra-red source is passed through a molecular sample, such as an organic compound, some frequencies will be absorbed[129].

The simplest example demonstrating the principles of iR adsorption is that of a diatomic molecule. In a diatomic molecule with masses m_1 and m_2, separated by distance r, a directional dipole moment will be set up as a result of the difference in electric charge between the two masses **Figure 2.9**[129]. As the molecule is in a state of perpetual vibration, the separation of the two masses r, will be constantly and periodically changing, causing an alternating electric field of frequency, $f = 1/\tau$. Therefore, if the incident iR radiation is of the same frequency, adsorption of that radiation will occur. The power of iR spectroscopy as an analytical tool is derived from the fact that each bond within a continuously vibrating molecule has its own characteristic frequencies of both stretching and bending vibrations.

Stretching frequencies result from vibrational changes in bond length, whilst those from bending are as a result of vibrational changes in bond angle. Stretching adsorptions appear at higher frequencies in the iR spectrum than bending for the same bond, due to the increased energy required for stretching in comparison to bending. In addition, the vibrational frequency of a bond increases if the bond strength increases or the atomic mass of either of the atoms decreases. For example the following bonds would change from high vibrational frequency to lower, in the following order; C=O > C=C > C-O > C-C[124].
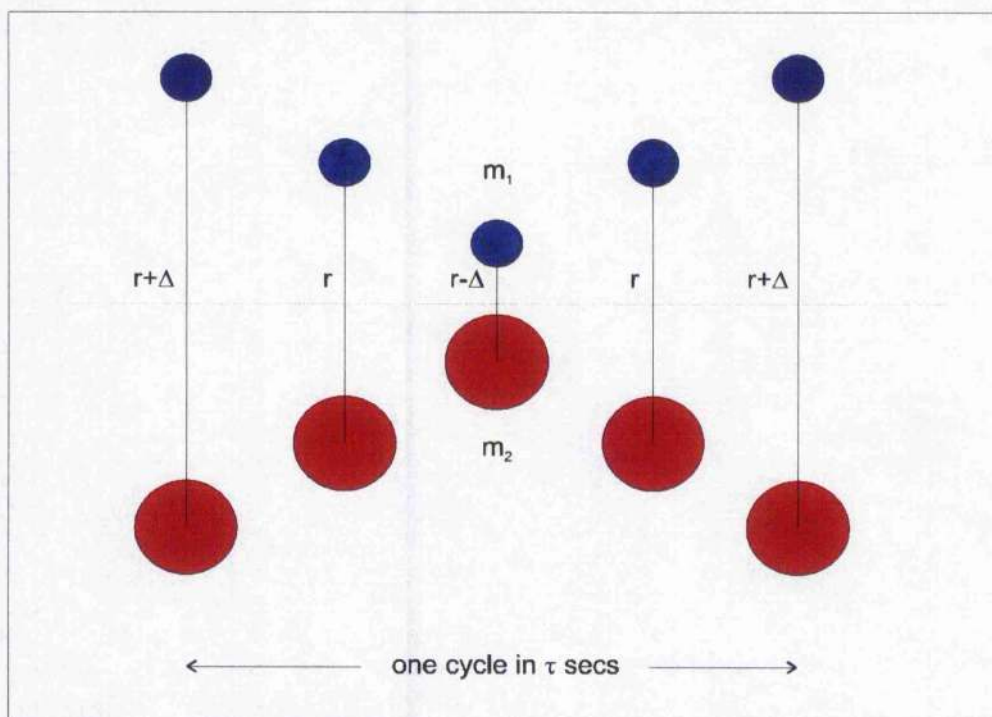
Figure 2.9 - A schematic representation of a diatomic molecule showing the vibrations that will adsorb iR radiation. The masses of the two molecules are represented by m_1 and m_2, r the distances between the two molecules and Δ the change in this separation.

For molecular assemblies containing a large number of atoms and bonds (such as proteins) there are many associated vibrational frequencies. For a non-linear molecule with N atoms, the number of vibrational degrees of freedom is $3N$-6 which, provided they satisfy the conditions required for adsorption described above, will produce characteristic vibrational frequencies somewhere within the iR spectra. Additionally, for linear molecules, the degrees of rotational freedom are reduced to 3N - 5, since only two degrees of rotational freedom are required[124,129,130]. The possible vibrational modes of both non-linear and linear molecules are illustrated in **Figure 2.10** using water and carbon dioxide as simple model examples.

A complex molecule has a large number of vibrational modes which involve the whole molecule. As a good approximation, however, some of these features are associated with the vibrations of individual bonds or functional groups (localised vibrations) while others must be considered as vibrations of the whole molecule.

The vibrations of the whole molecule give rise to a series of adsorption bands at low energy, below 1500 cm^{-1}. It is those peaks in the region of the spectrum greater than 1500 cm^{-1} that are, however, of particular interest as they show adsorption bands assignable to a number of functional groups.

(a) water molecule

symmetric stretch
3652 cm^{-1}

asymmetric stretch
3756 cm^{-1}

Bend
1595 cm^{-1}

(b) carbon dioxide molecule

symmetric stretch
no dipole movement
no absorption

asymmetric stretch
2349 cm^{-1}

Bend
667 cm^{-1}
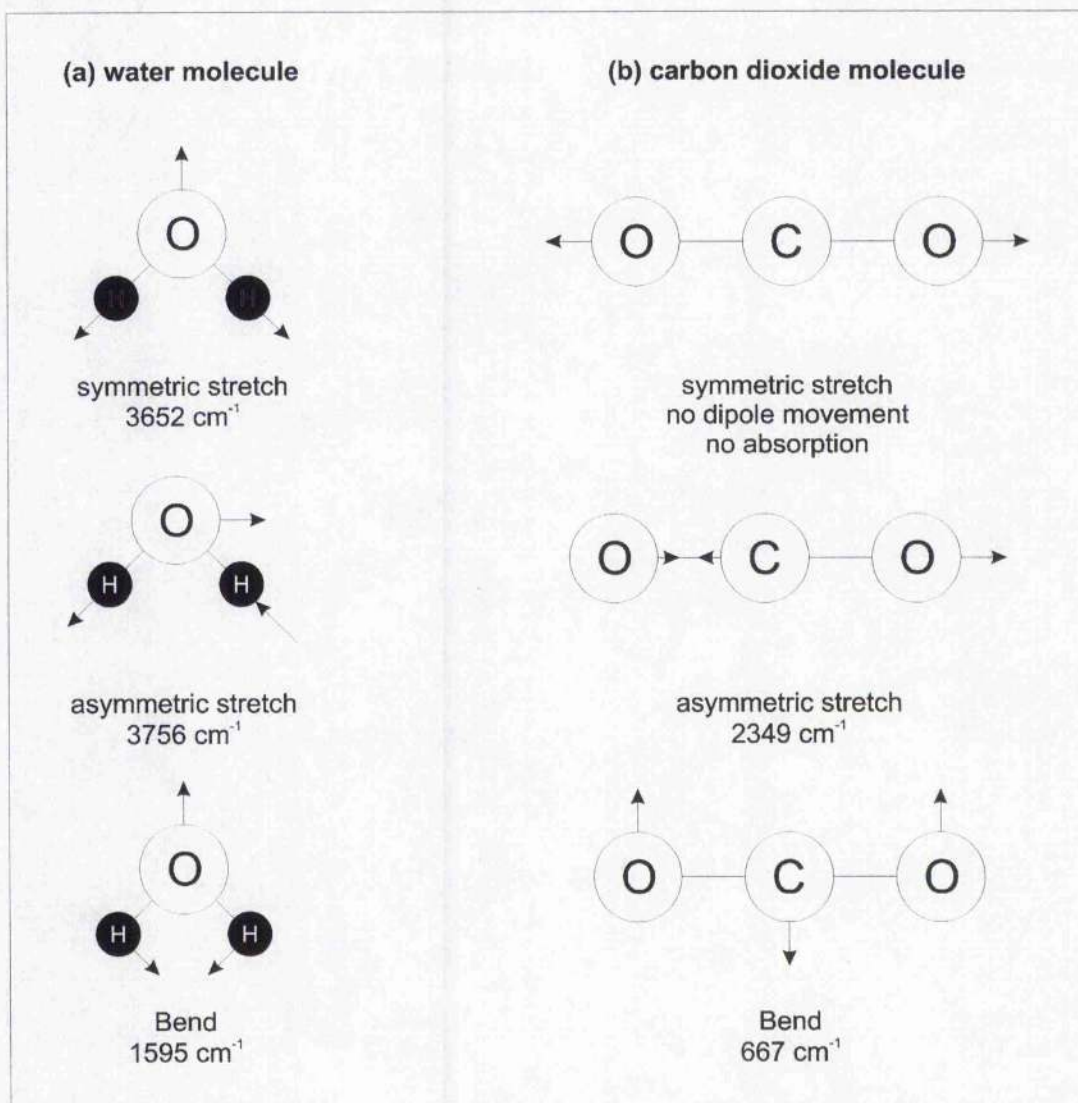
Figure 2.10 - Illustration of the fundamental modes of vibration of both a non-linear polyatomic water molecule **(a)**, and a linear polyatomic carbon dioxide molecule **(b)**. The magnitude of the adsorption value varies with the mode of vibration as illustrated. Arrows indicate the direction of the stretches or bends.

The regions of particular interest when considering protein immobilisation and adsorption at biosensor interfaces are those corresponding to the peptide bonds, which produce a strong characteristic signal. Peptide bonds have three related modes

31

of vibration, giving rise to three individual peaks in an associated iR spectrum; amide I, amide II and amide III. The amide I peak, 1600 - 1700 cm^{-1}, is the strongest of the three and is attributed to the C=O stretch. The amide II band, found between 1500 1600 cm^{-1}, is a strongly coupled interaction between C-N stretch and N-H bend vibrations. Finally the amide III is a weak peak associated with secondary N-H bend vibrations, found between 1200 - 1300 cm^{-1} **Figure 2.11**. The adsorption values for all of these peaks vary as the concentration of protein on the sample surface is varied[124,127,130-132].
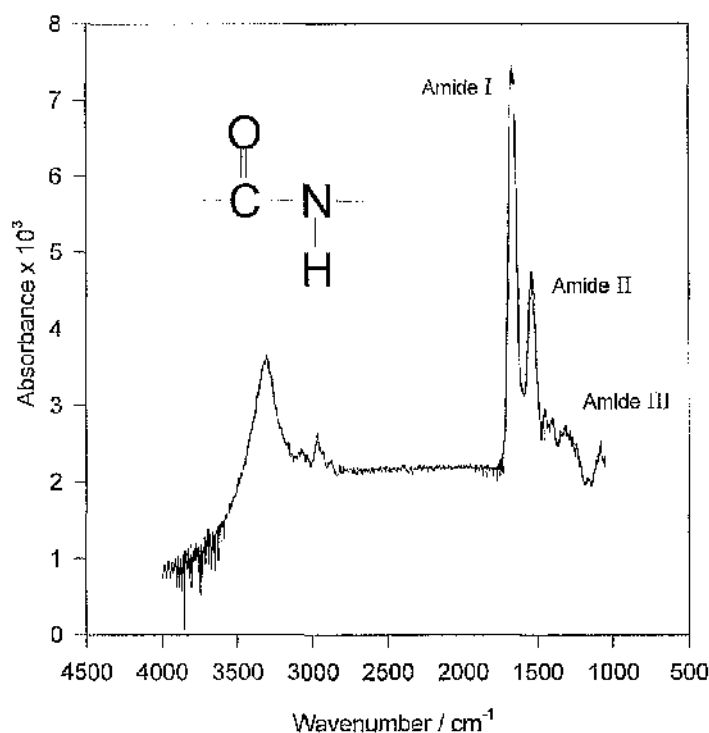
Figure 2.11 - A typical FT-iR spectra, collected for Bovine Serum Albumin adsorbed to a gold surface. The amide peaks of interest are illustrated. Spectra collected at an incident angle of 80° (grazing angle) at a 4 cm^{-1} resolution.
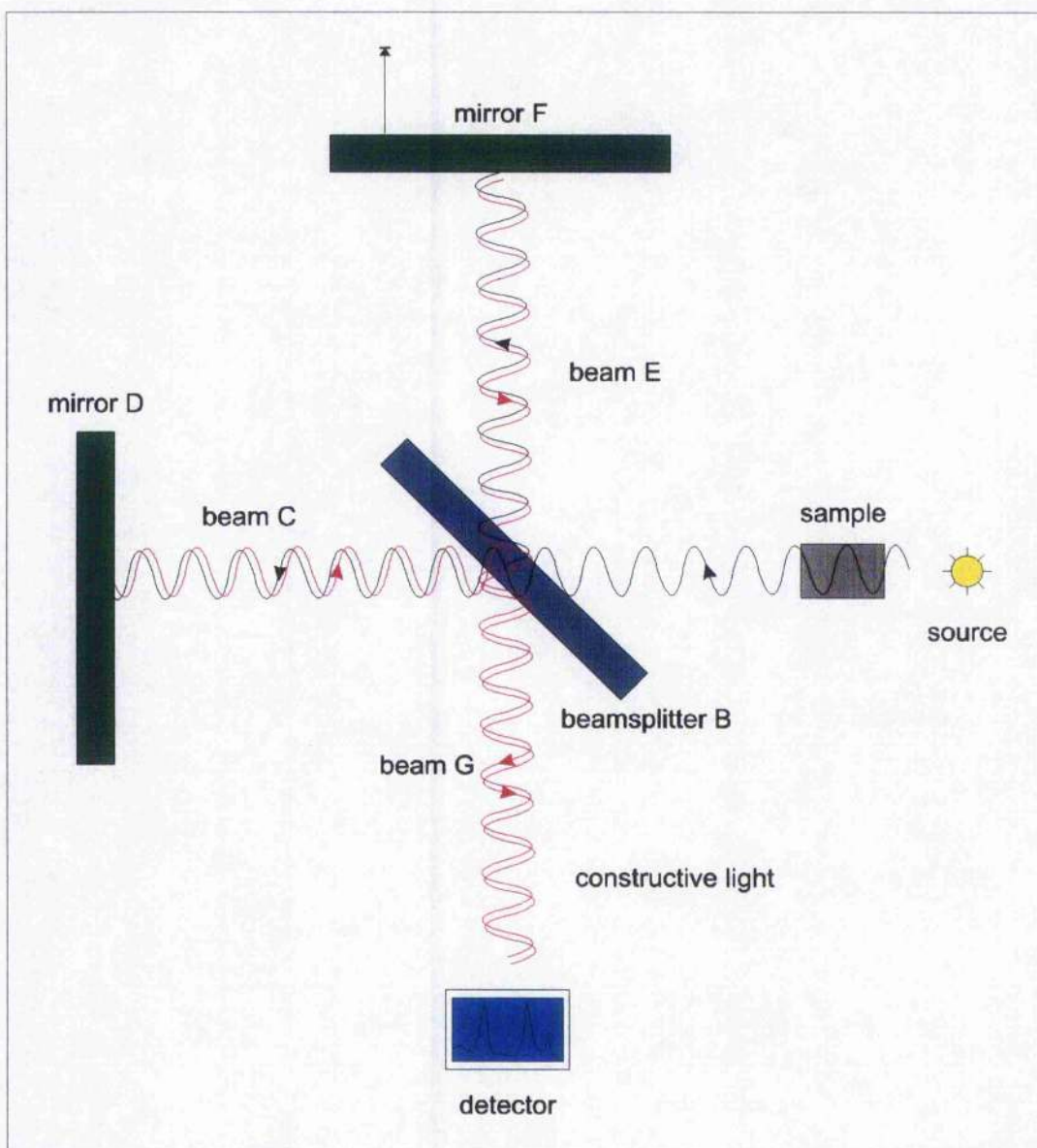
Figure 2.12 - A schematic of a Michelson interferometer illustrating the reflective pathway of the incident light prior to its detection and analysis.

The principle of FT-iR analysis is based upon infrared light from a p-polarised light source passing through a scanning Michelson interferometer[124] such that a Fourier Transformation of the energy gives a plot of intensity versus frequency. When a sample is placed in the beam, it absorbs particular frequencies (as previously described), so that their intensities are reduced in the interferogram and the subsequent Fourier Transform is the infrared adsorption spectrum of the sample.

The most fundamental component of the iR spectrometer is the Michelson interferometer whose function can be understood with reference to **Figure 2.12.**

Light from the source strikes the beam splitter B (usually a KBr or CsI plate coated with germanium for iR applications), which is designed to split beam A exactly in half. One half is transmitted, as beam C, to be reflected by the plane mirror D; the other half of beam A is reflected, as beam E, and reflected again by plane mirror F. Both of these reflected beams E and C are recombined at the beam splitter B to create beam G and passed onto the detector. Depending upon the position of plane mirror F (it is moved in the direction shown in the diagram) either constructive or destructive interference patterns i.e. light and dark images, will reach the detector and a Fourier Transform can be applied to the pattern to produce the intensity dependent iR spectrum for a particular sample.

For analysis of thin coatings on metal surfaces, or for samples with a very smooth surface, the iR spectrometer is used in grazing incidence reflectance (GIR) mode more commonly known as Reflectance Angle iR Spectroscopy (RAIRS). When operated in this mode the incident angle of the iR beam with (respect to the surface) can be varied from 10° (near normal) to 85° (grazing angle) depending upon the thickness of the adsorbed or bound layers on the sample. It is generally found that the thinner the sample, the larger the incident angle that has to be applied in order to obtain as much information from the sample, as possible.

Advantages offered by the RAIRS technique, over spectroscopies in other formats (e.g. 'in-line') include improved resolution and increased sensitivity. Practically, these advantages realise reduced time scales of experiments and increased signal to noise ratios.

Therefore, whilst XPS can be used to give excellent surface information, FT-iR is especially useful for probing the whole thickness of the adsorbed biomolecular layer.

2.4 Fluorescence Measurements[133]

Fluorescent probes enable researchers to detect particular components of biomolecular assemblies, with sensitivity and selectivity. In this thesis we use the immobilisation of a fluorescent probe at modified surfaces as a means of probing the molecular composition of that surface. When a fluorescent probe is used and the sample exposed to light energy of the correct frequency the sample will emit light by a process known as fluorescence.

Fluorescence is the result of a three-stage process that occurs in certain molecules called fluorophores (In this study we use a probe known as Fluorescien IsoThioCyanate FITC). A simple electronic-state diagram can be used to illustrate the production of fluorescence by such probes **Figure 2.13**.
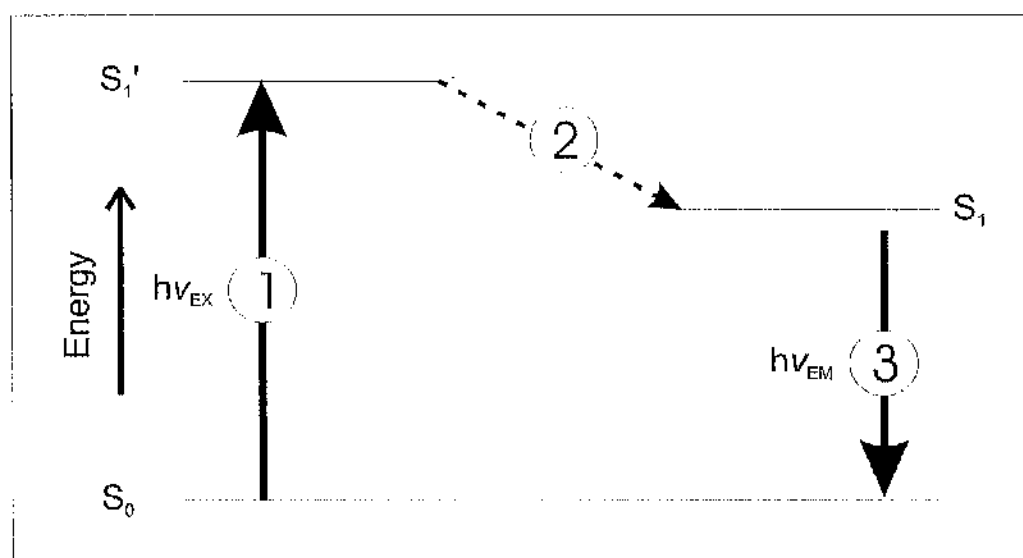
Figure 2. 13– A simple electronic state diagram showing the three stage process which describes fluorescence. In Stage 1 the fluorophore absorbs light energy $h\nu_{EX}$, creating an exited energy state S_1'. During the lifetime of this excited state some energy is dissipated though interactions within the molecular environment (Stage 2), such that the molecule possess a 'relaxed' state S_1. Finally the energy is released as an emission photon $h\nu_{EM}$ and the molecule returns to its ground state S_0 (Stage 3).

Initially a photon of energy $h\nu_{EX}$ is supplied by an external energy source, and absorbed by the fluorophore, creating an excited electronic singlet state (S_1'), Stage 1. This excited state exists for a finite time (typically $1\text{-}10 \times 10^{-9}$ seconds). It is during this time that the fluorophore undergoes conformational changes and is also subject to a multitude of possible interactions with its molecular environment, Stage 2. These processes have two important consequences. Firstly the energy of S_1' is partially dissipated, yielding a relaxed singlet excited state (S_1) from which fluorescence emission originates. Secondly, not all of the molecules initially excited by absorption (Stage 1) return to the ground state (S_0) via fluorescence emission, other processes such as collisional quenching and fluorescence energy transfer may also depopulate S_1. (A measure of the extent to which these processes occur is given by the fluorescence quantum yield, which is the ratio of the number of fluorescence photons emitted (Stage 3) to the number of photons absorbed (Stage 1)).

In the final stage a photon of energy $h\nu_{EM}$ is emitted, as the fluorophore returns to its ground state S_0 (Stage 3). It is due to energy dissipation during the excited-state lifetime that the energy of the emission photon is less than that of the excitation photon. The difference in energy or wavelength, represented by ($h\nu_{EX} - h\nu_{EM}$) is known as the Stokes Shift. The Stokes Shift is fundamental to fluorescence techniques as it allows emission photons to be detected whilst filtering out the excitation photons.

There are four essential elements for any fluorescence detection system, an excitation source, a fluorophore, wavelength filters (to isolate emission photons from excitation photons) and a detector that registers the emission photons. These four elements are illustrated in **Figure 2.14,** which represents the detection system used in this thesis.

36
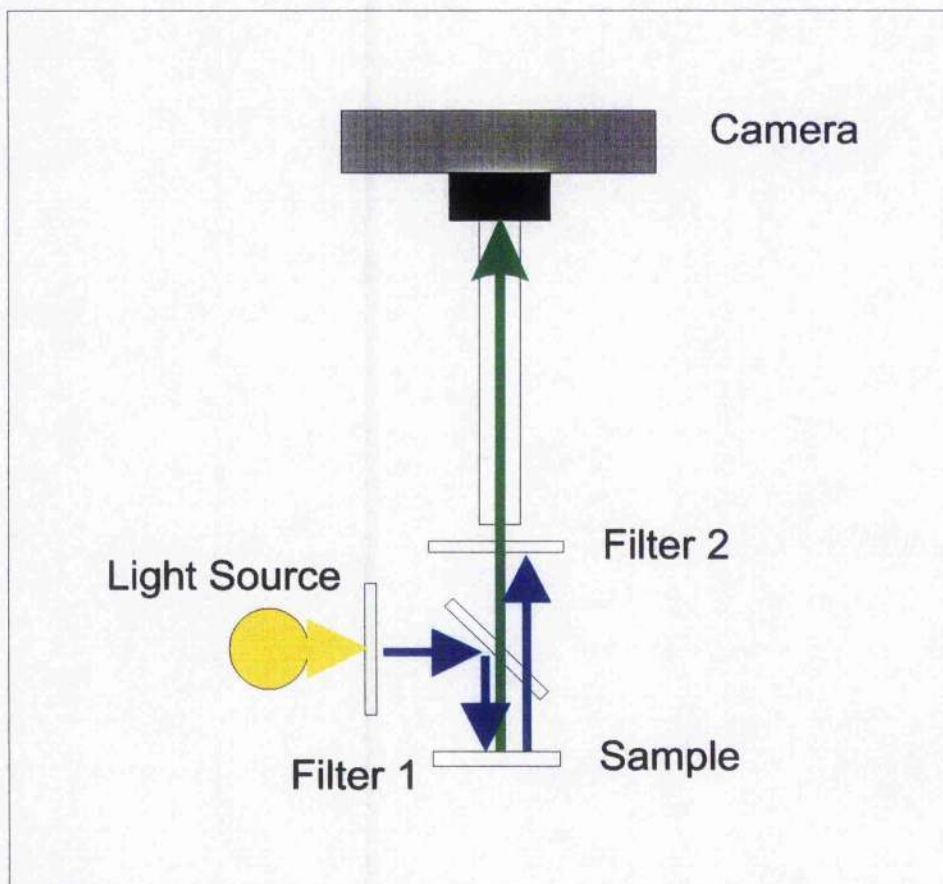
Figure 2.14 – The fluorescence detection system used in this thesis consists of the following elements. A helium light source which is filtered, by Filter 1, to allow only light having a wavelength suitable for excitation of the FITC labelled sample (FITCλ_{ex} = 494 nm). The photons that are collected from the sample are then filtered for excitation photons (FITC:λ_{em} = 520 nm) – Filter 2. Finally the photons are detected via a camera mounted on a microscope.

CHAPTER 3: X-RAY PHOTOELECTRON SPECTROSCOPY OF SELF ASSEMBLED MONOLAYERS

3.1 Introduction

Over the past decade, chemical modification of sensor surfaces has been recognised as a means of introducing both specificity and functionality[24,25,134-136]. For example, as long ago as 1983, Nuzzo and Allara showed that alkanethiols spontaneously chemisorb onto gold surfaces to form well organised structures known as self-assembled monolayers[29], thereby providing a means of introducing a degree of molecular functionality[137,138] **Figure 3.1**.
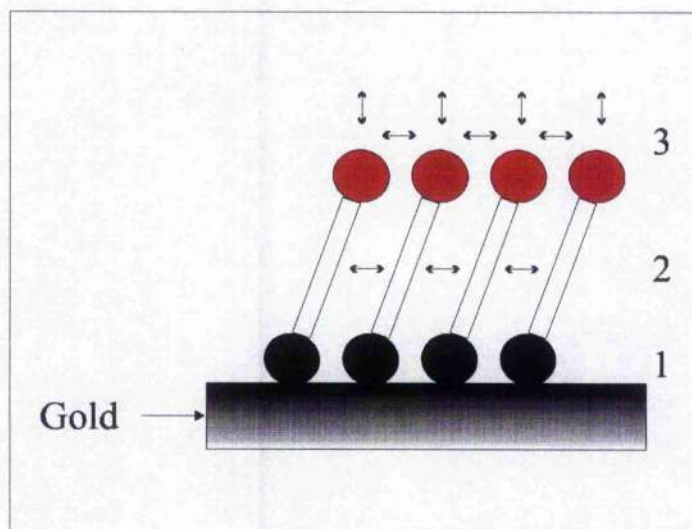
Figure 3.1 - Diagram representing a SAM formed on a gold surface, three main interactions determine the monolayer structure. The very strong chemisorption of the sulphur tailgroup to the gold surface, the lateral hydrophobic interactions between the acyl chains, which give the monolayer highly defined planar structure 2, and the headgroups, which determine the nature of the SAM's interaction with the solution phase and also influence the stability of the monolayer through headgroup/headgroup interactions 3, are shown.

In the context of understanding bio-interfacial interactions, the tail group of such a self assembled monolayer can be considered to tether the molecular structure to the gold surface, whilst the head group has the potential to act as a site for molecular recognition, e.g. for the selective immobilisation of a ligand binding protein (such as an antibody or streptavidin) as may be appropriate for a biosensor[37-43,48,134,139,140]. The abundance, and spatial distribution, of such headgroup recognition sites, has important implications on both the micro- and macroscopic properties of a bioelectronic interface. Indeed the introduction of mixed monolayers, composed of two or more head groups, can offer a method to control the optimum conditions for the functioning of either bound molecules, or those interacting with the surface.

In one example, which illustrates this latter point, immobilised antibodies show a decrease in response, when challenged by antigen, if the antibody surface density is too high, as a consequence of the effects of steric hindrance[42,43,48]. The addition of spacer alkanethiols into the alkanethiol monolayer to which antibody has been immobilised can be used to decrease the surface density of the immobilised antibodies. Similar results have been observed for the binding of avidin using mixed monolayers of biotinylated thiols and alcohol terminated thiols[47]. Control of the monolayer composition, therefore, provides a means by which the optimum surface density for the function of the immobilised protein can be attained

The use of long chain alkanethiols to produce mixed monolayers gold surfaces has received attention from a wide number of groups working in physics, biochemistry and the analytical sciences[135]. For example Takami et al have used Scanning Tunnelling Microscopy STM analysis to distinguish between different head groups in a mixed monolayer consisting of alkanethiols of chain lengths > 12 carbons atoms, demonstrating that the resulting (modified) surface reflected the molar ratio of headgroups in the (loading) solution[49]. Other research[44,45,51], producing mixed monolayers of CH_3- and OH-terminated long chain alkanethiols (of the same chain length) through co-adsorption has shown that the self-assembly results in true molecular mixing (with no single component domains).

39

Whilst long chain SAMs have the advantage of forming highly ordered structures[31,44-48], they do have the potential disadvantage that they serve to distance the solution phase from the underlying (sensor) surface, which may result in the reduction of the rate of electron transfer between a (solution phase) redox centre and the electrode[141]. In addition, long chain monolayers, by their nature often form a close packed, ordered barrier, which limits diffusion of a solution phase electroactive species, an arrangement which has practical limitations if such an interface were to be used for electrochemical sensing.

In common with other authors[50], we have prepared mixed monolayers of short chain alkanethiols by time dependant displacement of an initial modifier. In our work in chapter 3 we have found that the use of short chain thiols not only helps to maximise the rate of interfacial electron transfer between proteins, but also provides surfaces which are more amenable to quantification by X-ray Photoelectron Spectroscopy (XPS)[115,142].
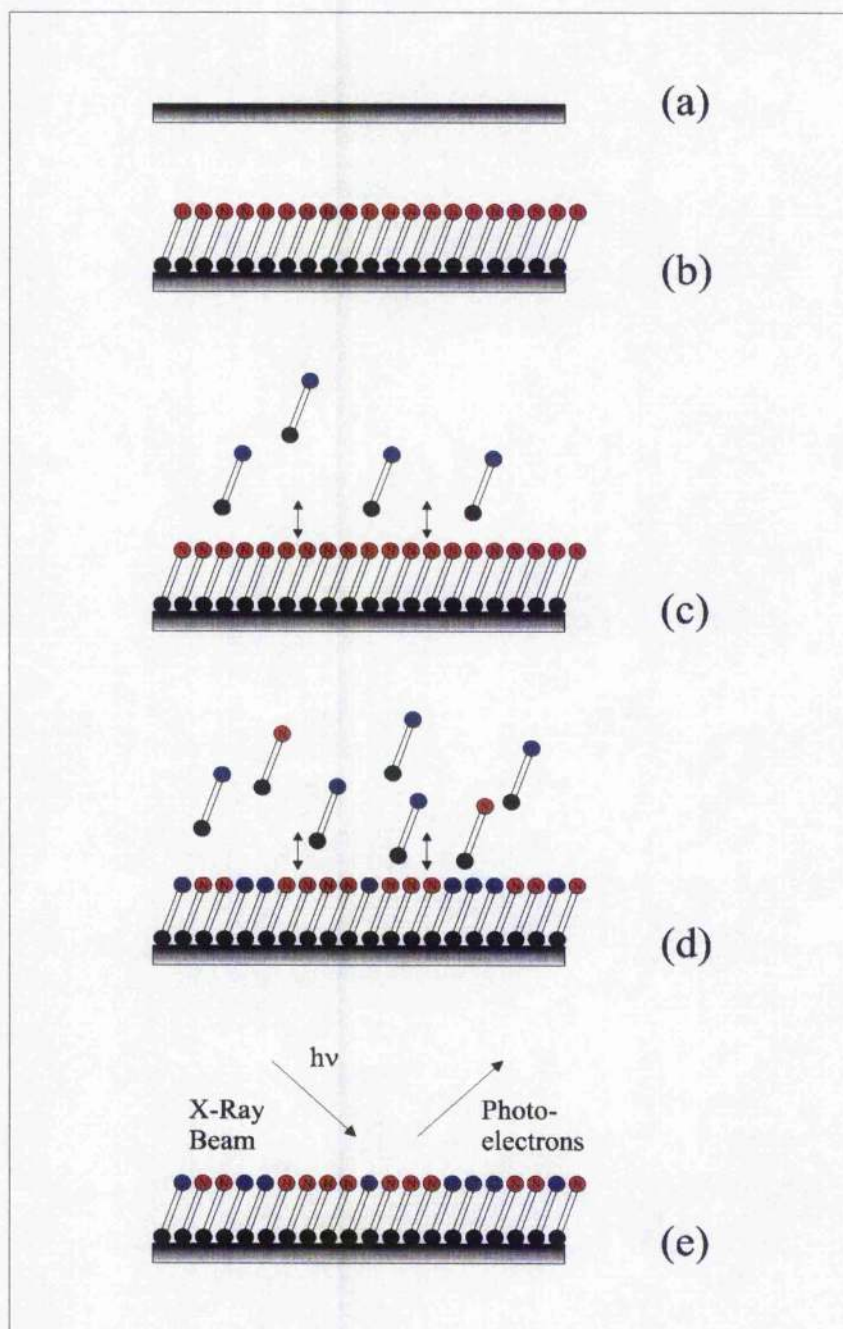
Figure 3.2 - Schematic representation of experimental procedures used in this study. A plain gold electrode (a), is cleaned by reactive ion etching (see later) prior to immersion in 1mM aqueous solution of mercaptoethylamine, to form a Au-mercaptoethylamine SAM (b). After washing thoroughly with RO water, this primary SAM is then immersed in a secondary modifying solution of 1mM mercaptopropanol (c). After varying periods of time the SAM is removed, and displacement of the thiol results in the formation of a secondary SAM composed of both mercaptoethylamine and mercaptopropanol (d). The secondary SAM is washed thoroughly in RO water and characterised by XPS analysis (e).

This latter aspect of the study is a consequence of higher ratios of head group specific signals (e.g. NH_2, COH) with respect to the alkyl backbone signals than would be the case for long chain thiols. Thus we have been able to probe the dynamics of mixed monolayer formation using spectroscopic studies **Figure 3.2**, and show that, by successive immersions of a gold substrate into single component thiol solutions, it is possible to control the ratio of two alkane thiols, containing head groups of differing functionality, within a mixed monolayer.

3.2 Experimental Section

3.2.1 Materials

2-Mercaptoethylamine and 3-mercaptopropanol were obtained from Sigma (Poole UK) and used without any further purification. 2-Mercaptoethylamine is susceptible to degradation in air and was therefore stored desiccated at 4°C. All 1 mM thiol solutions were prepared immediately prior to use, using reverse osmosis (RO) ultra-pure water (Millipore, UK). All metals were obtained from Goodfellows (Cambridge, UK).

3.2.2 Formation of Mixed Monolayers

3.2.2.1 Substrate Preparation

Glass slides (25 mm x 75 mm x 1.5 mm) were scribed using a diamond pen - into *ca.* 10 mm x 20 mm squares, prior to cleaning by sonication for 5 minutes in each of the following cleaning agents: Opticlear[TM] (G&S Inc.); acetone; methanol; and reverse osmosis (RO) water. After being dried in a stream of nitrogen gas the scribed and cleaned glass slides were finally baked at 50°C for 10 minutes in order to remove any residual water.

Gold electrodes, or substrates, were prepared for SAM formation by electron beam evaporation of a Ti/Pd/Au (10/10/100 nm) multilayer structure onto these scribed glass slides using a Plassys QD1 automated electron beam evaporation system. The use of this multilayer recipe of metals is well established and understood to give excellent adhesion of the metal to the glass substrate. Immediately prior to deposition of the thiol monolayer, the gold surface was cleaned using an optimised reactive ion etch, etching in a PlasmaFab ET340. Firstly for five minutes in an oxygen plasma to remove organic contamination, and then for a further five minutes in an argon plasma to remove adsorbed water(50 mT, 20 sccm, and 10 W)[143].

3.2.2.2 Monolayer Formation

After cleaning, the gold surface was immediately immersed in a 1 mM solution of an initial thiol modifier (i.e. an aqueous solution of 1 mM mercaptoethylamine) for 2 hours and then thoroughly rinsed using RO water. Mixed monolayers were subsequently prepared by drying the surface in a stream of nitrogen gas and then immersing in a second thiol solution (i.e. an aqueous solution of 1 mM mercaptopropanol) for between 10 seconds and 180 minutes, before rinsing.

$$HS-CH_2-CH_2-NH_2$$
Mercaptoethylamine

Tail   Head

$$HS-CH_2-CH_2-CH-OH$$
Mercaptopropanol
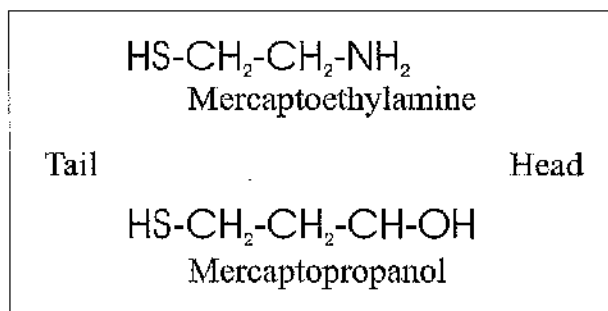
Figure 3.3 - Alkanethiols used in the following experiments. Alkanethiols were typically prepared in aqueous 1 mM solutions prior to application to gold substrates.

3.2.3 Characterisation of the Mixed Monolayers by XPS

All XPS spectra were collected using a Scienta ESCA300 spectrometer, with a rotating anode source providing Al Kα (1486.7 eV) radiation. After monochromation the radiation is focused on the sample, positioned such that the emitted electron take off angle (TOA) is 10° ($\pm$ 3°) relative to the substrate surface (discussed in **Section 3.3.1.3**). Self assembled monolayer films were prepared as described above, and S(2p), C(1s), N(1s) and O(1s) spectra were acquired using the Scienta Software. The slit width (0.8mm) and the TOA were kept constant for each of the samples measured, to probe each sample to the same depth. Prior to data fitting (SigmaPlot/Peak Fit, Jandel Scientific, Poole, U.K.), the binding energies of the spectra were adjusted to compensate for sample charging (as detailed in **Section 3.3.1.1**).

3.3 Results and Discussion

3.3.1 Some Analytical Considerations.

3.3.1.1 Adjustments for Charging Effects.

When using an insulating substrate, for example the glass base beneath the evaporated Au surface, the emission of photoelectrons results in the build up of a positive charge[115]. It is necessary therefore, to provide an additional compensating source of electrons. This is achieved by flooding the sample with monoenergetic source of compensating electrons (0eV bias voltage) using the flood gun. The absolute binding energy of an insulated sample is therefore difficult to measure and under these conditions it is best to use an internal reference[115]. In order to be able to compare peak positions between samples, the Au(4f $^{7}/_{2}$) spectrum (84.00 eV) was used as a reference, and all other collected spectra (S(2p), C(1s), N(1s) and O(1s))

44

were normalised with respect to this. Background counts (due to inelastic scattering) were also removed by the Shirley method, prior to fitting[122].

3.3.1.2 Gaussian Method of Peak Fitting.
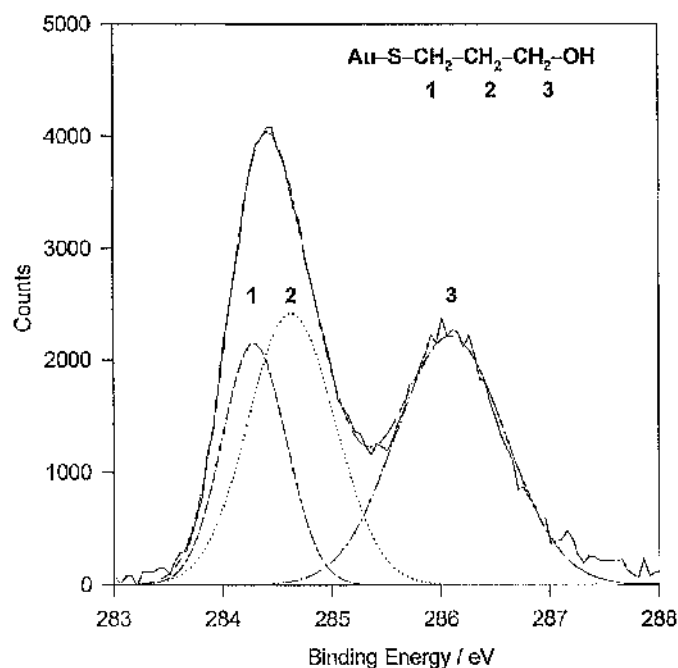
Figure 3.4 - C(1s) spectrum curve fit of a mercaptopropanol SAM, assembled on a gold substrate, fitted to the minimum number of Gaussian peaks. Numbered peaks refer to carbon centres as detailed in insert. (TOA 10°, Slit width 0.8mm and an AlKα source).

Figure 3.4 illustrates the typical data acquired during XPS measurements. It can be seen that the curve obtained for a given orbital(in this case for C(1s) spectra) is composed of counts detected for photoelectrons from several different atoms, each with bonds in their own particular molecular environment and, therefore, showing a range of binding energies. It is important to calculate the area and binding energy of each sub-peak within the spectra under study. A broadening of the sub-peaks, determined by the lifetime of the core hole (the time taken for the electrons to reorganise and fill the hole left by the leaving electron), instrumental resolution and satellite features all occur, such that these photoemmission peaks are generally

considered to be Gaussian in shape[115,122]. Deconvolution can, thus, be achieved by the fitting of the spectra to the least possible number of Gaussian shaped peaks, each peak being associated with an individual bond moiety within the sample as illustrated in **Figure 3.4.**

The area under each peak is related to the amount of that particular element there is present on the sample, such that after measuring the peak areas and correcting them for appropriate instrumental factors(described later), the percentage of each element in a sample, and the bonds it has formed, can be calculated.

3.3.1.3 Influence of TOA in Elemental Quantification of SAMs.

In this thesis, XPS measurements were generally performed using a TOA of 10°. This low TOA firstly, reduces the background signal due to emission of Au electrons, and secondly, maximised the surface area of the SAM that was sampled. As a consequence, it was possible to collect spectra with a good (high) signal to noise ratio before significant x-ray damage to the SAM occurred. Typical collection times were approximately 40 minutes, and examination of XPS spectra obtained over varying lengths of time (at 1 hour intervals, up to 4 hours after irradiation) showed little change in line shape, indicating a lack of X-ray damage. However, the collection of spectra at low TOA highlights the atomic centres closest to the sample/vacuum interface[115]. The manner in which SAMs form on gold produces a surface in which the sulphur tail group is always close to the gold surface whereas the tail group is always nearer the solution interface. As a consequence when XPS experiments are performed at a low TOA significantly less photoelectrons escape from the atoms which anchor the molecule to the gold surface than those nearer the solution interface. The variation in measured photoelectron intensity with SAM thickness and TOA is described by a simple model based on Beer-Lambert law:

$$I/I_o = \exp\left(-d/(\lambda \sin \theta)\right) \qquad\qquad \textbf{Equation 3.1}$$

Where I denotes the photoelectron intensity escaping at the surface of the SAM, and the initial intensity of photoelectrons produced a distance (d) from the film's interface as I_o, λ is the mean free path of the emitted photoelectron in the material being examined (ca. 25 Å for the transitions of this study) and θ is the TOA, or escape angle, of the photoelectrons (with respect to the sample surface) **Figure 3.5**[144].

For the SAMs under consideration in this work, the sulphur tail group is approximately 4.5 Å further from the photoelectron interface than is the tail group. If we assume, that the 'tails' forming the SAM above the sulphur groups form a complete, homogenous layer 4.5Å thick, then, photoelectrons measured with a TOA of 10° will pass through $4.5/\sin(10°)$ Å of material before escaping, see below.
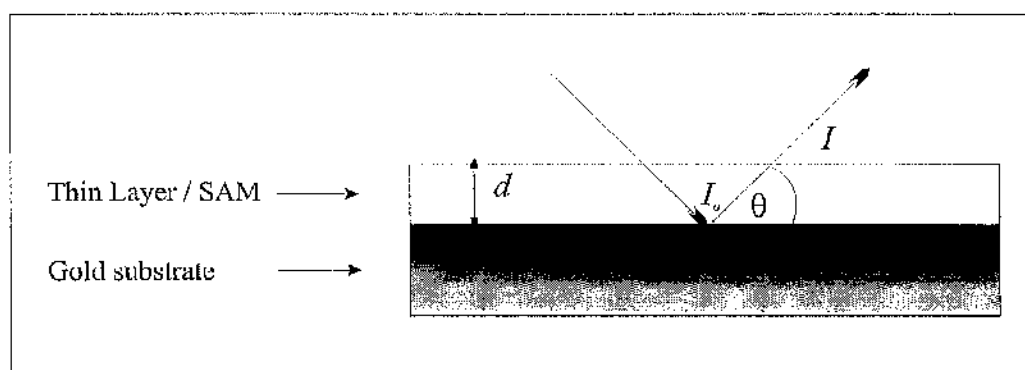
Figure 3.5 - Illustrating the variables in the simple model, based on the Beer-Lambert law, which describes the change in the intensity of measured photoelectrons with SAM thickness. I denotes the escaping photoelectron intensity at the surface of the SAM, I_o the intensity of photoelectrons at the source, d thickness of the SAM film and θ is the TOA, or escape angle, of the photoelectrons (with respect to the sample surface).

From **Equation 3.1**, it can be seen that the signals from the sulphur tail will be 65% less than those signals if they were at the sample/vacuum interface. It is important then, based on these assumptions, to note that the use of elemental quantification based on bulk sensitivity factors alone, will not give the stoichometric composition of the SAM, for the depth of the orbital within the molecule should also be accounted for. (*Note:* Sensitivity factors are used to correct for both differences in detector

sensitivity for each element, as well as the efficiency of production of photoelectrons by each element)[144]. Accordingly, the Gaussian peak responses were constrained to be of increasing areas for centres closer to the outer interface of the SAM, the peak area that corresponds to the carbon centre adjacent to the sulphur species on the gold was also constrained to be less than that derived from quantification of the sulphur species on the Au surface (by integration of the S(2p) spectrum). While the closeness of the C(1s) binding energies, as well as the instrumental resolution, can lead to uncertainties in the fitting of Gaussian peaks, it was noted that sets of curves with a similar goodness of fit varied most in the relative peak heights, rather than the peak positions or half-widths.
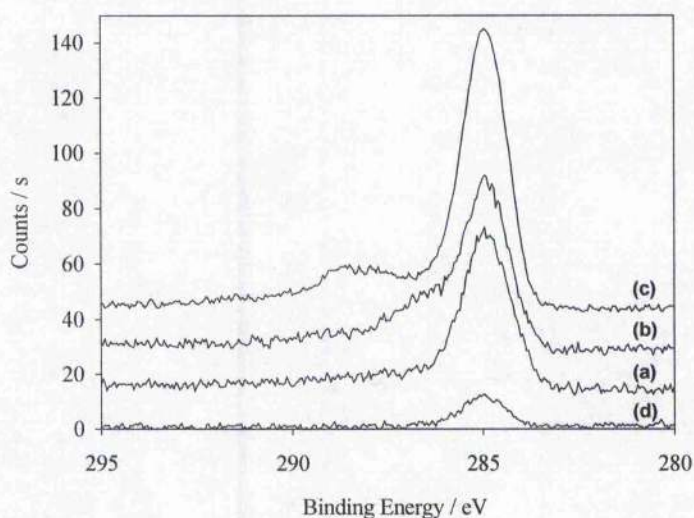
Figure 3.6 – C(1s) spectra of thin film gold electrodes evaporated onto glass substrates. (a) Sample measured within 4 hours of evaporation, note the low level of non C-C, or C-H species. (b) Sample as in (a) after immersion in phosphate buffer for 1 hour, showing the increase in counts at ca. 286 eV corresponding to C-O species. (c) Shows a sample measured two days after evaporation (stored within a closed container), note the increase in spectra at ca. 288 eV corresponding to C=O species, possibly human contamination such as skin rather than hydrocarbon contamination which has no C=O. Finally spectrum (d) shows sample (a) after 2 min Ar plasma etching, with only residual carbon due to contamination within the Au film. (10° take off angle).

3.3.1.4 Effect of Contamination.

As a further consequence of the low TAO used in this study in order to highlight the atomic centres near the sample/vacuum interface, the requirement for stringent precautions to minimise the inevitable surface contamination was paramount. Surface contamination is usually as a result of the adsorption of adventitious

hydrocarbons, for example aerosols of vacuum pump oil typically present in an analytical laboratory. Even by the momentary exposure of a clean sample to the atmosphere it is possible to introduce such large C(1s) contamination peaks so as to mask the signal of interest. **Figure 3.6.**

In the experiments shown, any contamination present did not typically contain significant amounts of nitrogen and as a result the evaluation of SAM composition based on N(1s) spectra was less prone to error due to contamination. However, any variations due to such contamination could be adjusted for by normalisation of N(1s) counts using the S(2p) signal (see later). Of the SAMs studied, it proved impossible, to prepare homogeneous mercaptoethylamine SAMs containing low levels of carbon contamination. This was in contrast to SAMs prepared using mercaptopropanol, mercaptopropionic acid or mercaptopropane. This is discussed later and thought to be due to the large amount of charged nitrogen groups found in the monolayer.
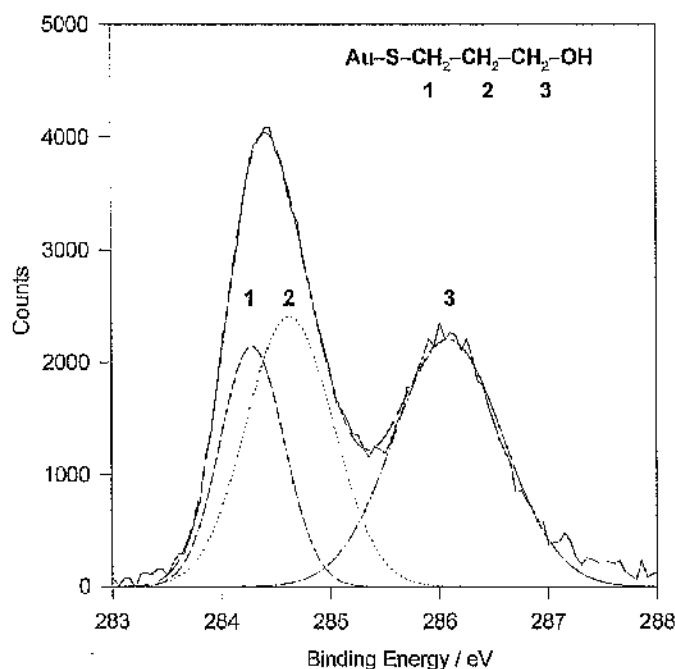
Figure 3.7 - C(1s) spectrum curve fit of a mercaptopropanol SAM, assembled on a gold substrate, fitted to the minimum number of Gaussian peaks. Numbered peaks refer to carbon centres as detailed in insert. (TOA 10°, Slit width 0.8mm and an AlKα source).

It is also important to note that oxygen is also present in contamination, and as the peaks due to contamination tend to appear at the same binding energy as those from oxygen in samples it, therefore, proved unreliable for use in analysis of the SAMs.

3.3.2 The XPS Measurement of Homogeneous SAMs.

3.3.2.1 Electronic Effects in the C(1s) Spectra.

Fitted spectra for the homogeneous SAMs of mercaptopropanol and mercaptoethylamine are shown in **Figures 3.7** and **3.8**.

Figure 3.8 - C(1s) spectrum curve fit of a mercaptoethylamine SAM, assembled on a gold substrate, fitted to the minimum number of Gaussian peaks. Numbered peaks refer to carbon centres as detailed in the insert. The large unnumbered peak represents a layer of physisorbed contamination. (TOA 10°, Slit width 0.8mm and an AlKα source).

Mercaptopropanol, is a liquid and was not, therefore, suitable for XPS measurements of the bulk phase. Measurements were, however, possible for thin films of mercaptoethylamine, **Figure 3.9**. The distinct shifts in binding energy of both the

50

carbon centres joined to the tail group(S-Au or S-H), and those bound to the head group (NH_2 or OH) are clearly seen. The electro-negativities of both the head group (oxygen or nitrogen) and that of the sulphur group, have a large influence on the binding energy of those electrons associated with the carbon centre adjacent to the sulphur group (indicated by 1 in **Figure 3.7**) causing a rise in the relevant C(1s) binding energy. However, when this sulphur group is bound to a gold surface there is also a significant electron donation effect from this electropositive surface, which has an effect which lowers the binding energy. Thus, whereas a general aliphatic carbon centre would have a binding energy of 285 eV, we can observe a negative shift for the carbon at position 1 (see **Figure 3.7**), as a direct result of the domination of the electron donating effect of the gold centre, over the electronegative effect of the head group.
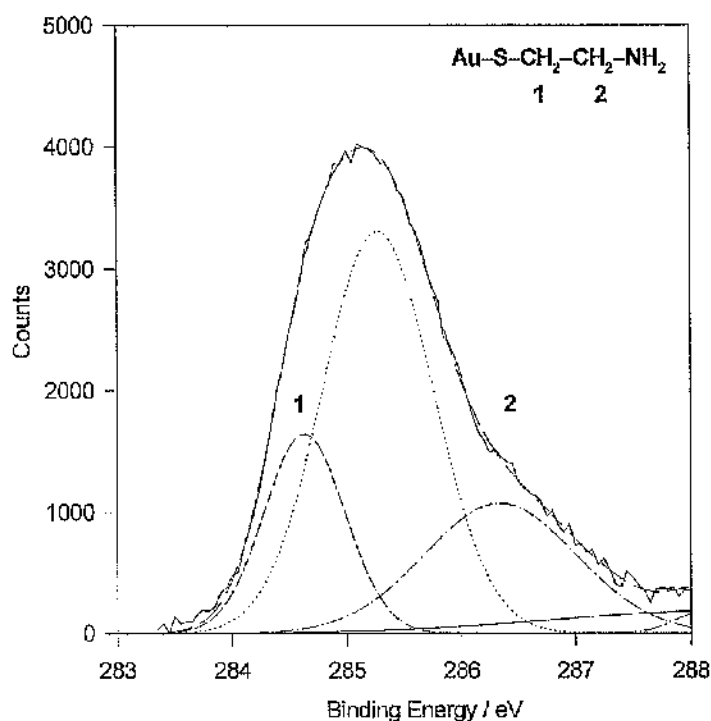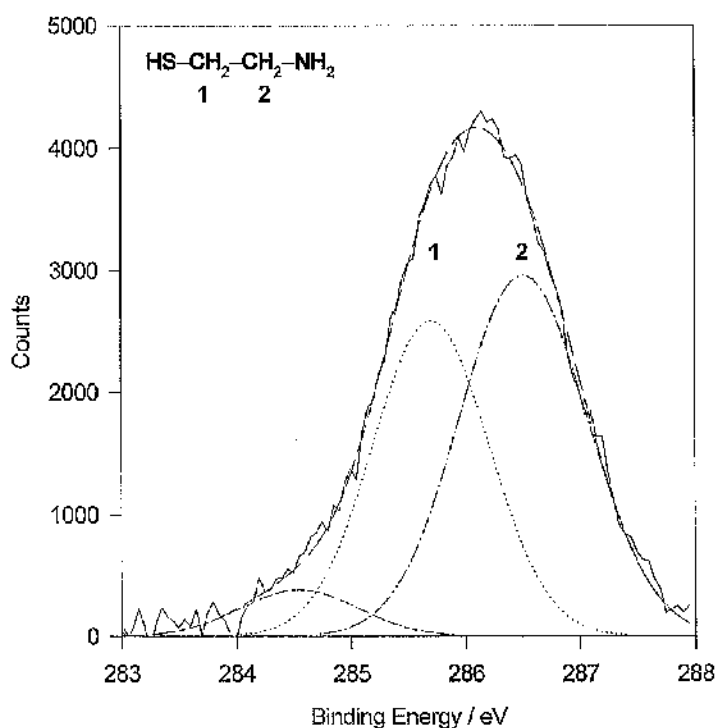

Figure 3.9 - C(1s) spectrum curve fit of a thin film of mercaptoethylamine, cast on a gold substrate, fitted to the minimum number of Gaussian peaks. Again, the numbered peaks refer to carbon centres as detailed in insert small unnumbered peak at 284.6 eV corresponds to chemisorbed mercaptoethylamine (Au-S). (TOA 10°, Slit width 0.8mm and an AlKα source).

51

By the comparison of the mercaptoethylamine C(1s) in **Figures 3.8** and **3.9**, a 1.1 eV reduction in peak position for the carbon at position 1 due to the electropositive Au is clearly seen. (*note:* the large peak in **Figure 3.8** seen at ca. 285.1 eV corresponds to contamination by adventitious carbon containing molecules discussed later). The small peak with low binding energy (ca. 284.6 eV) seen in **Figure 3.9** corresponds to gold bound mercaptoethylamine observed through 'thin' regions of the bulk film when a 90° TOA is used. As mentioned the proximity of the electronegative head group also has an effect on the position of the peak for the position 1 carbon. Oxygen is far more electron withdrawing in nature than nitrogen, and, because of the difference in chain length of the SAM's combined with the proximity of the head group to the carbon (position 1), the binding energy observed for mercaptoethylamine is 284.3 eV as opposed to 284.6 for mercaptopropanol **Table 3.1**.

Tail Group	Carbon no.			Head Group	C(1s) binding energy					
					dist. from tail group		dist. from head group			
	1	2	3		Carbon no. 1		Carbon no. 2		Carbon no. 3	
Au–S–CH$_2$–CH$_2$–CH$_2$–OH					284.3 eV		284.6 eV		286.1 eV	
					1.82 Å	4.49 Å	3.35 Å	2.96 Å	4.88 Å	1.43 Å
Au–S–CH$_2$–CH$_2$--------NH$_2$					284.6 eV		286.5 eV			
					1.82 Å	3.00 Å	3.35 Å	1.47 Å		
H–S–CH$_2$–CH$_2$--------NH$_2$					285.7 eV		286.5 eV			
					1.82 Å	3.00 Å	3.35 Å	1.47 Å		

Table 3.1 - C(1s) Binding energies for different carbon centres in homogeneous mercaptopropanol and mercaptoethylamine SAMs, as well as mercaptoethylamine thin films on gold. *NB:* 1. Peak positions were determined by deconvolution of spectra in **Figure 3.7** using Gaussian basis curves. 2. Estimates of distances between carbon centres and head/tail groups correspond to simple summation of the appropriate 'standard' bond lengths; i.e., no account is taken of the bond angles.

The 'electronic effects' on the carbon at position 1 are a consequence of the electropositivity of the gold surface. In the case of mercaptopropanol, the electronegativity of the head group also plays a significant role on those binding energies observed for the carbon at position 3. This results in a binding energy of 286.1 eV for that carbon (position 3) as opposed to ca. 285 eV for a general aliphatic carbon centre. This interplay, between the proximity of the headgroup and the electropositive character of the gold, is again seen when considering the carbon at position 2 in mercaptoethylamine. Here the result is a fractional lowering of the

headgroup adjacent carbon's binding energy (ca. -0.1 eV) than that observed in the bulk species see **Table 3.1**.

It is important to note that the half-widths observed for the C(1s) spectra can be seen to decrease with proximity to the sulphur centre - the carbon adjacent to sulphur group has a half width of ca. 0.7 eV, whilst that carbon closest to the head group is >1.0 eV, a fact which may be attributed to a reduced vibrational freedom. This change is also observed when comparing the half-widths of sulphur centres bonded to the gold surface with those which are physisorbed.

3.3.2.2 Homogeneous SAM N(1s) Spectra.

The influence of the electron donating gold surface on the distribution of photoelectron peaks is further manifested in a more significant lowering of the N(1s) binding energy in the SAM (399.1 eV) **Figure 3.10** from that found in the bulk (400.0 eV). The increase in electron density about the nitrogen group, through the anchoring of the molecule to gold surface implied by this measurement would also suggest an increased basicity of the SAM when compared with the same species in solution. This is also evidenced by the high binding energy shoulder frequently found in an N(1s) spectra collected from a mercaptoethylamine SAM, see **Figure 3.10**.
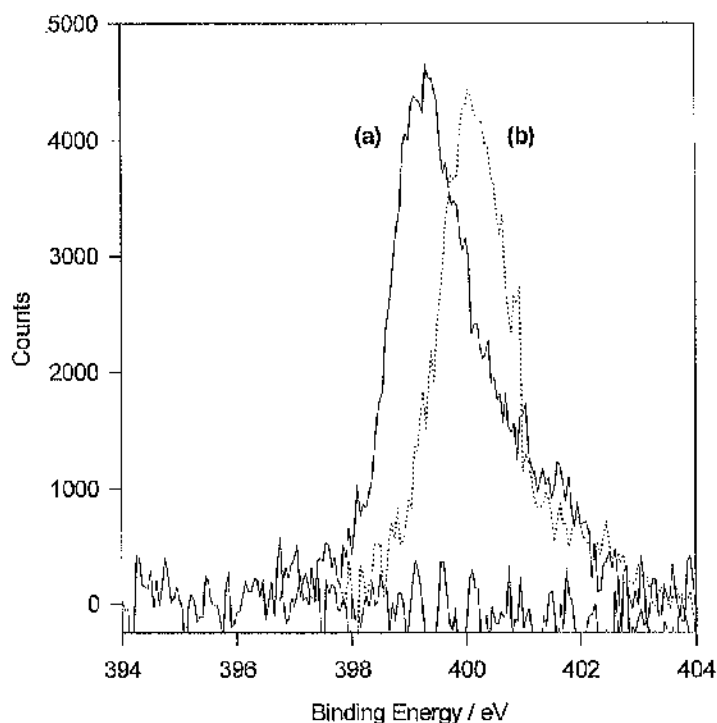
Figure 3.10 - N(1s) spectra for a mercatoethylamine/Au (a) SAM after immersion in a 1 mM mercaptopropanol solution for 90 mins together with a mercaptoethylamine thin film (b) cast on a gold substrate. (TOA 10°, Slit width 0.8mm and an AlKα source).

An N(1s) spectra would usually be expected to be Gaussian in shape, the broadening observed would suggest the presence of a number of nitrogen centres bearing positive charge, possibly as a consequence of this increased basicity. The increase in the number of charged centres is also often associated with a higher than average amount of surface contamination. This contamination is most evident in the C(1s) spectra, as shown in **Figure 3.8** where it can be observed as a peak at approximately 285.1 eV.

Figure 3.11 - N(1s) spectra for mercatoethylamine/Au SAMs after immersion in a 1 mM mercaptopropanol solution for varying periods of time (1, 10, 20, and 90 min, a-d), together with a mercaptopropanol/Au SAM which has been left in RO water for 50 min (e) (TOA 10°, Slit width 0.8mm and an AlKα source).

3.3.3 Evaluation of the Composition of Mixed SAMs.

3.3.3.1 Composition Based on the N(1s) Spectra.

The N(1s) spectra of mercaptoethylamine monolayers, following immersion in mercaptopropanol for increasing periods of time, as well as the N(1s) spectra of a mercaptopropanol monolayer left soaking in RO water for an extended period of time, are both shown in **Figure 3.11**. The absence of contamination with nitrogen containing species, is clearly illustrated by the lack of any N(1s) signal in the mercaptopropanol spectra **Figure 3.11e**. The spectra suggests that immersion in mercaptopropanol solution leads to a loss of nitrogen groups from the surface of the SAM. This loss is not observed when a mercaptoethylamine SAM is incubated in RO water for a similar period of time.
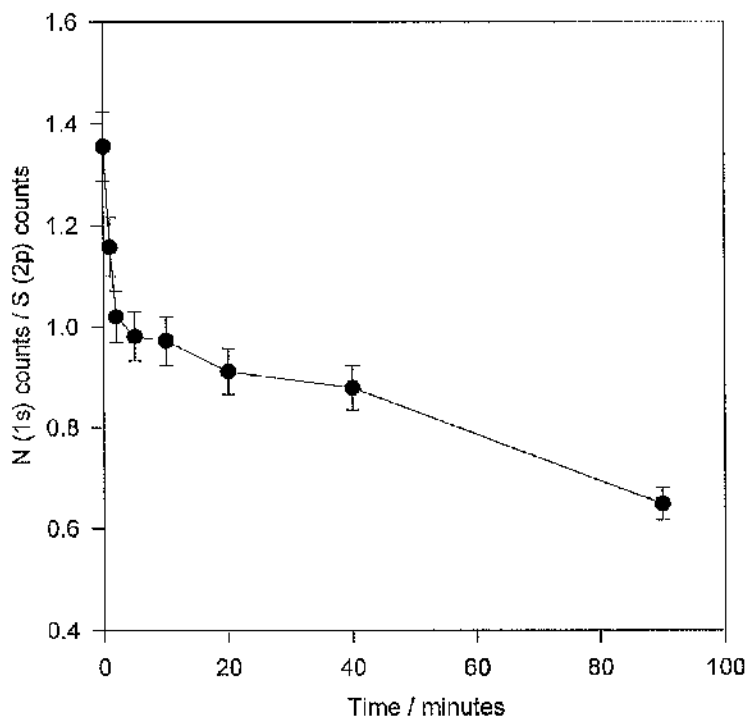
Figure 3.12 - Ratio of N(1s) to S(2p) photoelectron counts for mercaptoethylamine/Au SAMs after different lengths of time immersed in a 1 mM mercaptopropanol solution. Error bars estimated from variations in fitting the underlying baseline to the N(1s) and S(2p) spectra. (TOA 10°, Slit width 0.8mm and an AlKα source).

Figure 3.12 shows the time course for the nitrogen group displacement by mercaptopropanol. The difference in the nitrogen functionalities present over time is shown as a change in the ratio of N(1s) photoelectrons with respect to those originating from S(2p) centres which correspond to those in the SAM tail. Normalisation in this manner corrects for small variations in SAM surface coverage, surface contamination and instrumental parameters (e.g. TOA and X-ray flux). The ratio of N(1s) to S(2p) photoelectrons, in a homogeneous mercaptoethylamine SAM illustrates the attenuation of photoelectron intensity with film thickness. This ratio, measured to be ~1.36, which when bulk sensitivity factors (1.73 and 2.08, respectively) are used to calculate elemental composition gives a N:S atomic ratio of 1.6:1 (rather than 1:1 as would be expected from the chemical composition).

With the breaking of the aliphatic backbone chain highly unlikely, this 'high' N:S ratio therefore confirms, in the absence of N containing contamination, that the interfaces under study are ordered with the S group further from the outer interface than is the N group. The N:S ratio does however more closely approach 1:1 when examining highly contaminated samples which, through poor rinsing, participate in strong electrostatic interactions with solution molecules, leading to additional physisorbed layers. This reduced N:S ratio, judged by multiple values of S(2p) binding energies which reflect a more random orientation of molecules in the interface, correlates with a significant amount of physisorbed thiol on top of the underlying SAM.

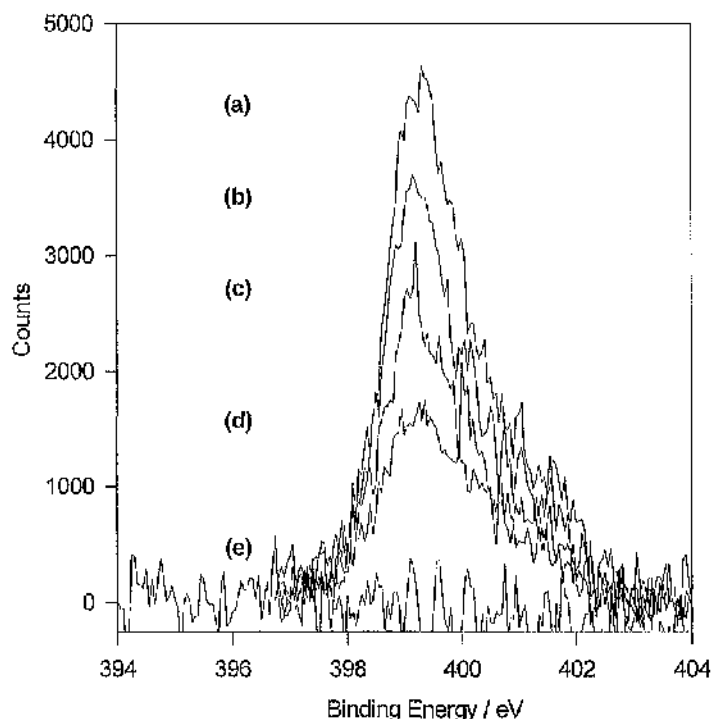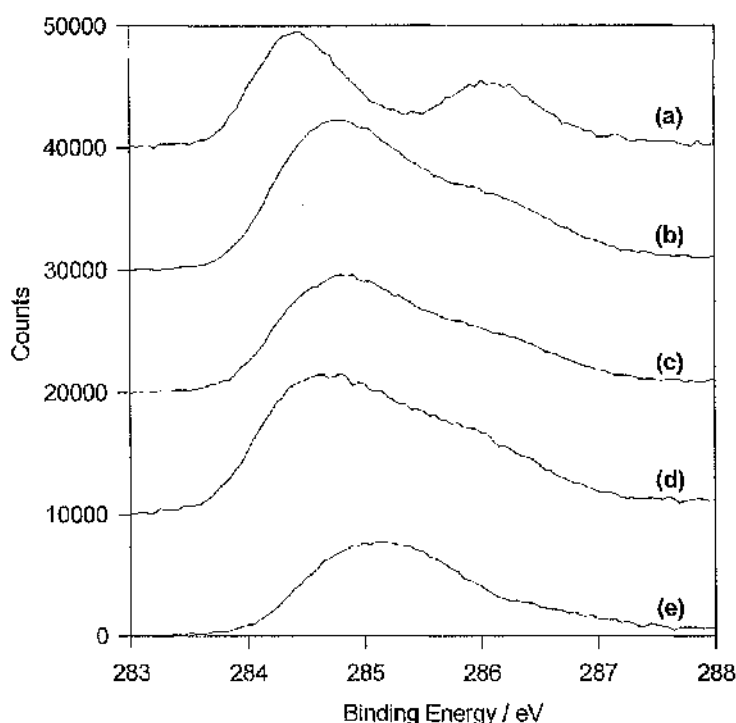**Figure 3.13** - Evolution of C(1s) spectra for mercaptoethylamine/Au SAMs on immersion in 1 mM mercaptopropanol solution for varying periods of time (b, 2 min; c, 20 min; d, 90 min), together with the C(1s) spectra for homogeneuos mercaptoethylamine/Au (a) and mercaptopropanol/Au (e) SAMs (TOA 10°, Slit width 0.8mm and an AlKα source). The spectra are offset horizontally for purposes of clarity.

3.3.3.2 Composition Based on the C(1s) Spectra.

Although clearly demonstrating a loss of nitrogen functionality in the SAM, the analysis of N(1s):S(2p) ratio of photoelectrons does not indicate if this loss is as a result of the adsorption of mercaptopropanol, with the concurrent loss of mercaptoethylamine. However, by comparing the C(1s) spectra of variously prepared SAMs **Figure 3.13**, a change in the line shape of the spectra indicates a progression of pure mercaptoethylamine to one containing a significant mercaptopropanol proportion.

Whilst the deconvolution of these C(1s) spectra by the use of combinations of Gaussian peaks derived from the homogeneous SAMs, half-widths, positions and relative heights constrained to those found in the homogeneous SAMs, is possible, the large number of parameters, requires very complex fitting techniques. An alternative, used with success in previous studies[145], involves combinations of library spectra for the two component SAMs in a spectral decomposition process. By using combinations of these library spectra in an unconstrained manner, it was possible to produce a set of degenerate solutions if an additional component, a spectrum due to surface contamination, was included. When the fit was performed in an unconstrained manner, the component corresponding to surface contamination was abnormally large in comparison to data from our previous studies. By using the size of the N(1s) signal for each monolayer we applied a constraint to the proportions of the SAM library spectra.

The deconvolution process for the C(1s) spectra **Figure 3.14**, therefore, followed the following steps.

1. A difference spectrum was created by subtracting a library mercaptoethylamine SAM spectrum from the mixed monolayer spectrum. This spectrum had been proportioned according to the magnitude of the N(1s) signal in the mixed monolayer.

2. This difference spectrum was then fitted using a mercaptopropanol SAM C(1s) library spectrum such that the residual (contamination) spectra contained minimal intensity between 286-287 and 283 - 284.5eV.

3. The residual spectrum corresponded, therefore, to a Gaussian peak centred on 285eV.

Mercaptoethylamine library spectra were used from two sources, either the 'as measured' spectrum **Figure 3.8**, or a spectrum synthesised from the curve fitting of those spectra in **Figure 3.8** such that the spectra contained no component resulting from contamination. In either case the quantification of SAM compositions were generally within 5%. The results presented in **Figures 3.14** and **3.15** show those obtained by use of the synthetically derived mercaptoethylamine spectrum. This deconvolution method relies on the low level of nitrogen present in any surface contamination introduced by experimental procedure (as shown in **Figure 3.11e**).

The comparison of **Figures 3.12** and **3.15** show that both methods of XPS analysis give similar estimates of SAM composition. However, the requirement to use a mercaptopropanol spectrum in calculating the data of **Figure 3.15** supports the assertion that a mixed mercaptopropanol/mercaptoethylamine SAM is being formed.
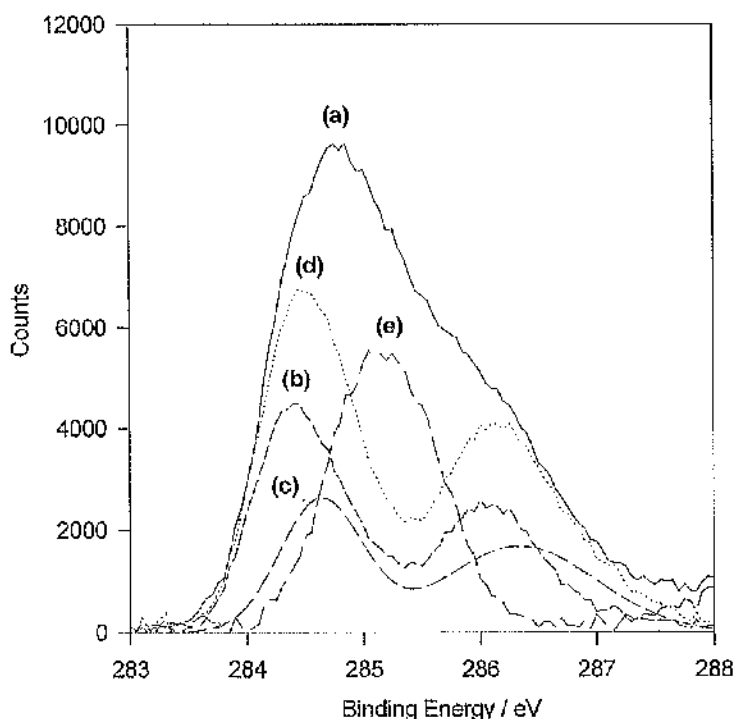
Figure 3.14 - Spectral decomposition of mercaptoethylamine/Au SAM which has been immersed in a 1mM mercaptopropanol solution for 5 min. Curve (a) corresponds to the measured spectrum. The component spectra corresponding to proportioned library spectra are as follows: mercaptopropanol/Au (b) and mercaptoethylamine/Au (c) (derived from the peak fitting of figure 1b). The composite spectrum is labelled (d) with the residual spectrum labelled (e). (TOA 10°, Slit width 0.8mm and an AlKα source).

The physisorption rather than chemisorption of either of the SAM components would contradict this assumption. However, it should be noted that the S(2p) signals for all of these monolayers suggest that >95% of the sulphur species are bound to Au. This is indicated by binding energies ~162 eV (Au-S) as opposed to ~163 eV as would be expected for physisorbed species. This lack of physisorbed species is in contrast to observations by others, for carboxylate terminated or other very polar SAMs[146].
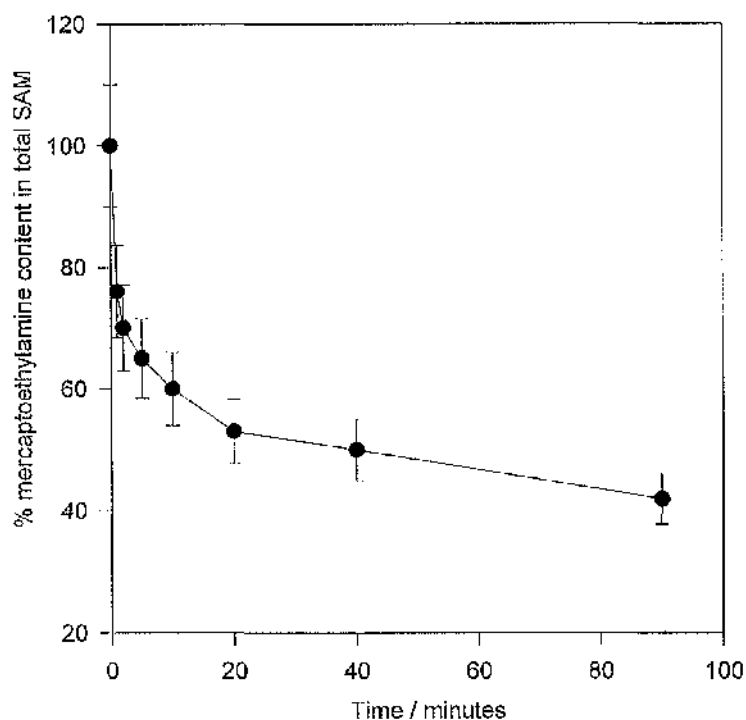
Figure 3.15. The percentage of mercaptoethylamine remaining in mercaptoethylamine/Au SAMs after their immersion in 1mM mercaptopropanol for varying periods of time as evaluated by spectral decomposition of C(1s) spectra. (TOA 10°, Slit width 0.8mm and an AlKα source).

3.3.4 Reaction Mechanism for the Formation of Mixed SAMs.

In was noted that the S(2p) binding energy in mercaptopropanol monolayers was 0.1 eV lower (162.0 eV) than that observed for mercaptoethylamine SAMs. These values compare with the 161.3 eV binding energy our group has measured for Na_2S derived SAMs and 163 eV for physisorbed species. This higher S(2p) binding energy, observed in mercaptoethylamine, suggests that the outer S(3s) and S(3p) electron densities are further from the sulphur centre as a consequence of the combined electron-withdrawing and -donating effects of atoms bonded to the sulphur.

This observation is important when considering a mechanistic explanation for the displacement of a mercaptoethylamine SAM by mercaptopropanol, particularly when

61

combined with observations of the C(1s) binding energy. The binding energies of the tail group C(1s) electrons in a mercaptoethylamine SAM are seen to possess higher binding energies than those observed for mercaptopropanol, indicating that the electrons in the Au-S bond are centred closer the Au than to the S. This suggests, possibly, that the Au-S bond is longer and consequently weaker than the Au-S bond in the mercaptopropanol monolayer. An indication that the change of composition of the SAM is not by an initial dissociative step comes from our observations that the N(1s) signal does not diminish appreciatively on immersion of the mercaptoethylamine monolayer in (thiol free) water of various pHs, for similar extended periods of time.

Thus, a possible mechanism would involve a transition state in which a disulphide bond exists between the solution species and the thiol in the SAM. The dissociation of this transition state would then lead to a SAM composed of thiol species with the stronger Au-S bond; i.e. in this case a mercaptopropanol SAM. Recent work by others suggests that a SAMs composed of mercaptopropanol enjoy significant stabilisation as a result of their capability to form hydrogen bonds when assembled as a monolayer between their head groups[147], an ability that mercaptoethylamine does not share to the same extent. Further investigation of this mechanism would require examination of far infrared reflectance ($\sim$200cm^{-1}), or Raman, spectra in the region corresponding to Au-S vibrations.

In summary, the XPS measurements on mercaptoethylamine SAMs immersed in mercaptopropanol solutions indicate that by using readily manageable solution concentrations (millimolar) and immersion times (minutes) it is possible to control the proportions of these two species in the resultant mixed SAM. Since prolonged immersion leads to larger levels of contamination (predominately C containing), hampering the deconvolution of C(1s) spectra and obscuring N(1s) signals, it is not possible to state if the level of mercaptoethylamine still present in the SAM after 90 minutes represents an equilibrium or a kinetic state. Confidence in the determination of the fractional mercaptoethylamine or mercaptopropanol content in the SAMs comes from the similarity of the results obtained for both C(1s) deconvolution and

the N(1s) quantification. **Figures 3.12** and **3.15**. A final point to note is the absence of an increase in the high binding energy region of the C(1s) spectra for the treated mercaptoethylamine SAMs, indicating that the nitrogen functionality has not been lost by oxidation to a carboxylate species.

3.4 Conclusion

We have shown that the degree of head group functionality in a SAM on gold can be altered in a time dependant fashion by displacement of an initial alkanethiol by a second thiol containing an alternative head group. Such control over the head group composition of a SAM on gold, should in turn, enable a degree of regulation of biomolecular recognition at biosensor interfaces. The use of short chain molecules has the potential of allowing molecular control without a concurrent loss of sensitivity due to the introduction of a long chained, highly ordered, insulating SAM. Indeed the use of mercaptopropanol as a surface modifier, led to a noticeable decrease in physisorbed contamination, and could be used as an anti-fouling layer on metal electrode surfaces.

CHAPTER 4: USE OF SELF–ASSEMBLED MONOLAYERS TO CONTROL PROTEIN RECOGNITION AT METAL SURFACES

4.1 Introduction

The use of self-assembled alkanethiol monolayers on gold has received much attention as a means of manipulating the molecular architecture of a sensing surface[32,137,138]. Such control is of vital importance in the fabrication of biosensors and other bioelectronic devices, where providing the optimal environment for the sensing enzyme to function is paramount[4,5,67,135,136]. Using X-ray Photoelectron Spectroscopy (XPS)[115] studies, we have shown previously in chapter 3, that by the immersion of a primary alkanethiol layer on gold in a secondary modifying thiol, it is possible to manipulate the molecular composition of a thiol SAM on gold. In this chapter we demonstrate how simple control of alkanethiol composition can be used to manipulate molecular recognition at that gold surface.

The electrochemistry of metalloproteins is a subject of great interest[136], and work in this area[39,148-153] is of importance in shaping our understanding of electron transfer between biological molecules and electrode surfaces. Initially, therefore, we used the electrochemistry of horse heart cytochrome c to probe the monolayer composition, providing further evidence of the mechanism of alkanethiol displacement by the use of a wider variety of thiols than that discussed in the previous chapter. In doing so, we also demonstrate the ability to manipulate the interaction of redox metalloproteins with sensing surfaces.

In a second area of study, within this chapter, we demonstrate the ability of thiol monolayers to diminish the non-specific binding of proteins to surfaces an issue of importance for all devices contacting biological samples, offering an alternative to some traditional methods[154-157].

65

4.2 Experimental Section

4.2.1 Materials
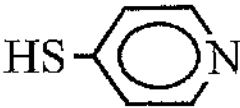
$$HS - CH_2 - CH_2 - CH_2 - OH \qquad \text{Mercaptopropanol}$$

$$HS - CH_2 - CH_2 - NH_3^+ \qquad \text{Mercaptoethylamine}$$

$$HS - CH_2 - CH_2 - CH_3 \qquad \text{Mercaptopropane}$$

$$HS - \bigcirc N \qquad \text{Mercaptopyridine}$$

Figure 4.1 - Structure of the thiols used in the experiments described.

Unless otherwise stated, the thiols (**Figure 4.1**) and all other chemicals and solvents used were purchased from Sigma (Poole UK) and used without any further purification. All solutions were made using reverse osmosis (RO) ultrapure water (Millipore, UK). Lyophilised horse heart cytochrome c (Sigma type IV) was reconstituted in 20 mM phosphate buffer pH 7 (containing 100 mM sodium perchlorate as the supporting electrolyte) and stored until required at -20°C in individual 100 μL, 14 mM aliquots. When required an aliquot of cytochrome c was diluted to the appropriate concentration (0.7 mM) by the addition of phosphate buffer and electrolyte (as described above). Bovine serum albumin BSA (Sigma,UK) at 5 μg/ml was made up from its lyophilised form, again immediately prior to use in PBS (pH 7.4).

66

Gold electrodes (diameter = 2 mm) were either fabricated as a Ti/Pd/Au (10/10/100 nm) multi-layer structure using standard photolithographic procedure, described below, or supplied as polycrystalline gold electrodes by BioAnalytical Systems (Luton, UK). The materials used to fabricate electrodes, titanium (Ti), palladium (Pd) and gold (Au) were purchased, from Goodfellows (Cambridge, UK). In addition, a Ag|AgCl reference electrode (MF-2063) was also obtained from BioAnalytical Systems (Luton, UK).

4.2.2 Microfabrication of Electrodes

4.2.2.1 Substrate Cleaning

Glass substrates were cleaned, prior to photolithography and electron beam evaporation, by sonication for 5 minutes in each of the following cleaning agents: Opticlear™ (G&S Inc.); acetone; methanol; and finally reverse osmosis (RO) water. The samples were dried in a stream of nitrogen, and then baked for 10 minutes at 50°C, in order to ensure removal of any remaining residual water.
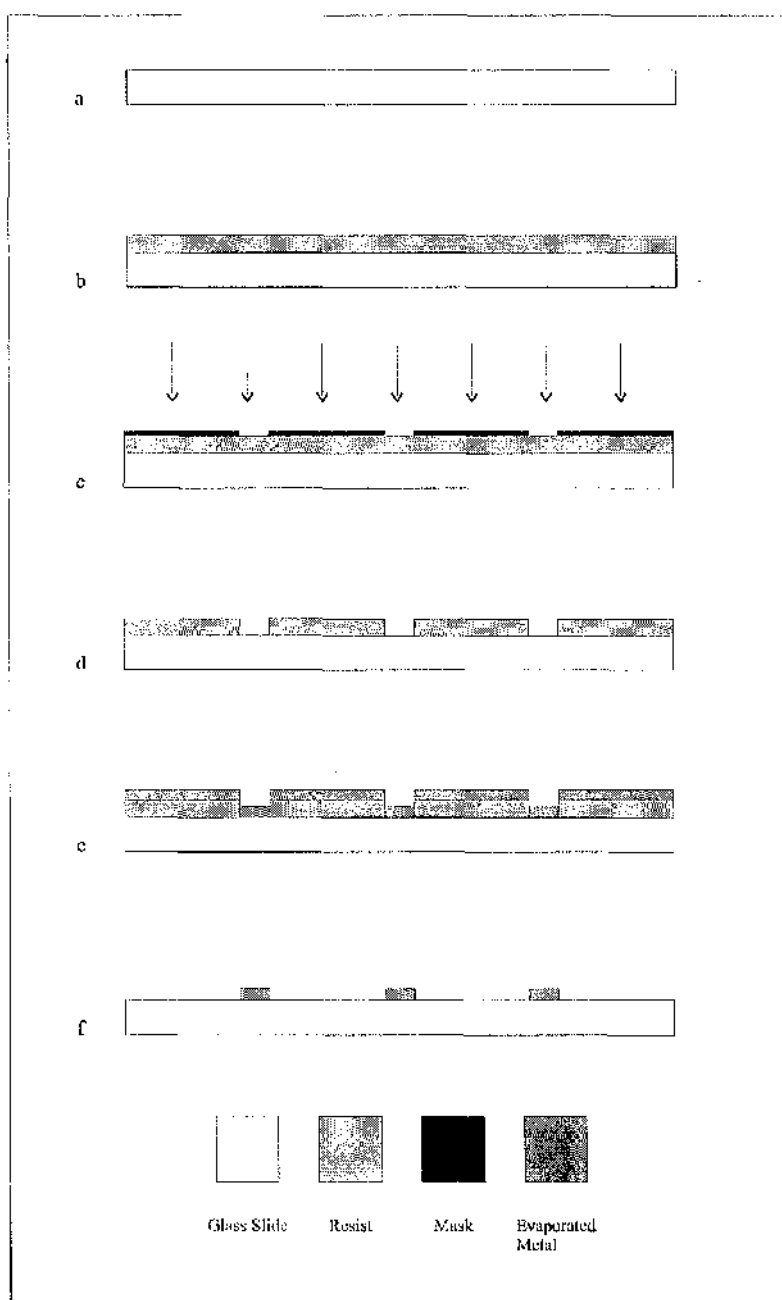
Figure 4.2 - Gold electrodes were prepared by photolithography followed by electron-beam evaporation of a Ti/Pd/Au (10/10/100 nm) multi-layer structure. A clean glass substrate **A** was coated by a 1.8 μm layer of S1818 resist (Shipley, UK) by spinning for 30 seconds at 4000 rpm, **B**. The required electrode pattern was transferred to the resist, by UV exposure through a ferric oxide mask (14 seconds, Hybrid Technology mask aligner, 32J cm^{-2}, 364nm), **C**. After development for approximately 80 seconds in Microposit developer (1:1 mix with RO water) **D**, the multilayer metal structure was deposited by e-beam evaporation using a Plasyss QD1 automated e-beam evaporation system **E**, 'lift-off' was performed by dissolving the resist in acetone the metal remaining defined the electrodes **F**.

4.2.2.2 Photolithography

In order to produce photographically defined, 2mm diameter electrodes, cleaned glass samples were spin-coated (at 4000 rpm) with S1818 resist (Shipley Inc.), which had been pre-filtered using a 0.25μm particle filter. In order to define metallic electrodes with clean, sharp edges, after fifteen minutes baking time at 90°C, the samples where soaked for 10 minutes in chlorobenzene, prior to a further fifteen minutes bake, also at 90°C. Patterning of the photoresist was achieved by UV exposure through a purpose made ferric oxide photomask, for 14s on a Hybrid Technology mask aligner, (photon flux = 32J cm^{-2}, λ = 364nm). The pattern was developed by the immersion of the sample, for approximately 80 seconds, in Microposit developer (Shipley Inc.) mixed 1:1 with RO water. Samples were finally dried in a stream of nitrogen and then baked for 10 minutes at 50°C to remove any residual water.

4.2.2.3 Metal Evaporation and Lift-off

Metals were deposited on clean slides and those which had been photolithographically modified by electron beam evaporation (Plassys QD1 automated e-beam evaporation system), as a Ti/Pd/Au (10:10:100nm) multi-layer structure. This well established recipe provides excellent adhesion of the electrode to the underlying substrate and gives good electrochemical stability at high oxidative potentials. A 30 nm layer of nickel - chromium (60:40) (NiChrome) was also evaporated on to the electrode structure, which could be removed by etching with a standard nichrome etch (3.5 ml glacial acetic acid and 20 g ammonium ceric nitrate dissolved in 100 ml of RO water). This final evaporated layer served as a sacrificial protective coating and enabled electrodes to be produced which were "clean" (i.e. free from particulate contamination). Following electron beam evaporation of metals, the electrode patterning was finally achieved by the 'lift-off' of the remaining photoresist by incubation in acetone the electrode pattern had been clearly developed. Finally it was necessary to take the sample from the 'lift-off' solution whilst under a flow of RO water, in order to ensure that none of the metal particles re-adhere to the sample. See **Figure 4.2** for a diagramatic representation of this process.

4.2.3 Cleaning of electrodes.

4.2.3.1 Polycrystalline Gold Disk Working Electrodes.

Polycrystalline gold working electrodes (BioAnalytical Systems Inc.) were cleaned by polishing with a 0.3 μm alumina slurry, sonication in reverse osmosis (RO) water for 15 minutes, and then treatment for two minutes in a solution of freshly prepared 1:4 piranha solution (30% H_2O_2 : 98% H_2SO_4) prior to a final rinse with RO water.

4.2.3.2 Electron Beam Evaporated Gold Substrates

Immediately prior to deposition of the thiol monolayer, the gold surface was cleaned either:

1. by a reactive ion etch for 5 minutes (50 mT, 20 sccm, and 10 W) first in an oxygen plasma and then in an argon plasma using a PlasmaFab ET340; or

2. by cyclic voltammetry in a 0.1 mM H_2SO_4 solution (containing), 0 - 1.8 V, scan rate 50 mVs^{-1}. **Figure 4.3.**

4.2.4 Experimental Set-Up For Electrochemical Measurements

All electrochemical responses of electrodes were recorded using a low current potentiostat (BAS CV-37, Stockport, UK) with data collected using an 'in-house' data acquisition system comprising a PC30AT multi-function analogue and digital input/output Amplicon board (Brighton, UK), installed in an IBM compatible personal computer. Experiments were performed in an all-glass cell which had a working volume of 1.0 ml. The cell incorporated a conventional three electrode configuration[109] accommodating, either a 2mm diameter polycrystalline or electron-beam evaporated gold working electrode, a fixed counter electrode of platinum wire and a Ag|AgCl reference (3.0 M NaCl, 190 mV vs. NHE). Cyclic voltammetry was performed between -200 mV and +200 mV at scan rates (v) of between 5-100 mV s^{-1} in a solution of 700 μM horse heart cytochrome c (Sigma type

70

VI) (supporting electrolyte 20mM sodium phosphate, pH 7.4, plus 100mM sodium perchlorate) at a temperature of 22 ± 2 °C.

4.2.5 Formation of Mixed Monolayers.

After cleaning, the gold surface was immediately immersed in a 1 mM solution of an initial thiol modifier (i.e. 1 mM mercaptoethylamine) for 2 hours and then thoroughly rinsed using RO water. Mixed monolayers were subsequently prepared by drying the surface in a stream of nitrogen and then immersing them in a second thiol solution (i.e. 1 mM mercaptopropanol) for between 10s and 180 min, before rinsing.

4.2.6 FT-iR Analysis of Non-Specific Protein Binding to SAMs on Gold.

Prior to FT-iR analysis, electron beam evaporated gold substrates were prepared and modified by various methods **Table 4.1**. Each method was composed of the following sequential steps;

1. Reactive-ion etching of evaporated gold substrates for 5 minutes (50 mT, 20 sccm, and 10 W) first in an oxygen plasma and then in an argon plasma using a PlasmaFab ET340 (cleaning step).
2. SAM formation, as described previously, followed by RO water wash.
3. Protein adsorption step: substrate immersed in a solution of 5 μg ml^{-1} BSA in PBS (with or without 0.5% Tween 60 detergent).
4. Excess protein removed by thorough rinsing with PBS.

FT-iR spectra were collected using a Bomen MB-120 spectrometer with a mercury cadmium telluride (MCT) detector, running Bomen GRAMS/32 software (Gallactic Industries Corporation). The analysis by FT-iR was performed in a grazing-angle reflectance mode (IRAS) using p-polarised light at an incident angle of 80°, with spectra recorded at 4 cm^{-1} resolution and an iris aperture of 8 mm. Nitrogen purging

71

was maintained throughout the experiments to flush the atmosphere of water molecules which produce strong absorption bands at 3300 cm^{-1} and 1600 cm^{-1}.

SAM formed	Protein Adsorbtion
none	None
none	5 μg ml^{-1} BSA
none	0.5% Tween 60
none	5 μg ml^{-1} BSA and 0.5% Tween 60
MPOH	None
MNH$_2$	None
MPOH	5 μg ml^{-1} BSA
MNH$_2$	5 μg ml^{-1} BSA
MPOH	5 μg ml^{-1} BSA and 0.5% Tween 60
MNH$_2$	5 μg ml^{-1} BSA and 0.5% Tween 60

Table 4.1 - The various treatments to RIE cleaned evaporated gold samples. Note the following abbreviations: MPOH - mercaptopropanol, MNH$_2$ - mercaptoethylamine, BSA - bovine serum albumin.

A reference spectrum from a RIE cleaned gold sample was collected for each sample to minimise the possible errors from contaminant (particularly water) adsorption. The data was recorded as transmission spectra and converted into absorbence data prior to analysis using the relationship described by **Equation 4.1**.

$$\%abs = -\log (trans/100) \qquad\qquad \textbf{Equation 4.1}$$

4.3 Results and Discussion.

4.3.1 Electrode Cleaning by Acid Cycling.
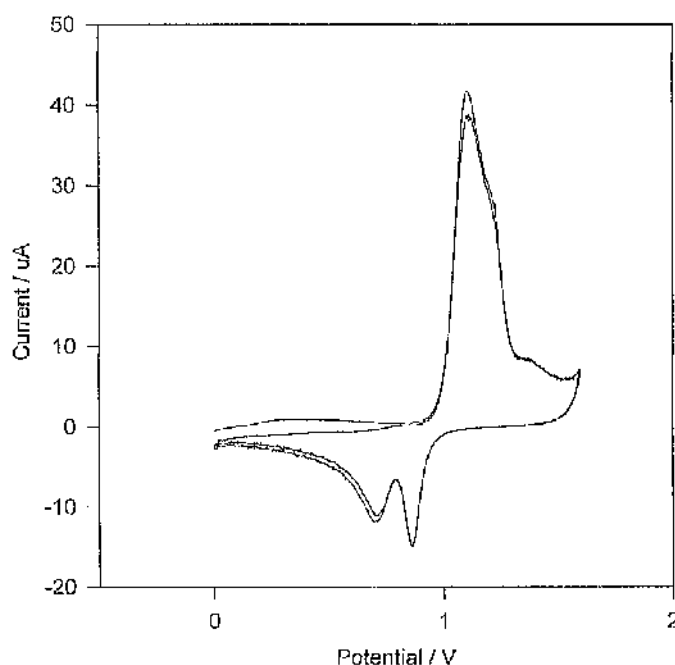
Figure 4.3 - Cleaning of evaporated gold disc electrodes (2mm diameter, 100 nm thick) by the potential cycling in 0.1 mM H_2SO_4 solution (containing 5 mM NaCl) at a scan rate of 50 mVs^{-1}.

Surface cleaning, prior to modification is a crucial factor particularly when using SAMs where even a small degree of contamination can have significant effects on the electrochemical characteristics of that interface[158]. The experiments described above, whilst performed on macro scale electrodes, are of particular interest with regard to their application within microsensors. These sensors are commonly fabricated by photolithography, and are not suitable for cleaning by alumina polishing as described for macro electrode, due to the thin (10 - 100 nm) planar nature of the evaporated gold surfaces. Consequently, two alternative cleaning methods were used involving either potential cycling in acid[159,160] **Figure 4.3** or plasma cleaning[161], when using electron-beam evaporated gold substrates. Although both methods gave satisfactory cleaning results (as evidenced by

"acceptable" cytochrome c electrochemistry), potential cycling is established as a method where the microscopic roughness of the gold surface is increased[160]. As a result, the surface area of the electrode is also increased[162], leading to increased peak anodic currents observed when performing cyclic voltammetry. It is, therefore, important, when comparing data recorded at electrodes cleaned in this manner, to ensure that each electrode has been cleaned in the same manner, an equal number of times. Despite this disadvantage, acid cycling is easier (and cheaper), to perform than plasma etching, and is desirable where such facilities are not readily available.

4.3.2 Electrochemistry of Cytochrome c at Mixed Monolayers.

The electrochemistry of redox proteins such as cytochrome c has been extensively researched for a number of years[39,50,57,148-153,163]. In this context, the distance dependence on the rate of electron transfer between the redox centre and the electrode have been described[164,165], and the experimental evidence suggests, that the probability of charge transfer decreases exponentially as the distance increases, such that:

$$K = K_0 \exp (-\beta [r - r_0])$$
Equation 4.2

Where K is the electronic transmission coefficient, K_0 its value when the separation is r_0, r is the distance between the centres, and β is a constant (experimentally estimated to be 12 nm^{-1}). This would imply that for every 0.2 nm increase in distance between the electrode and the protein redox centre, the magnitude of the electronic transmission coefficient decreases by an order of magnitude. This is of particular importance when considering the asymmetric redox protein cytochrome c.
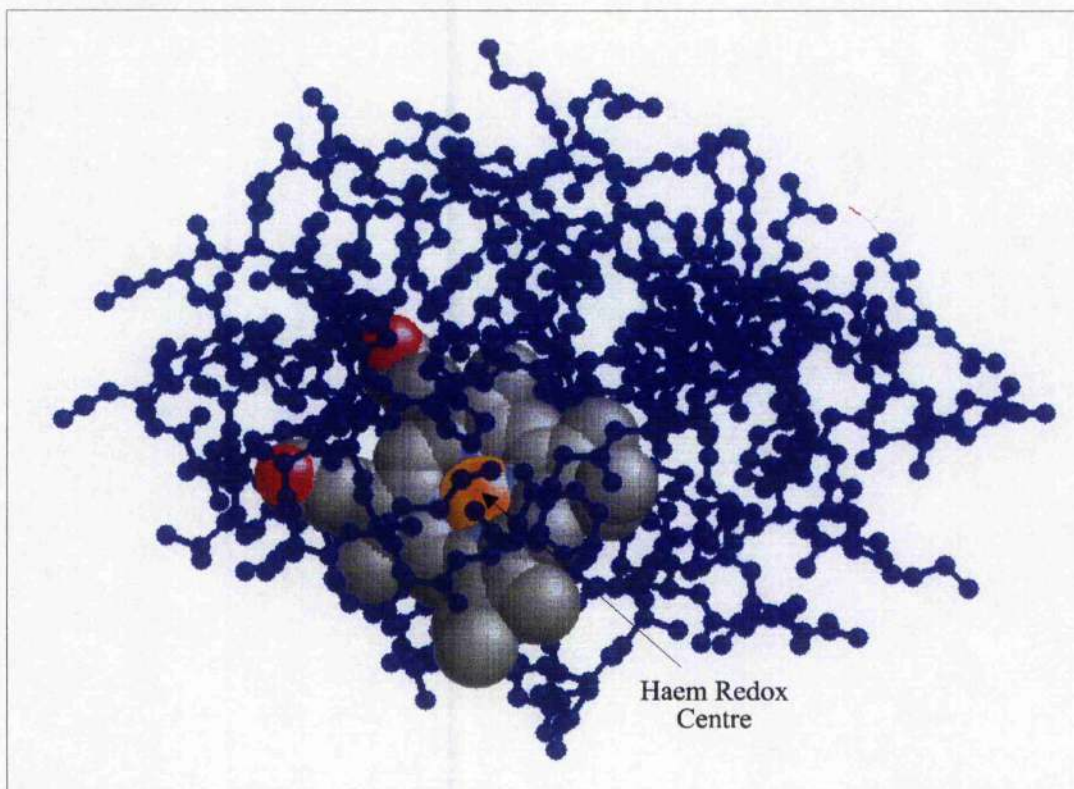
Haem Redox
Centre

Figure 4.4 - The asymmetric protein cytochrome, showing the heame redox centre. For fast electron transfer to occur, it is important that the redox centre is aligned close to the electrode surface, as possible.

Cytochrome c **Figure 4.4** is approximately 3.4 nm in diameter and the haem redox centre is located near to the periphery[136]. There are, therefore, a number of orientations that the redox protein can present to the electrode for an electron transfer event, each with a different distance over which electron transfer can occur and therefore with different probabilities of a transfer event occurring as shown schematically in **Figure 4.5**.

Also illustrated (in **Figure 4.5b and 4.5c**) is the complimentary effect that thiol length might be expected to have on electron transfer. In this case the thiol serves to distance the redox protein from the electrode surface and the rate of electron transfer will, therefore, depend upon the length of the thiol used. The primary motivation in our choice of short chain modifying thiols is a consequence of this effect on the rate of electron transfer, for example the difference in chain length between a $C_{10 \text{ and }}$ a C_4

molecule is approximately 1.0nm whereas the difference in the relative rates of electron transfer (k(rel)) is approximately 10^4.
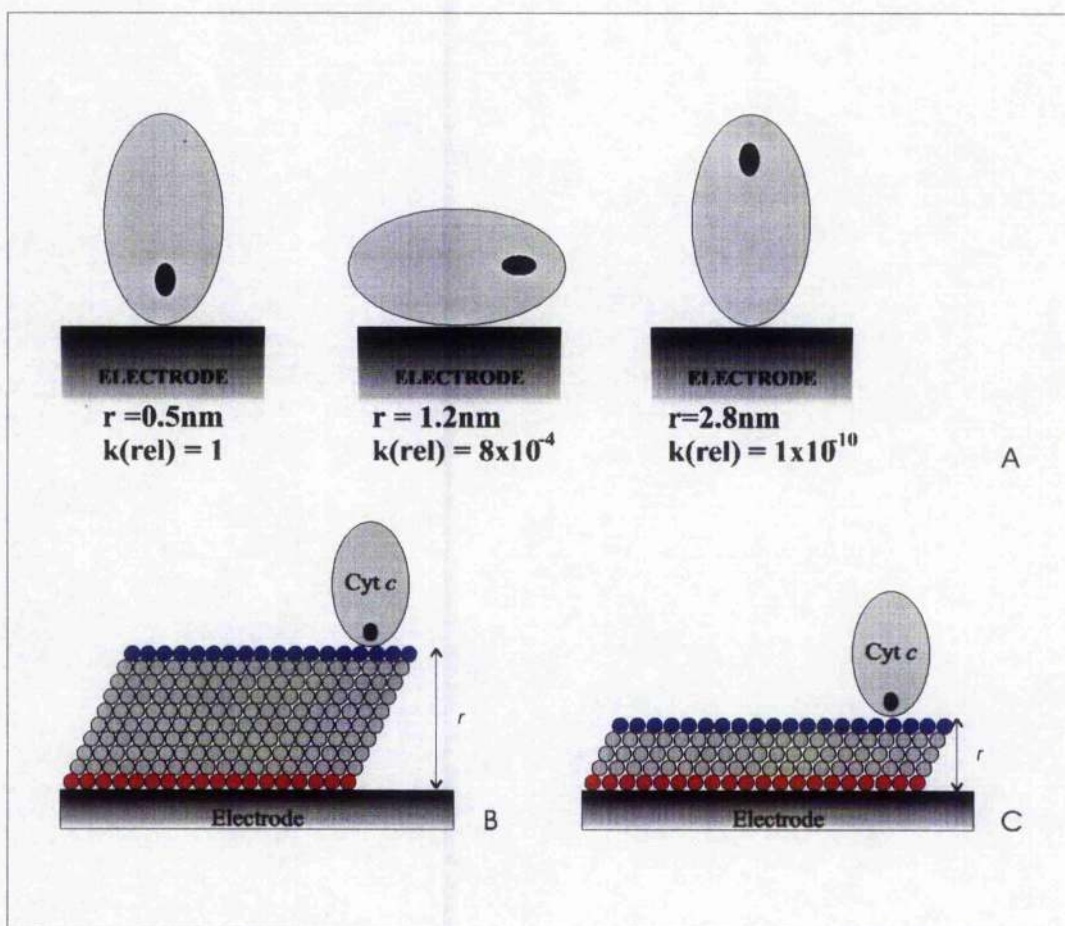
Figure 4.5 - The rate of electron transfer occurring between a protein and an electrode surface is dependant upon the distance that the electron transfer centre of the protein is from the electrode surface. The asymmetric protein Cytochrome*c* , can be seen to have several possible orientations for electron transfer, with markedly different rates of electron transfer.

Generally the rate of electron transfer between an electrode and metaloproteins is extremely slow. This can be explained using the mechanism of electron transfer between cytochrome c and an electrode proposed by Albery et al. whereby an adsorption event takes place at the electrode surface before the electron transfer event itself can occur[149]. It is suggested that in order to overcome the substantial activation energy for the electron transfer step, a considerable binding energy for the proceeding adsorption step is essential. In the case where an electrode is either

76

unmodified or modified with a poor bioelectrochemical promoter, then the binding energy is low and electron transfer less probable than when the electrode is modified with a promoter which encourages electrostatic binding.

Electron transfer therefore depends upon the ability of the modifying ad-layer not only to orientate the protein correctly, but also to promote a high binding energy.
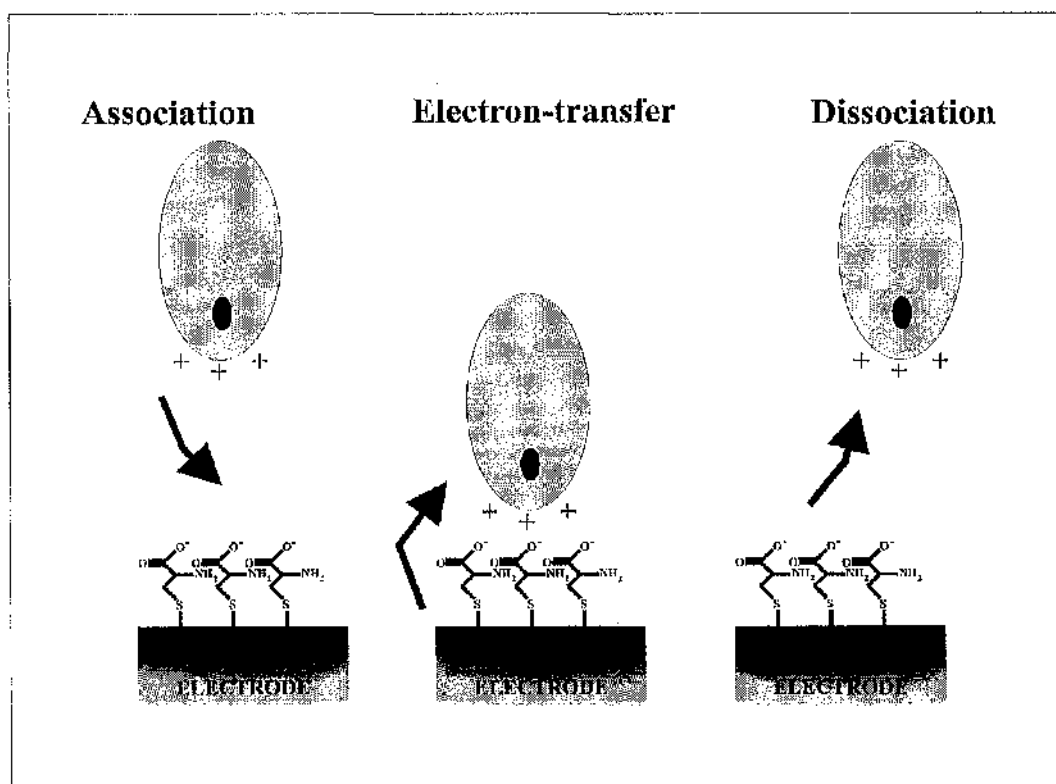
Figure 4.6 - Good promoters of cytochrome *c* electrochemistry have the ability to form hydrogen bonds with the lysine residues surrounding the heme crevice on the protein, thereby producing the best orientation for electron transfer.

The ability of alkanethiols bearing certain head groups to promote electron transfer at gold electrodes is well documented. For example, over a decade ago, Allen et al. produced a comprehensive survey of over 50 thiol-containing molecules studied for their ability to promote the electrochemistry of cytochrome *c* at gold electrodes[39]. Their studies shows that for a compound to be an effective electron transfer promoter it is essential that it has the ability to form hydrogen bonds with the terminal amine

groups on the lysine residues which surround the heme crevice on cytochrome c **Figure 4.6.** It is the presence of these lysine residues that enable the cytochrome c to perform its biological function, acting as sites whereby aspartates present on cytochrome c peroxidase can bind electro-statically, enabling electron transfer.

Figure 4.7 - Representative cyclic voltammograms of a 0.7 mM solution of horse heart cytochrome c, recorded at a gold electrode (diameter 2 mm^2), scan rate 50 mVs^{-1}. (a) shows the scan of a clean unmodified electrode, whilst (b) shows the voltammetry observed at an electrode modified by incubation in 1 mM aqueous solution of mercaptopropanol for 30 minutes. The anodic peak current (i_{pa}) and cathodic peak current (i_{pc}) as well as the peak to peak separation (ΔE) are labelled. Electrolyte conditions were 20 mM sodium phosphate buffer pH 7.0, containing 100 mM sodium perchlorate as the supporting electrolyte.

In this respect, it might be expected that mercaptopropanol has an ability to promote the redox chemistry, while the protonated NH_3^+ group of mercaptoethylamine that exists at pH 7.0, the pyridine group of mercaptopyridine and the aliphatic mercaptopropane do not **Figure 4.1**.

Figure 4.7a shows how, as expected, the distinctive electron-transfer peaks of horse heart cytochrome c are *not* observed when cyclic voltammetry is performed at an unmodified gold electrode. **Figure 4.7b** however, shows the voltammetry which is

observed at a gold electrode which has been modified with mercaptopropanol, showing well-defined, diffusion controlled, reversible cytochrome c electrochemistry (the peak to peak separation $(\Delta E) = 61$ mV and the ratio of the anodic and cathodic currents $(I_{pa}/I_{pc}) = 1$, both indicating a high degree of reversibility)[111,114].
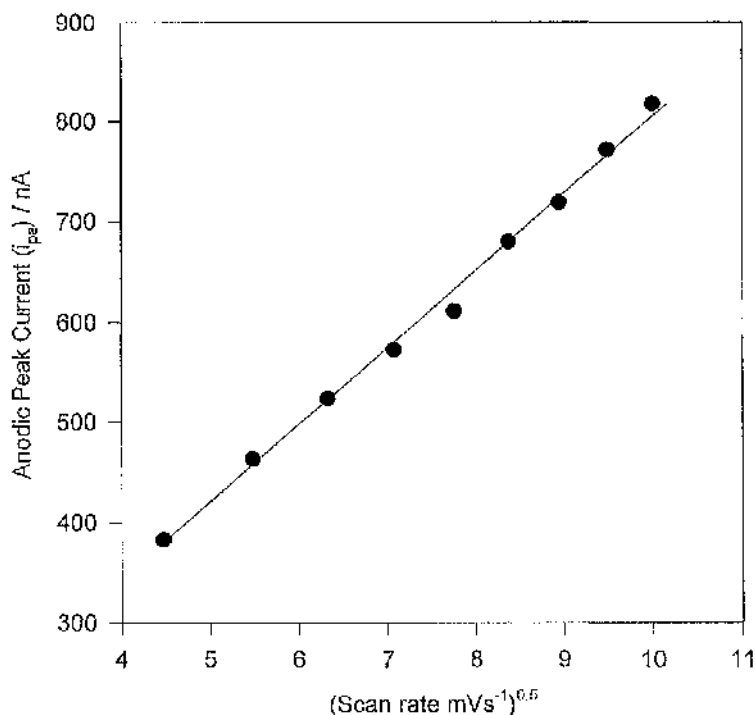
Figure 4.8 - Variation of peak current (i_{pa}) with square root of scan rate $(v^{1/2})$ for cyclic voltammograms of a 0.7 mM solution of horse heart cytochrome c, recorded at a gold electrode (diameter 2 mm^2) modified by incubation in 1 mM aqueous solution of mercaptopropanol for 30 minutes. Electrolyte conditions were 20 mM sodium phosphate buffer pH 7.0, containing 100 mM sodium perchlorate as the supporting electrolyte.

In common with other studies[50], the size of both cathodic (i_{pc}), not shown, and anodic (i_{pa}) peaks were proportional to $v^{1/2}$ in the range 10-100 mVs^{-1}, indicating that the electrochemical reaction is fast and diffusion controlled **Figure 4.8**. In contrast, electrodes modified with mercaptoethylamine, mercaptopyridine or mercaptopropanol gave very poor voltammetric responses, **Figures 4.9**.
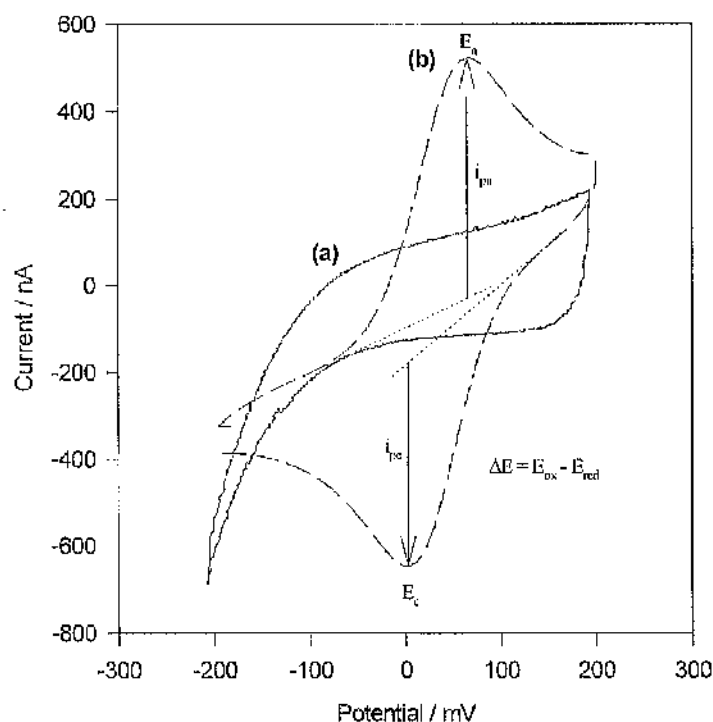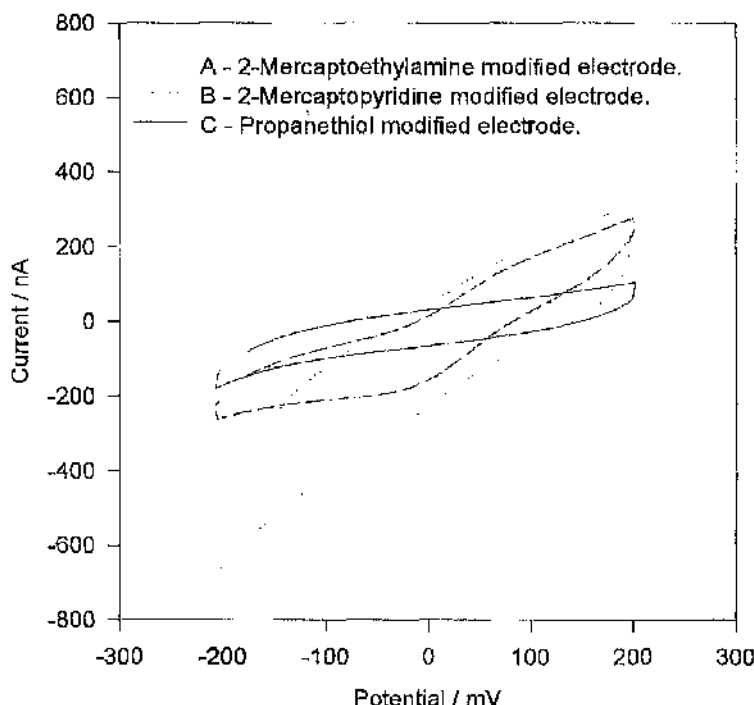
Figure 4.9 -Representative cyclic voltammograms of a 0.7 mM solution of horse heart cytochrome, recorded at a gold electrode (diameter 2 mm^2), scan rate 50 mVs^{-1}. (a) shows the scan of an electrode modified by incubation for 30 minutes in an aqueous solution of 1 mM 2-mercaptoethylamine, (b) that of an electrode modified by incubation for 30 minutes in an aqueous solution of 1 mM 2-mercaptopyridine and (c) the scan observed at an electrode modified by incubation for 30 minutes in an aqueous solution of 1 mM propanethiol. Electrolyte conditions were 20 mM sodium phosphate buffer pH 7.0, containing 100 mM sodium perchlorate as the supporting electrolyte.

As a consequence we sought to use the electrochemistry of cytochrome c to probe the molecular composition of SAMs prepared by displacement of an initial thiol modifier with a secondary thiol. The change in peak anodic current (i_{pa}) following immersion of the primary monolayer in a solution secondary thiol for varying lengths of time was sought not only to corroborate information obtained by XPS measurements (**Chapter 2**) but also to demonstrate the use of mixed monolayers to control molecular recognition at a gold interface.

Figure 4.10 - Cyclic voltammograms of a 0.7 mM cyctochromc solution, obtained when a gold electrode (diameter 2 mm²), modified with mercaptoethylamine, was placed in a solution of mercaptopropanol for repeated periods of time (0 - 120 min). Increasing peak heights occur for increasing lengths of immersion time, seeFigure 4.11 for precise values. Solution and instrumental parameters were as for **Figure 4.9**.

Figure 4.10 shows the consequence of immersion of a mercaptoethylamine modified electrode in a 1 mM mercaptopropanol solution, over a period of time (10s - 180 minutes). Two main effects are observed: first the peak currents (I_{pa} or I_{pc}) increase in size as a function of the time of exposure to mercaptopropanol, **Figure 4.11**; second the peak to peak separation decreases with time. Both results are indicative of an increase in the rate of biological electron transfer (despite the increased length of mercaptopropanol over mercaptoethylamine), an observation which can be attributed to the displacement of mercaptoethylamine by mercaptopropanol, as substantiated by previous XPS studies. Similar change in peak current is not observed for various control conditions illustrated in **Figure 4.13**.

81
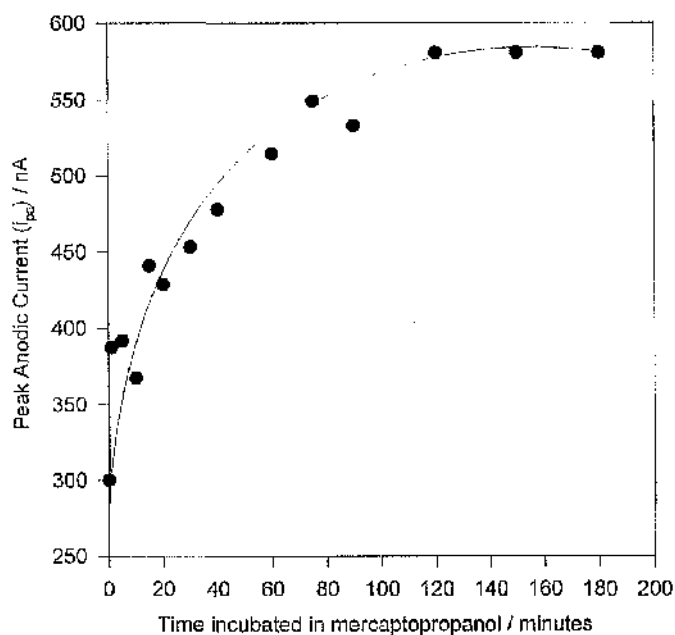
Figure 4.11 - Variation of i_{pa} with immersion time of the anodic peak current for electrodes prepared and treated as in **Figure 4.10**.
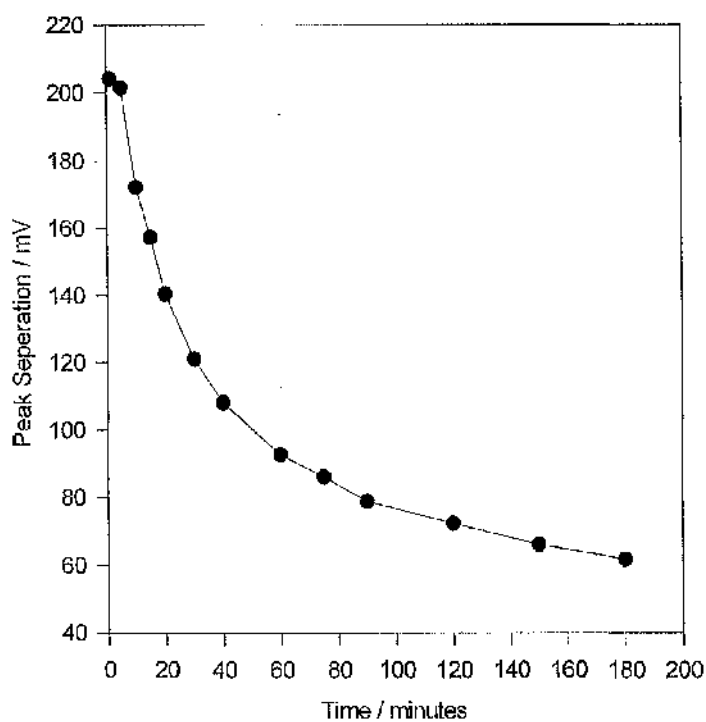
Figure 4.12 - Showing the decrease in the separation between i_{pa} and i_{pc} for electrodes prepared and treated as in **Figure 4.10**

82

Similar results are observed when mercaptopyridine is used as a primary modifier, suggesting that this species is also displaced by the promoter mercaptopropanol **Figure 4.14 and 4.15**. It is also possible to displace mercaptopropanol by incubation in mercaptopropane **Figure 4.16 and 4.17**.
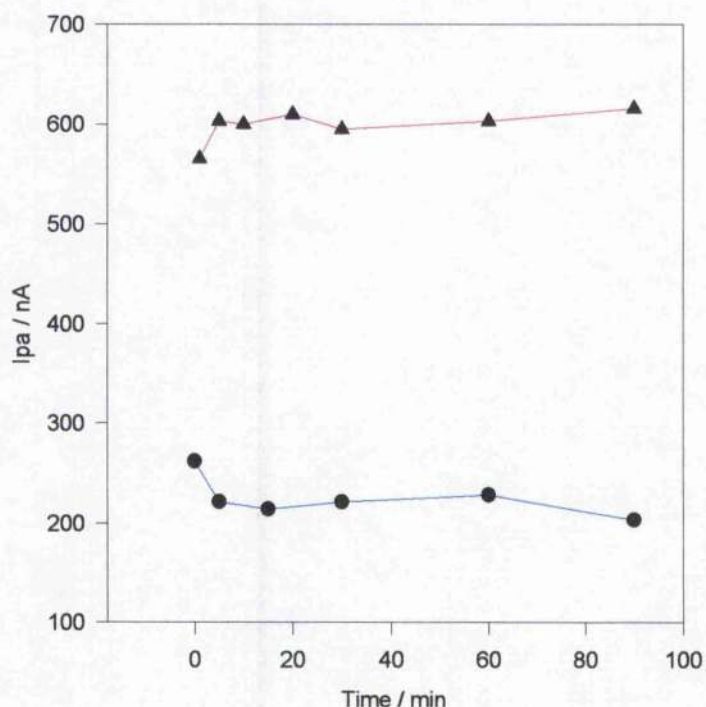
Figure 4.13. Variation with immersion time of the anodic peak current for control electrodes. Electrodes were prepared and tested as described in **Figure 4.9** with the exceptions that; one electrode was not modified with mercaptoethylamine before incubation in (▲) and the other was incubated in RO water rather than mercaptopropanol after initial modification with mercaptoethylamine (●).

It is interesting to note that the reverse displacement reactions shown (i.e. mercaptopropanol incubated in either mercaptoethylamine or mercaptopyridine) yield no change in the peak currents observed, even after over prolonged periods of time (> 12 hours), suggesting no change in monolayer composition. This is in agreement with our previous observations from XPS data, and the work of others indicating that displacement occurs as a result of a more stable monolayer being formed by the incoming thiol[147]. Consequently it is possible to create a hierarchy

83

corresponding to the ability of a solution thiol to displace a surface species **Table 4.2,** and thus create mixed SAMs containing controlled quantities of multiple thiols.

Modifying Thiol	Surface Thiol			
Mercapto-	-propane	-propanol	-pyridine	-ethylamine
-propane	-	Displacement	Displacement	Displacement
-propanol	SAM stable	-	Displacement	Displacement
-pyridine	SAM stable	SAM stable	-	N/A
-propanol	SAM stable	SAM stable	N/A	-

Table 4.2 – Showing the ability of each thiol used in this study to displace another. Where dispalcement does not occur this is indicated by 'SAM Stable', otherwise if displacement does occur this is indicated by the term 'displacement'.
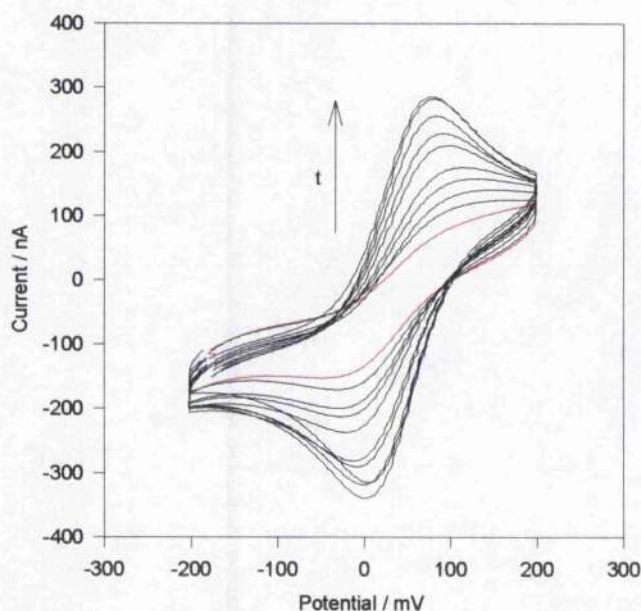
Figure 4.14. Cyclic voltammograms of a 0.7 mM cyctochrome*c* solution, obtained when a gold electrode modified with mercaptopyridine (surface area 2 mm^2), was placed in a solution of mercaptopropanol for different periods of time (0 - 120 min). Increasing peak heights occur for increasing lengths of immersion time, see**Figure 4.15** for precise values. Solution and instrumental parameters were as for **Figure 4.9**.
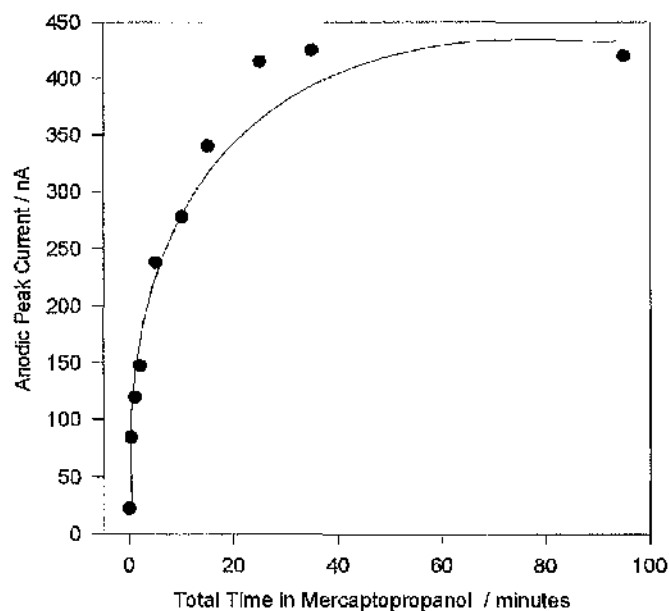
Figure 4.15. Variation with immersion time of the anodic peak current for electrodes prepared and treated as in **Figure 4.14.**
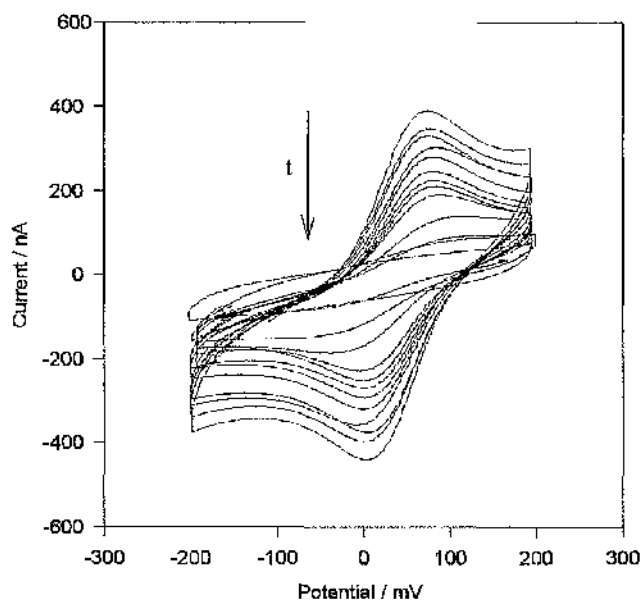
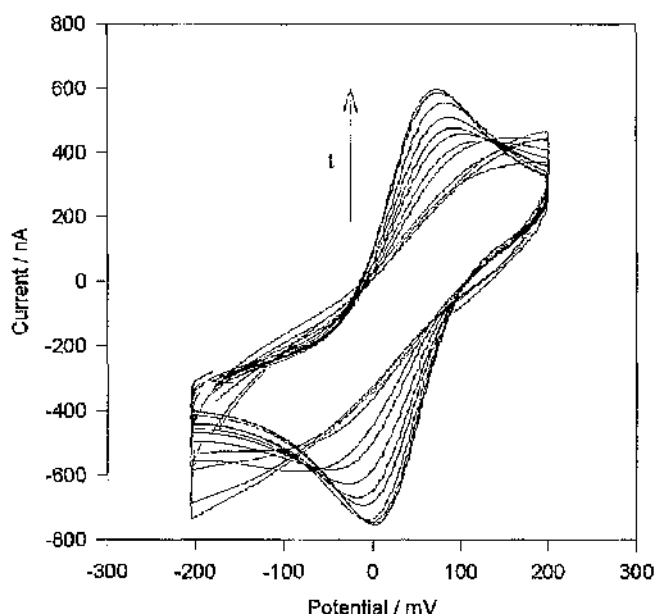**Figure 4.16** - Cyclic voltammograms of a 0.7 mM cyctochrome*c* solution, obtained when a gold electrode (diameter 2 mm^2) modified with mercaptopropanol was placed in a solution of mercaptopropane for repeated periods of time (0 - 60 hours). Decreasing peak heights occur for increasing lengths of immersion time, see**Figure 4.17** for precise values. Solution and instrumental parameters were as for **Figure 4.9**.
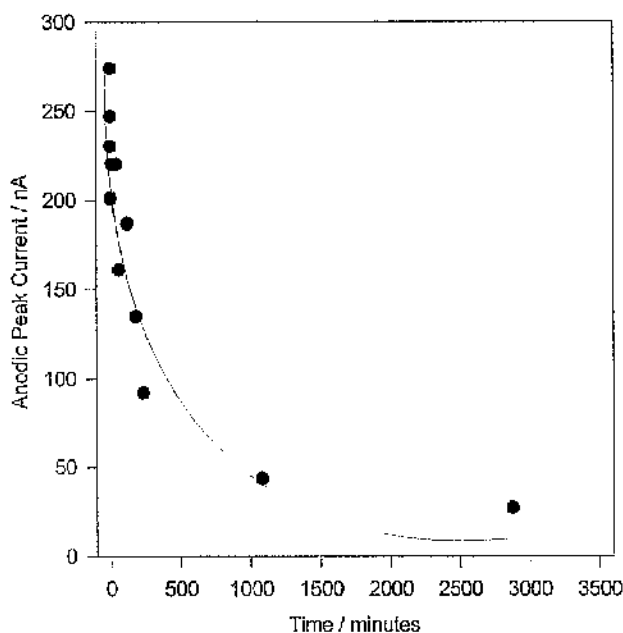
Figure 4.17 - Variation with immersion time of the anodic peak current for electrodes prepared and treated as in Figure 4.16.

The results shown above demonstrate that it is possible to use the displacement of thiols to control the degree of molecular recognition between redox proteins and an electrode surface. The resolution, as a consequence of the large size of the protein in comparison to the thiols, will of course be limited, however, if we consider the cytochrome c as a probe, it can give us information as to the composition of the electrode surface as regards to head groups present. In this manner the suggestion, indicated by XPS measurements (Chapter 2) that displacement is occurring is supported, and it also indicates possible control over protein immobilisation at modified electrode surfaces by the use of head group specific binding strategies.

4.3.3 Investigation of Non-Specific Protein Binding at SAMs Using FT-iR.

In accordance with our XPS measurements, that suggest an unusually low amount of physisorbed contamination observed at mercaptopropanol SAMs (Chapter 2), we also investigated the ability of these SAMs, to prevent non specific protein

adsorption. Using FT-iR spectroscopy we were able to compare protein adsorption at reactive ion etch cleaned evaporated gold samples, which had been modified by various means **Table 4.1**.

The characteristic chemical groups of interest when analysing the amount of protein physisorbed to the various surfaces are shown for an reactive ion etch cleaned gold sample immersed in 5 µg ml^{-1} BSA **Figure 4.18**. Of particular interest are the amide I band (1600-1700 cm^{-1} associated with the stretching vibration of peptide C=O group) and the amide II band (1400-1500 cm^{-1} due to N-H bending with a contribution from C-N stretching). These amidic peak positions were found to correspond well with those described in the literature[145].
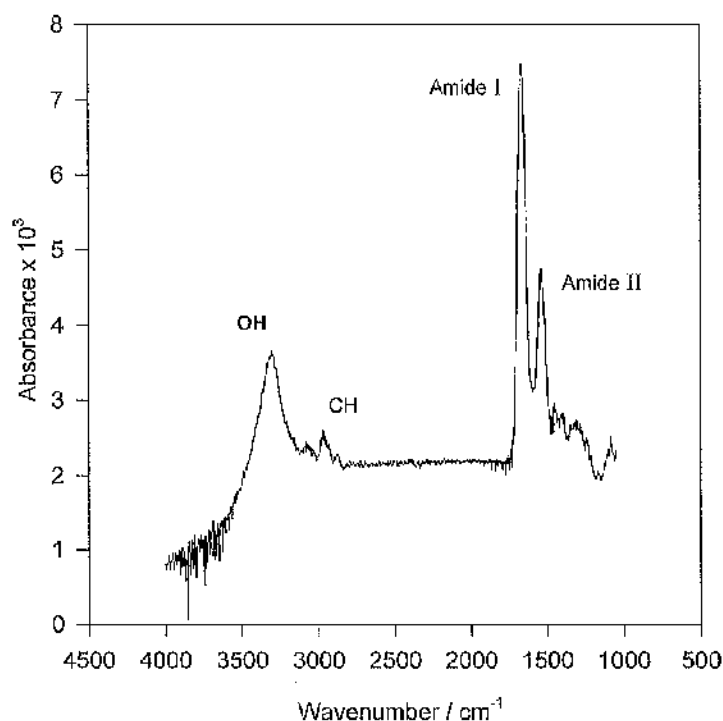
Figure 4.18 - The FT-iR absorption spectra of BSA physisorbed onto reactive ion etch cleaned evaporated gold, from a solution of 5 µg ml^{-1} protein in PBS. The peaks observed, can be attributed to the Amide I and II regions associated with adsorption as a result of peptide bond vibrations within the enzyme, and the OH and CH stretching regions.

By following the change in the absorbence at wave numbers characteristic of the two amidic peaks **Figure 4.19**, we were able to infer the relative amount of protein physisorbed to each surface **Figure 4.20**.

It can be seen that a SAM composed of mercaptopropanol results in approximately a 72 % decrease of physisorbed protein compared that observed at a plain gold surface. SAMs composed only of mercaptoethyalamine, however, only show ca. 38% decrease in protein absorption. This is in accordance with our XPS data presented earlier where lower contamination as a consequence of hydrocarbon physisorbtion were observed for SAMs composed of mercaptopropanol than for those of mercaptoethylamine. The higher incidence of fouling noted in the mercaptoethylamine is probably as a result of the formation of hydrogen bonds between the "contamination" and the charged NH_3^+ headgroup of mercaptoethylamine.
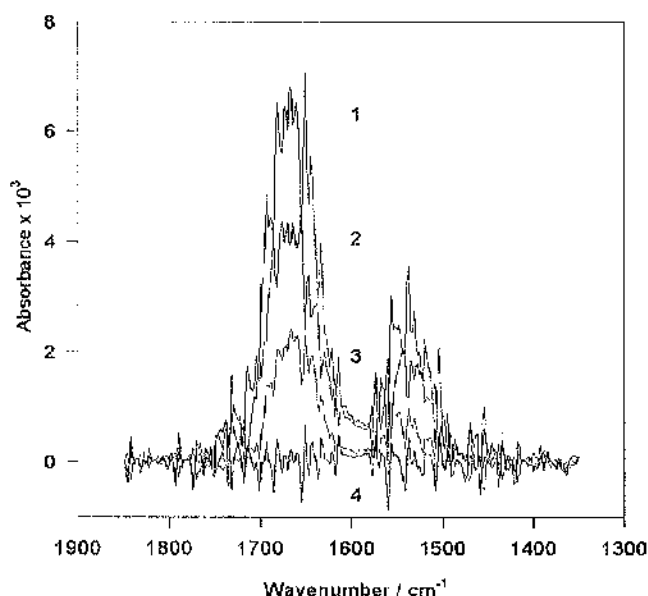
Figure 4.19. The variation in the Aimde I and Amide II absorbence spectra recorded at evaporated gold surfaces modified as described in Section 4.2.6, prior to immersion in a PBS containing BSA. Spectra 1 shows an unmodified gold surface, with physisorbed protein; spectra 2 a gold surface modified with mercaptoethylamine prior to protein physisorbtion; Spectra 3 a gold surface modified with mercaptopropanol prior to protein physisorbtion; and finnaly spectra 4 an unmodified gold surface immersed in PBS containing 5 μg ml⁻¹ BSA and 0.5 % Tween 60.
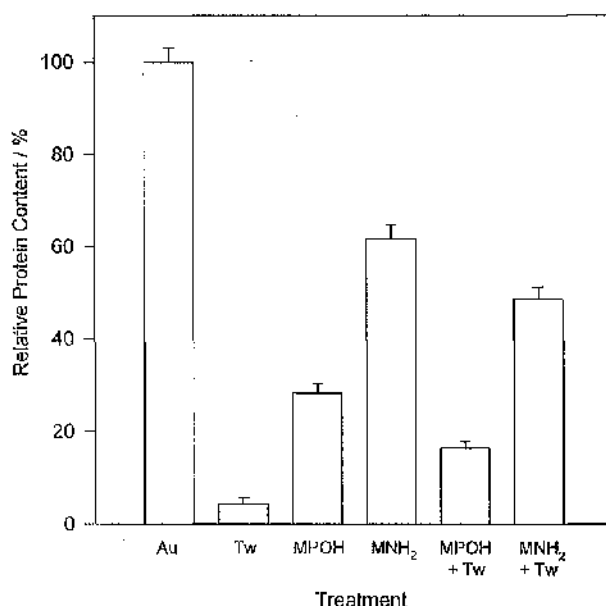
Figure 4.20 – The relative amount of protein absorbed to modified gold surfaces are immersed in a PBS solution containing 5 μg ml⁻¹ BSA, shown as a percentage of that adsorbed to a plain unmodified gold surfaces. Relative protein adsorbtion is inferred by the integration of the Amide I and Amide II absorption peaks seen in FT-IR spectra recorded as described in **Figure 4.18**. Modifications prior to physisorbtion step: *Au* - plain gold; *Tw* - plain gold with 0.5% Tween 60 included in protein solution; *MPOH* - mercaptopropanol SAM; *MNH₂* - mercapethylamine SAM; *MPOH + Tw*- mercaptopropanol SAM with Tween 60 included in protein solution; *MNH₂ + Tw*- mercaptoethylamine SAM with Tween 60 included in protein solution.

For comparison the effect of Tween 60 (polyethylene sorbitan monostearate) commonly used as a biological detergent to prevent non-specific protein adsorption, was also investigated. The anionic detergent Tween 60 is thought to prevent protein adsorption by the formation micelles around proteins[66,166] **Figure 4.21**.
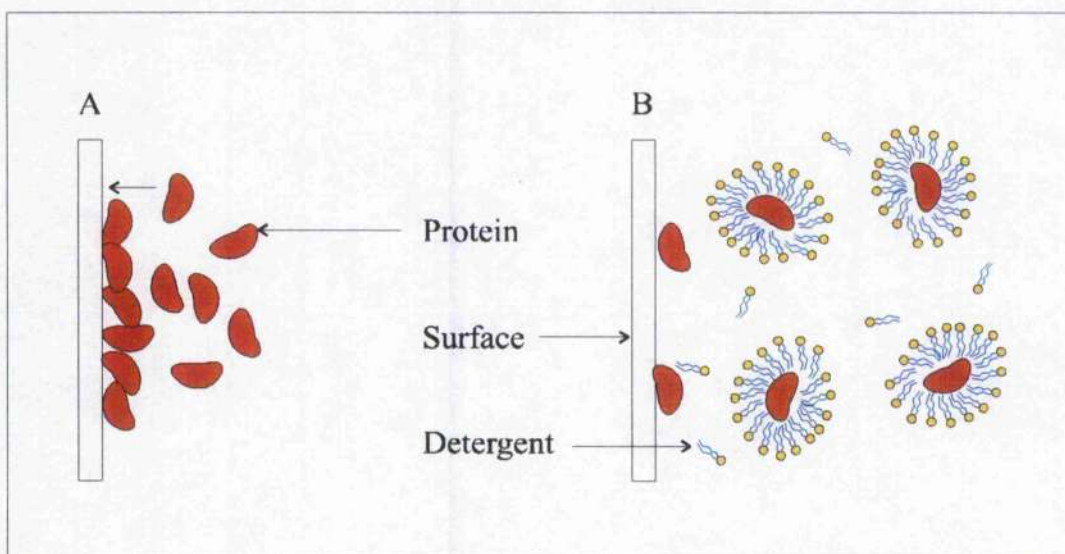
Figure 4.21 - Detergents such as Tween 60,are believed to help prevent the adsorption of proteins to surfaces such as electrodes **A**, by forming micelles around the protein, as a consequence of their ampiphatic nature, thereby stabilising the protein in solution and preventing hydrophobic interactions of the protein with the electrode **B**.

Correspondingly when we use Tween 60 as a component of our absorption buffer we noted almost a 100% reduction in protein binding, when using RIE cleaned gold surfaces. However, a similar decrease is not observed when a thiol modified gold surface is used, where only a small, further, reduction of protein adsorption is seen **Figure 4.20**.

In the FT-iR spectra collected for those cases where Tween 60 is included in the adsorption buffer, an increase in the peak corresponding to CH stretching is observed, as indicated in **Figure 4.22**. This increase which is most probably a consequence of Tween 60 binding to the gold surface.
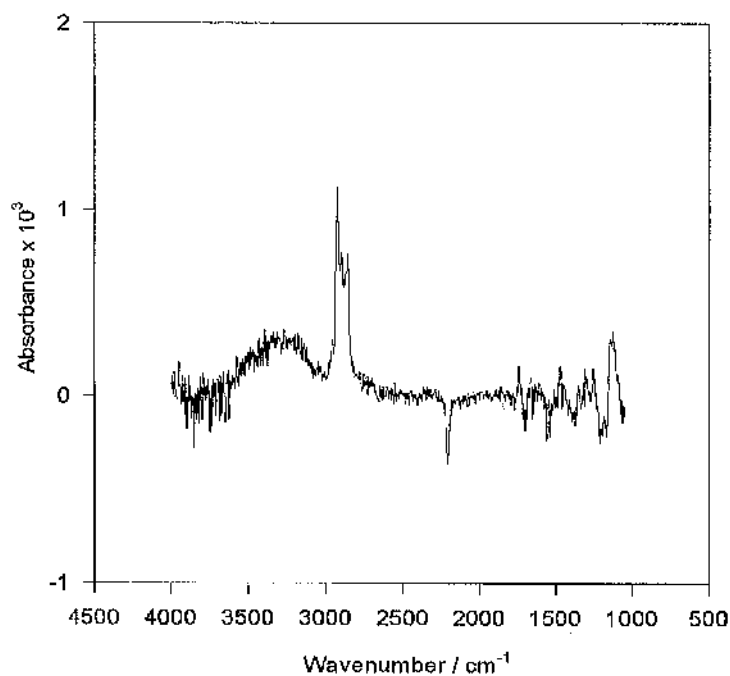
Figure 4.22 - The FTIR absorption spectra of an RIE cleaned evaporated gold sample immersed for 2 hours in a solution of PBS containing 0.5% Tween 60. The large peak observed at approximately 3000 cm^{-1} is due to absorption through CH stretching in the Tween 60 molecules. This distinctive peak is observed in all protocols where Tween 60 is included.
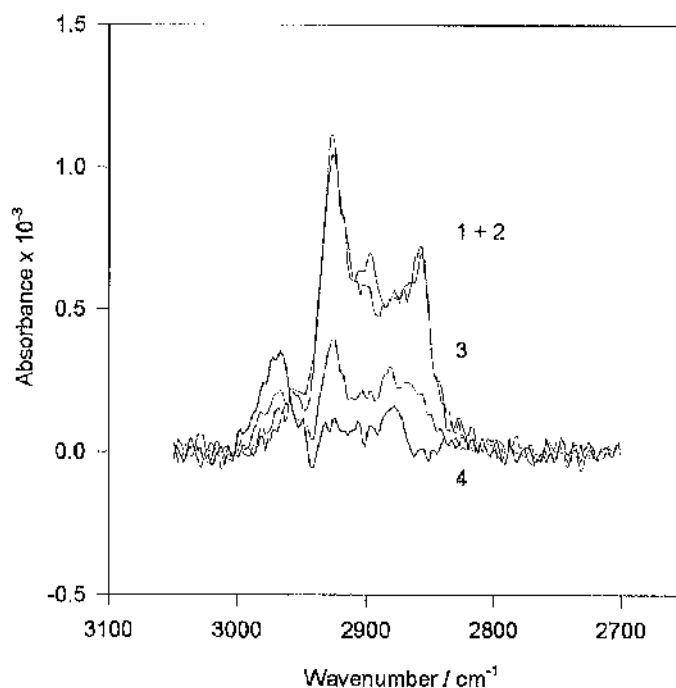
Figure 4.23 - The absorption peaks corresponding to CH stretching observed in FT-iR spectra collected at RIE cleaned, evaporated gold samples modified in the following fashions prior to immersion in a PBS containing 5µg ml^{-1} BSA as well as 0.5% Tween 60 (described in Section 4.2.6): 1. Plain RIE cleaned evaporated gold washed no BSA included in adsorption buffer; 2. Plain RIE cleaned evaporated gold washed with BSA included in adsorption buffer; 3. mercaptopropanol SAM, ; 4. mercaptoethylamine SAM.

91

It is probable therefore, that the reduction of NSB to almost zero (as described above for an RIE cleaned gold substrate), is as a consequence of the Tween 60 playing two roles. Firstly the stabilisation of protein in solution by micelle formation, and secondly the adsorption of Tween 60 to the gold, thereby blocking those potential binding sites previously available for protein adsorption.

This hypothesis can also be used to explain why, only a slight reduction in NSB is observed in those samples where a thiol monolayer already exists. In these cases only a small Tween 60 signal is observed in the FT-iR spectra **Figure 4.23**, indicating that the reduction in NSB is probably due only to micelle formation and not as a result of blocking of potential binding sites by Tween 60 **Figure 4.24**. Although effective at reducing the NSB, the adsorption of Tween 60 at the electrode surface may not be appropriate when performing bioelectrochemical measurements, where proteins are immobilised to the electrode surface. Cases such as these may offer an effective alternative to detergents in order to reduce non-specific interactions.
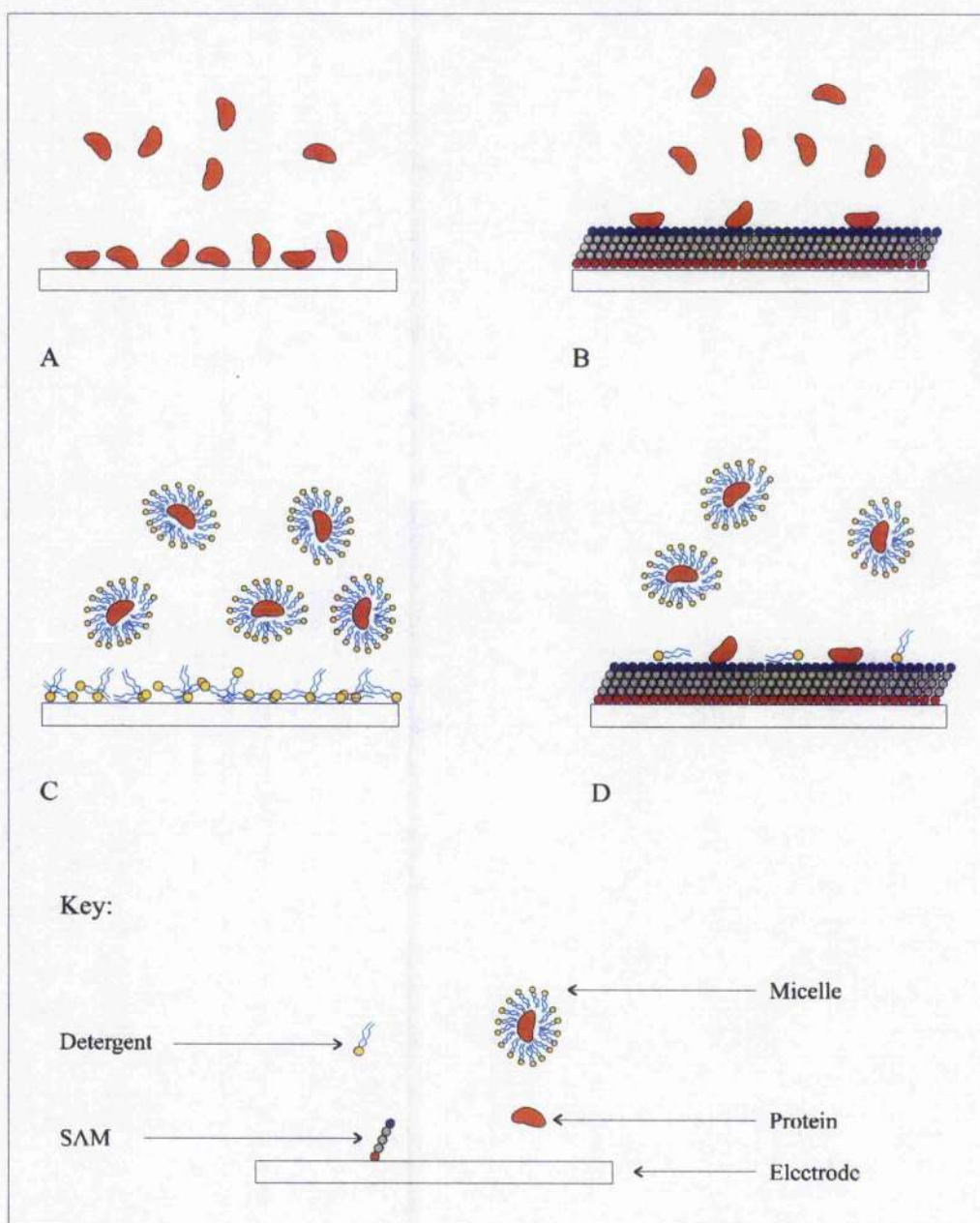
Figure 4.24 - At plain gold electrodes (**A**) protein adsorbs to the surface as a consequence of weak non-covalent interactions (van der Waals, ionic and hydrophobic forces). In the presence of a pre-formed alkanethiol SAM such as mercaptopropanol (**B**) there is a degree of reduction in physisorbtion. Detergents such as Tween 60 prevent protein binding at unmodified gold electrodes (**C**) by binding to the surface and stabilising the protein in solution. When a pre-formed SAM is present (**D**), the detergent can not bind to the surface but still stabilises the protein in solution, protein can still bind to the SAM but to a lesser extent.

4.4 Conclusion

We have shown that mixed SAMs, formed by displacement reactions on gold surfaces, can be used as a method of controlling the interactions of proteins with micro-engineered devices. The possible applications cover the promotion of reduction/oxidation reactions, directed protein immobilisation, the reduction of non-specific protein adsorption as well as possible cellular engineering applications (controlling cell growth through molecular gradients). These results demonstrate the wide range of uses that SAMs of alkanethiols on gold can impart. With such a variety of both alkanethiols and bi-functional cross-linking agents available to be exploited in this manner, the formation of mixed monolayers by "displacement" could be used as a tool to enable a high degree of control over the molecular architecture of gold surfaces used both in biosensor and bioengineering fields.

CHAPTER 5: PROTEIN IMMOBILISATION AT MIXED MONOLAYERS

5.1 Introduction

The nature of the surface molecular environment in which a molecule is immobilised has considerable implications on the sensing properties of that surface[8,37,41,136,167,168]. As a consequence, the control of protein immobilisation and the subsequent manipulation of the surface molecular architecture is of importance for many areas of science and technology.

In one example, which illustrates this point, immobilised antibodies show a decrease in response, when challenged by antigen, if the antibody surface density is too high, as a consequence of the effects of steric hindrance[48]. Prevention of this reduction in antigen binding could be achieved by the addition of spacer alkanethiols into an antibody immobilised on alkanethiol monolayer resulting in a decrease the surface density of the immobilised antibodies **Figure 5.1**. Similar results have been observed for the binding of avidin using mixed monolayers of biotinylated thiols and alcohol terminated thiols[47]. Control of the monolayer composition, therefore, provides a means by which the optimum surface density for the function of the immobilised protein can be attained.

In this chapter, therefore, we present techniques which allow the control of protein immobilisation at a surface, in a custom which allows for the manipulation of the quantity and "quality" of material bound to that surface (i.e. in the latter case, by reducing steric effects and controlling orientation as described later). Using both mixed monolayers and the manipulation of avidin/biotin chemistry, we are able to produce a variety of protein gradients over a gold surface. Although suitable for the preventing loss of activity through steric hindrance if used in conjunction with photo-lithographic procedures, these techniques would allow the formation of surfaces suitable for on sensor calibration.
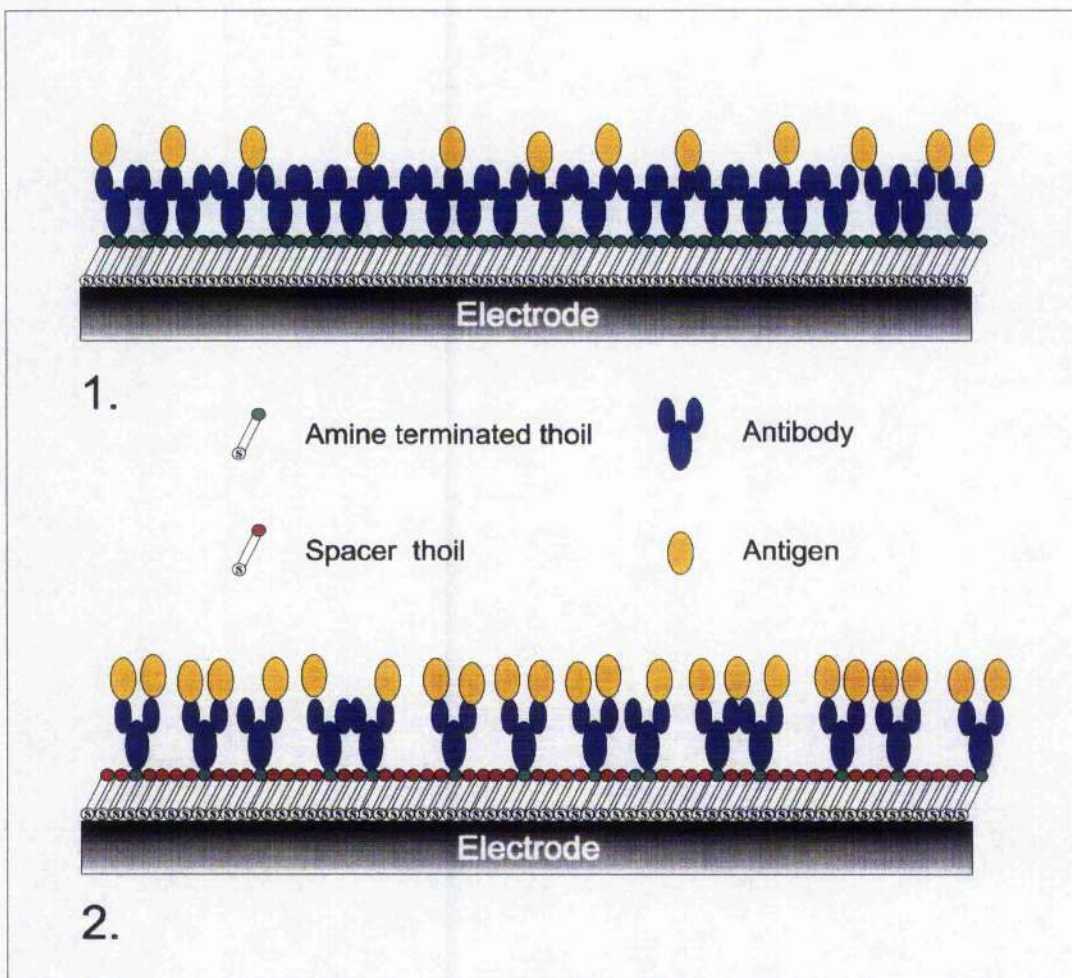
Figure 5.1 - Steric hindrance can cause ineffective antigen binding when the density of antibody immobilised at a SAM is too high as shown in figure 1, this problem can be overcome by the addition of spacer thiols into the SAM, figure 2.

Further to possible biosensor applications, the formation of protein gradients are of particular interest for their employment in the investigation of the behaviour of cells at bio-material surfaces[84,169,170]. This is as a consequence of the influences that the properties of the surface have on the cell adhesion, spreading and growth. In addition, it is believed that many aspects of cellular movement are controlled by gradients of molecules known as chemokines.

Finally, as stated above, whilst each of the methods used allows us to control the density of the immobilised protein, they also have the potential to be used to define the orientation of immobilisation, giving a possible method of preventing the loss of protein activity on immobilisation, as a result of inappropriate protein orientation[167,168].

5.2 Experimental

5.2.1 Materials

All chemicals and solvents were purchased from Sigma (Poole, UK) and used without any further purification. Glutaraldehyde was stored at -20°C until required. All solutions were made up using reverse osmosis (RO) ultrapure water (Millipore, UK). All proteins were reconstituted from lyophilised form with 100mM phosphate buffered saline pH 7.0 (PBS) and stored frozen at -20°C until required. Fluorescein IsoThioCyanate (FITC)- labelled proteins were stored guarded from exposure to light in order to prevent photobleaching of the fluorophore. Stock solutions of biotin were prepared by dissolving 10 μg in 5 ml of Dimethyl-Sulphoxide (DMSO) before diluting to the required concentration by the addition of PBS.

Titanium (Ti), palladium (Pd) and gold (Au), used for the fabrication of 2 mm diameter photolithographically defined gold working electrodes, were all purchased from Goodfellows (Cambridge, UK). In addition, a Ag|AgCl reference electrode (MF-2063) was obtained from BioAnalytical Systems (Luton, UK).

5.2.2 Gold Substrate Preparation

5.2.2.1 Electron Beam Evaporation

All of the following experiments were performed using gold surfaces prepared by the electron beam evaporation of a Ti/Pd/Au multilayer structure on to glass substrates.

When clearly defined surfaces for electrochemical measurements were required, the glass substrate used had been patterned photolithographically to produce 2 mm diameter gold electrodes prior to metal deposition by electron beam evaporation. These processes have been described in more detail in chapters 4 and 6.

5.2.2.2 Cleaning of Gold Substrates by Reactive Ion Etching

Immediately prior to modification of the gold substrates, the samples were cleaned by a reactive ion etch for five minutes first in an oxygen plasma and then in an argon plasma using a PlasmaFab ET340 (50mT, 20 sccm, and 10 W).

$$HS-CH_2-CH_2-NH_2 \qquad (1)$$

$$HS-CH_2-CH_2-CH_2-OH \qquad (2)$$
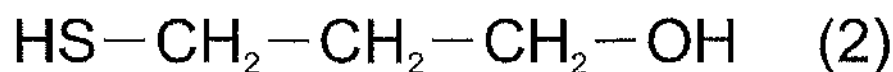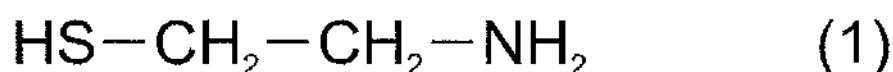
Figure 5.2 - Alkanethiols used to create SAMs, mercaptoethylamine (1) and mercaptopropanol (2).

5.2.3 Alkanethiol Self-Assembled Monolayer Formation

5.2.3.1 Formation of Homogenous and Mixed Monolayers

After cleaning, homogeneous monolayers of a single alkanethiol **Figure 5.2** were produced by immersing the gold substrate into a 1 mM aqueous solution of the thiol for two hours and then by thoroughly rinsing using RO water. Where mixed monolayers were required, the surface was then blown dry in a stream of nitrogen gas and then immersed in a secondary thiol solution for periods between 10 seconds and 180 minutes before rinsing as described previously in Chapter 4.

5.2.3.2 Alkanethiol gradients over whole glass slides

Gold substrates, prepared by the electron beam evaporation of metals onto glass slides (75mm x 25mm x 1.5 mm), were initially modified by immersing in 1mM aqueous solution of mercaptoethylamine as described above. After rinsing in RO water and blow drying in a stream of nitrogen gas, the slides were placed up-right in a slide holder (volume 85 ml). Over the course of ninety minutes, 1 mM mercaptopropanol was added to the holder (5 ml every 4 minutes) until the slide was covered to within 1 cm of the top **Figure 5.3**. The slide was immediately washed in RO water and dried in a stream of nitrogen gas prior to further modification by the immobilisation of proteins at its surface.

Slide

Slide Holder

A   B   C   D
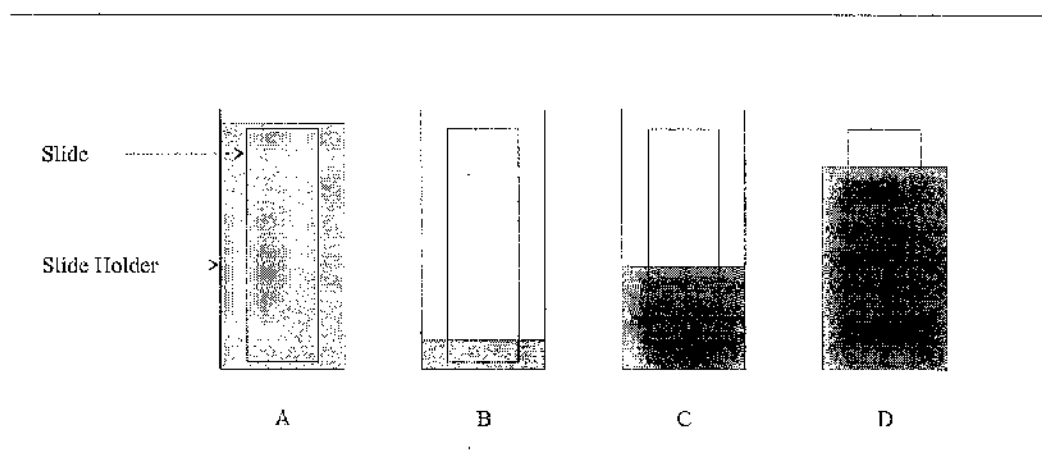
Figure 5.3 - A continuous gradient of protein was prepared on gold slides, by modifying the substrate, in a time dependent fashion whilst held in an appropriate holder, with the primary thiol 1 mM mercaptoethylamine **A**. After washing with RO water, the secondary modifying thiol, 1 mM mercaptopropanol was added slowly over a period of time **B-D**. Following a further wash with RO water, a glutaraldehyde immobilisation of FITC labelled IgG was performed.

5.2.4 Protein Immobilisation at Alkanethiol SAMs

Proteins were immobilised to SAMs containing amine terminated alkanethiols, by an optimised glutaraldehyde amine directed cross-linking[171] method as first described by Williams and Blanch[25]. This procedure is illustrated schematically in **Figure 5.4**. The samples were immersed in 10% glutaraldehyde solution (made up using RO water) for one hour at room temperature. After washing with RO water, the samples were then immersed in a solution of 100 mM PBS pH 7 containing the protein to be immobilised at a concentration of 20 μg ml^{-1} and 0.5% v/v Tween 60 for 40 minutes at room temperature (note: before this stage, it is important to ensure that all excess glutaraldehyde has been removed by washing thoroughly with RO water in order to prevent cross-linking of the protein in solution to other solution proteins.) The samples were finally rinsed thoroughly in order to remove any unbound protein by vortexing, at least four times, in a 100 mM PBS solution containing 0.5% Tween 20, and at least two times in PBS only.

5.2.5 Fluorescence measurements

In those cases where FITC-labelled proteins were bound to SAMs, the samples were examined using a Nikon Microphot fluorescent microscope (FITC: λ_{ex} = 494 nm, λ_{em} = 520 nm). Relative fluorescence was estimated as the 'in focus' exposure time at a fixed aperture when photographing the surface (thus using the camera to integrate the average fluorescent signal over an area of 100 x 100 μm). Exposure times for unmodified mercaptoethylamine SAMs were used to correct for background light levels.
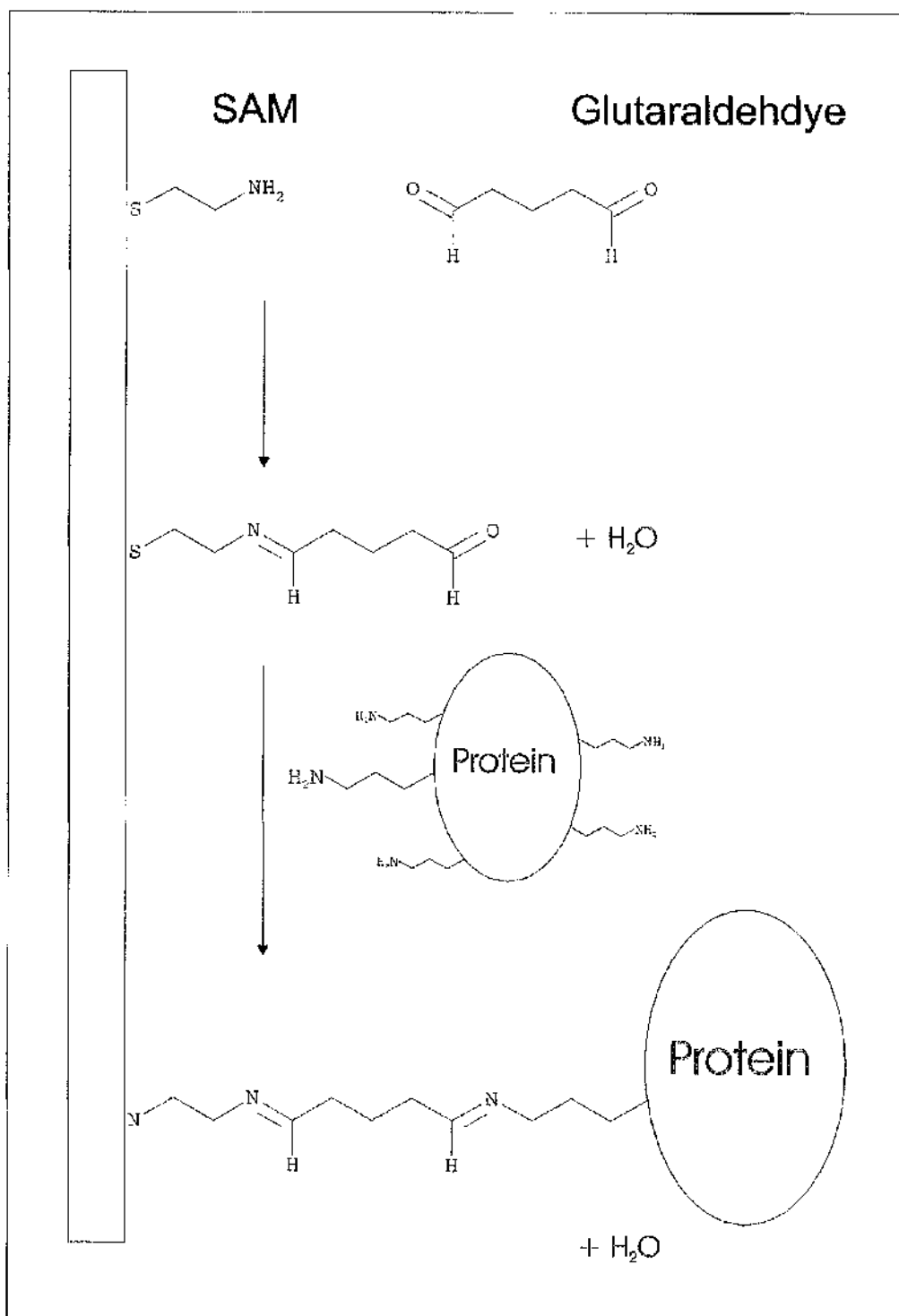
Figure 5.4 - The immobilisation of proteins at surfaces is achieved by an optimised method first described by Williams and Blanch[25]. Initially an amine terminated SAM is formed on a gold sample. To this glutaraldehyde is added and excess glutaraldehyde removed by washing. When the sample is subsequently immersed in 20μg ml⁻¹ BSA solution for 2 hours, the protein is bound at the surface. Excess protein is removed by washing in PBS.

101

5.2.6 Preparation of Biotin/Biotinylated Protein Gradients

Gradients of biotinylated horseradish peroxidase HRP and biotinylated IgG were prepared by incubating the biotinylated proteins, in the presence of various concentrations of free biotin to both avidin adsorbed in polystyrene microtitre plates and also to avidin immobilised at alkanethiol SAMs on gold, **Figure 5.5**.
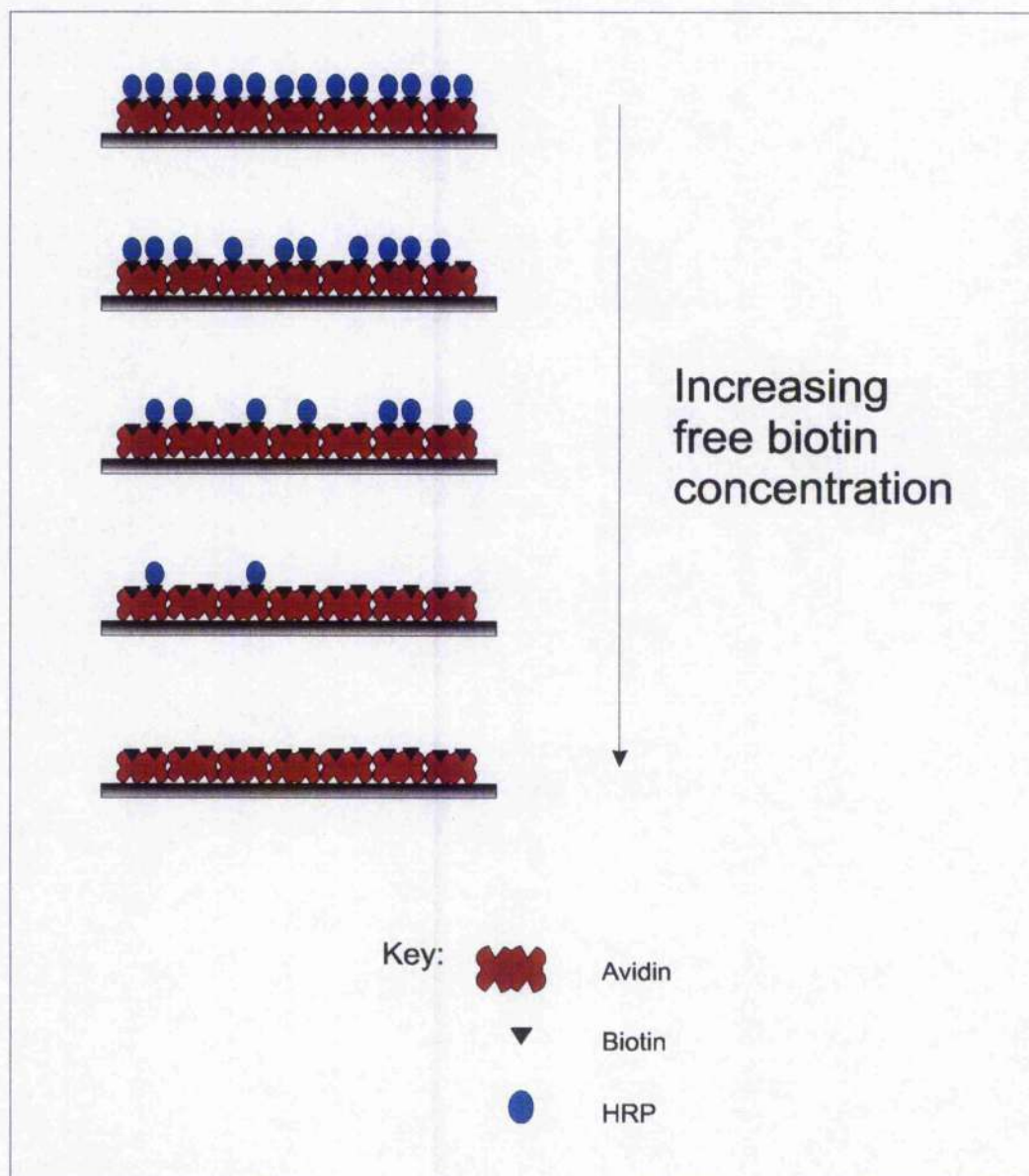
Figure 5.5 - Gradients of biotinylated proteins (e.g. HRP) have been fabricated by incubating a streptavidinated surface in a solution of the biotinylated HRP in the presence of increasing concentrations of free biotin.

5.2.6.1 HRP Protein Gradients for Colorimetric Characterisation.

Streptavidinated 96 chamber mictrotitre plates (R+D Systems, UK) were blocked for non-specific protein binding by the addition of 300 μl, pH 7.4 PBS (containing 1% BSA, 5% sucrose and 0.05% sodium azide) to each chamber and incubated at room temperature for two hours. After washing each chamber at least four times with PBS, to remove excess BSA, 100 μl biotinylated-HRP reaction mixture was added to each chamber. This reaction mixture consisted of a 1 μg ml^{-1} solution of biotinylated HRP in 100 mM PBS pH 7.4 with between 0 and 1000 ng/ml free biotin. After a further 2 hour incubation at room temperature, the chambers were again washed at least four times with PBS solution. The chambers were characterised colourimetrically using tetramethylbenzidine (TMB) substrate system for peroxidase assay (Sigma, UK) **Figure 5.6**. 200 μl of TMB substrate system was added to each chamber and incubated for 30 minutes at room temperature. After 15 minutes, 100 μl of acidic 'stopping' solution (0.5 M H$_2$SO$_4$) was added and the change in absorbence was determined by measurement at 450 nm using an EL$_X$ 800 (Bio-Tek Intruments) microplate reader.
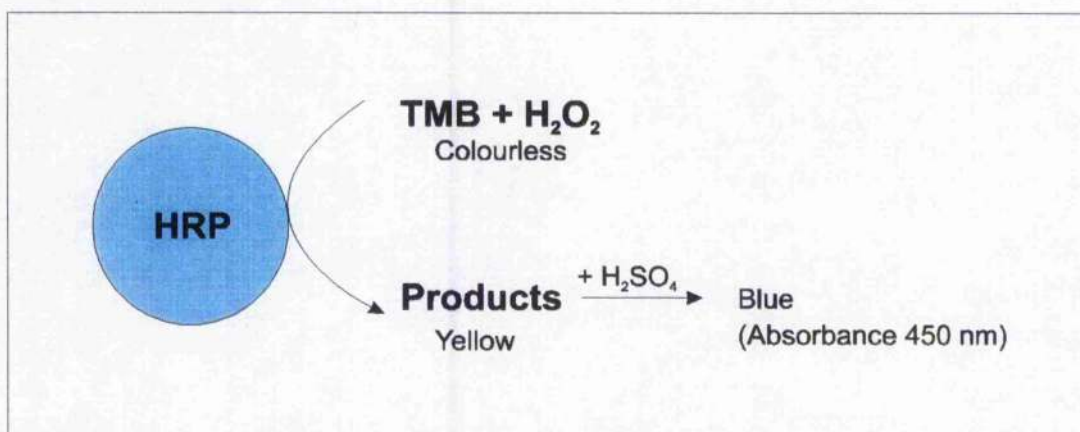
Figure 5.6 - Relative amounts of HRP bound to surfaces were quantified using TMB assay substrate system. HRP turns colourless TMB to yellow products in the presence of hydrogen peroxide. For end point experiments 0.5 M sulphuric acid can be used to stop the enzymatic process. The change in absorbence can then be measured at 450 nm.

The concentration of H_2O_2 in a 30% solution (as supplied) is inherently unstable even when stored at 4°C[172]. Consequently the actual concentration was confirmed by measuring the absorption at 240 nm (molar extinction coefficient = 43.6 M^{-1} cm^{-1}) using a U-2000 spectrophotometer (Hitachi Instruments, Inc.). i.e. 8 mM H_2O_2 (0.025%) has an optical density of 0.35 (optical pathway of 1 cm).

5.2.6.2 IgG Protein Gradients for Coulorimetric Characterisation.

Gradients of biotinylated IgG were prepared in a manner similar to that described for biotinylated HRP gradients in microtitre plates. Streptavidinated plates were purchased and blocked as described in section 5.2.5.2. To these plates 100 μl mixtures of a 1 in 1000 dilution of a biotinylated goat IgG (R+D Systems, UK) 50 μg ml^{-1} stock solution. Both the IgG and free biotin (0 - 1000 ng ml^{-1}) were added to each well before incubation for 2 hours at room temperature. After washing at least four times with PBS (pH 7.4), 100 μl of a secondary 'detection' antibody, alkaline phosphatase labelled rabbit anti-goat IgG (Sigma, UK) at a dilution of 1 in 8000 solution was added to each well and incubated for two hours at room temperature. After further washing with PBS, the microtitre plate was analysed colourimetrically using p-nitrophenyl phosphate (pNPP) liquid substrate system (Sigma, UK). 200 μl of pNPP liquid substrate system was added to each well and incubated for 30 minutes at room temperature. After 30 minutes, 50 μl of stopping solution (3M NaOH) was added and change in absorbence determined at 405 nm using an EL_X 800 (Bio-Tek Instruments) microplate reader.

5.2.6.3 HRP Gradients Prepared for Electrochemical Detection

Clean, photolithographically defined gold electrodes (diameter = 2mm), were immersed in an aqueous solution of aqueous solution of 1 mM mercaptoethylamine **Figure 5.2** for two hours at room temperature. Excess 1 mM mercaptoethylamine was then removed by rinsing, vigorously, in PBS pH 7.4. Glutaraldehyde immobilisation of streptravidin was then carried out as described above in section

5.2.4 After the final immobilisation step any remaining sites available for non-specific protein binding were blocked by incubation for two hours at room temperature in pH 7.4 PBS solution containing 1 % bovine serum albumin. Finally biotinylated horseradish peroxidase was immobilised at this surface by immersion of the electrode in a PBS solution containing 2 $\mu g\ ml^{-1}$ biotinylated HRP. Gradients were produced by incorporating free biotin (0 - 1000 ng ml^{-1}) in the biotinylated HRP reaction mixture **Figure 5.7**. After rinsing thoroughly with PBS, electrodes were characterised by chrono-amperometry, section 5.2.7.
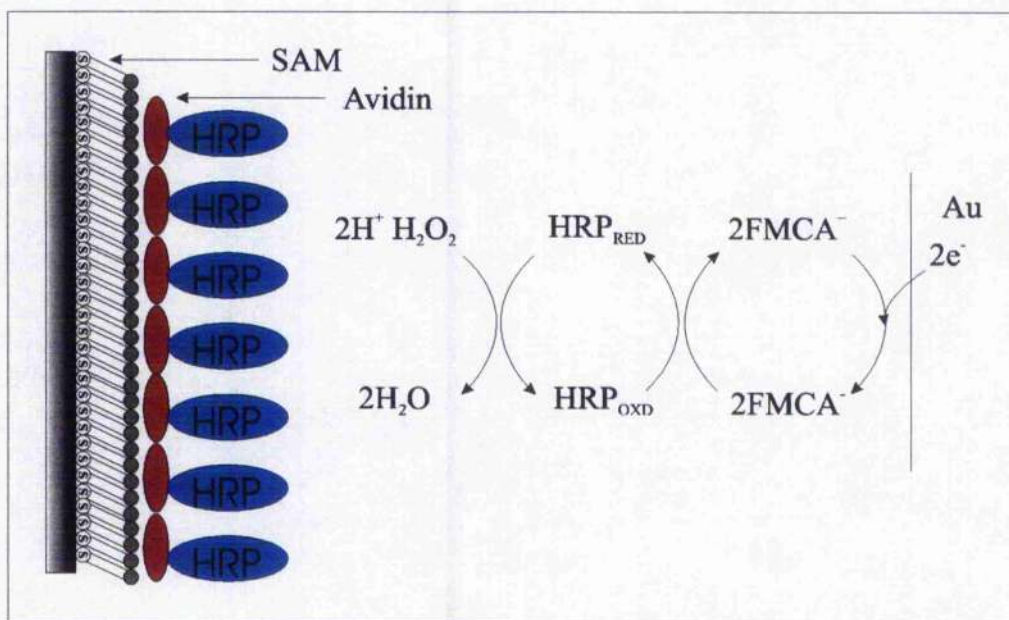
Figure 5.7 - HRP bound by an avidin/biotin link, can be characterised electrochemically using chronoamperometry. When the electrode was poised at 0 mV versus an Ag|AgCl reference electrode, in the presence of both hydrogen peroxide and FMCA an electron transfer reaction occurs and the consequent current can be measured.

5.2.7 Chronoamperometric Readings

Electrochemical responses recorded at electrodes modified with biotinyalted HRP as described in Section 5.2.5.1 were recorded at a low current potentiostat (BioAnalytical Systems CV-37, Stockport, UK) with data collected using an 'in-house' data aquisition set-up comprising a multi-function analogue and digital input/output board (Amplicon PC30AT, Brighton, UK), installed in an IBM

compatible personal computer. Experiments were performed in a 1 ml all glass cell with a working volume of 1ml. The cell incorporated a conventional three electrode configuration accommodating the 2 mm diameter photolithographically defined gold working electrode, a platinum wire counter electrode and a Ag|AgCl reference (3.0 M NaCl, 190 mV vs. NHE).

Measurements were taken by poising the working electrode at 0 mV with respect to the Ag|AgCl reference electrode and recording the change of current with time upon the addition of 10 mM hydrogen peroxide (10 mM peroxide is known to kinetically saturate the enzyme giving an optimal signal)[172]. The three methods used to create biotinylated protein gradients are illustrated schematically in **Figure 5.8**.
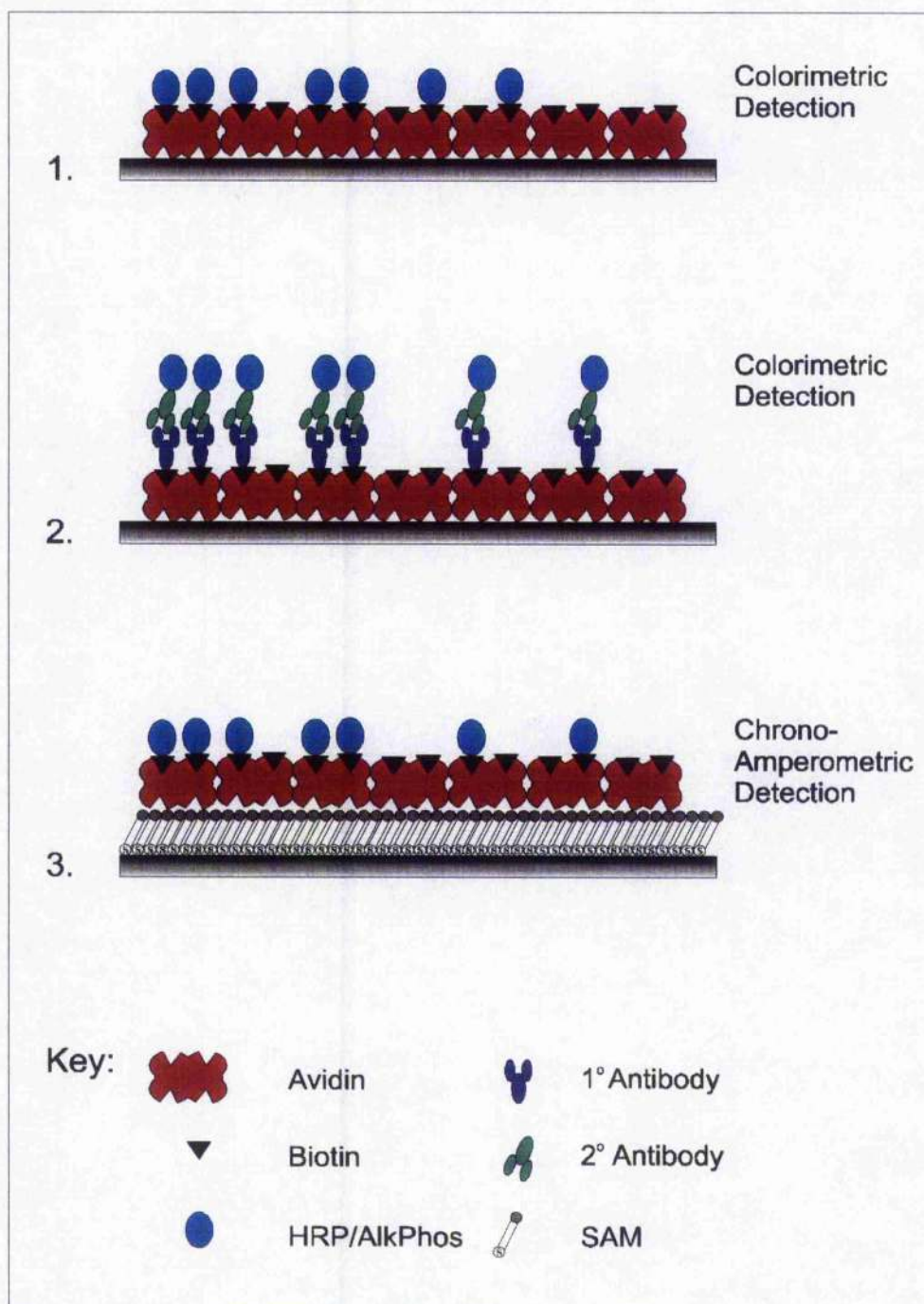
Figure 5.8 - Illustration of three methods used to create protein gradients by the manipulation of the competition for avidin biotin binding sites. Gradients of biotinylated HRP created in an avidinated 96 well microtitre plate, with colourimetric detection using TMB substrate assay system as shown in Figure 5.8.1. Gradients of biotinylated IgG were created in an avidinated 96 well microtitre plate, detection via an alkaline phosphatase labelled secondary IgG with pNPP substrate assay system, Figure 5.8.2. Figure 5.8.3 shows how gradients of biotinylated HRP were created at avidinated gold electrodes, detection by chronamperometry in presence of peroxide and FMCA.

5.3 Results

5.3.1 Immobilisation of FITC Labelled IgG at Mixed Monolayers.

The displacement of mercaptoethylamine by mercaptopropanol was used in order to manipulate the number of potential sites (NH_2 headgroups) for amine directed protein binding on gold surfaces, thereby allowing control over the amount of FITC labelled antibody (IgG), immobilised through a glutaraldehyde mediated coupling[171].

A number of gold samples were initially modified in 1 mM mercaptoethyalmine before being exposed to 1 mM mercaptopropanol for varying periods of time (between 1 and 90 minutes). All of these samples then underwent the same coupling (Section 5.2.4) procedure leading to the immobilisation of goat IgG (bearing the fluorophore FITC) to the available amine groups present in the monolayer.

Comparative measurements of the amount of antibody immobilised was determined by recording the intensity of emitted fluorescence (from the exposure time for a Nikon camera) at a fixed aperture with appropriate filters (FITC: λ_{ex} = 494 nm, λ_{em} = 520 nm). Using the metering system of a camera in this manner we were able to average a reading across a field of view decreasing the effect of any 'hot spots' or in-homogeneities in the sample. Results were corrected using background fluorescence values for native gold modified with mercaptoethylamine alone followed by scaling the fluorescence from IgG immobilised on a homogeneous mercaptoethylamine SAM. **Figure 5.9** shows the general trend that the fluorescence observed, after the immobilisation of antibody, decreases with the time that the mercaptoethylamine-modified gold sample is immersed in mercaptopropanol.
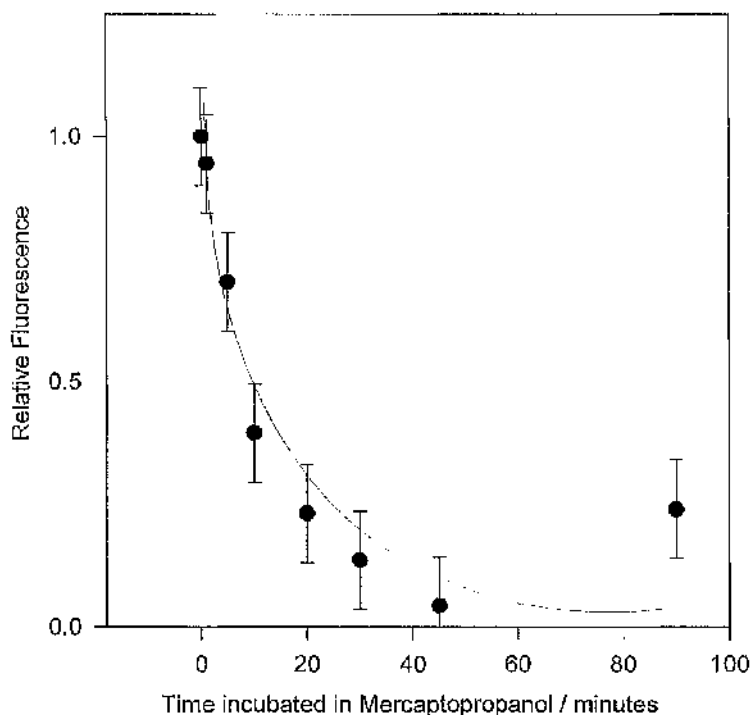
Figure 5.9 – Shows a plot of the change in the fluorescence observed at mercaptoethylamine modified gold samples after immersion in 1 mM mercaptopropanol for a specified time period, followed by the glutaraldehyde mediated immobilisation of FITC-labelled goat anti-rabbit IgG. (λ_{ex} 494 nm - λ_{em} 520 nm). Reading normalised to a pure mercaptoethylamine monolayer, modified with FITC-labelled goat anti-rabbit IgG.

This decrease in fluorescence is consistent with a reduction in the number of available surface amine groups as demonstrated by both XPS measurements (Chapter 2) and cytochrome c electrochemical characterisation (Chapter 3). In this manner we can, therefore, demonstrate control over the amount of protein bound to the SAM and as such this method shows that the immobilisation environment can be manipulated to control the nature of the sensing device.

5.3.2 Immobilisation of Fluorescent Antibodies - Continuous Gradient

Having obtained control over the quantity of protein immobilised at any one surface, the possibility of producing gradients of proteins over a single gold surface was also investigated.

A gradient of immunoglobulin was produced on a gold surface by slowly increasing the amount of the displacing (secondary) thiol in a purpose built glass slide holder containing an evaporated gold covered glass slide **Figure 5.3**. IgG was immobilised at this monolayer by amine directed glutaraldehyde immobilisation of FITC-Labelled goat IgG. Fluorescence measurements were taken at discrete intervals along the length of the slide, as described above (Section 5.3.1). The results **Figure 5.10** show how a gradient of fluorescence exists along the length of the slide, indicating that a gradient of immobilised IgG exists along the length of the slide.
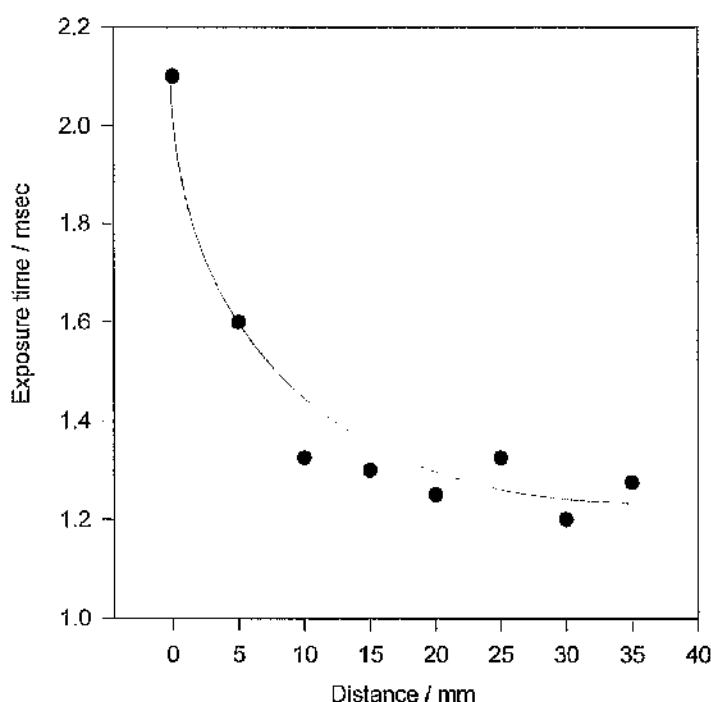
Figure 5.10 - Change in the fluorescence observed along a mercaptoethylamine modified gold slide after the immersion in 1 mM mercaptopropanol as shown in **Figure 5.3**, followed by the glutaraldehyde immobilisation of FITC-labelled goat ant-rabbit IgG. (λ_{ex} 494 nm - λ_{em} 520 nm). The distance along the slide is proportional to the time spent in the displacing thiol, hence the decrease in immobilised protein as the slide is traversed.

This method shows that thiol and hence protein gradients can be produced over the distances required (a few millimeters) for both microsensor calibration strips and cellular engineering experiments. Further investigations are, however, required using more sensitive spectroscopic techniques such as XPS or FT-iR in order to allow more detailed characterisation of these monolayers.

110

5.3.3 Fabrication of Protein Gradients Using Competition for Avidin Binding Sites.

The use of competition between biotin and biotinylated proteins for a limited number of streptavidin binding sites was also investigated as a means of creating protein gradients **Figure 5.5**. Optimal gradients were attained when a solution of biotinylated HRP was mixed with biotin to give various solutions, all containing 1 μg ml^{-1} of biotinylated-HRP and between 0 and 1 ng ml^{-1} of free biotin. These mixtures, when added to streptavidinated 96 well microtitre plates, gave protein gradients as indicated by the change in optical density after addition of a TMB substrate assay system (Sigma, UK) **Figure 5.11**.
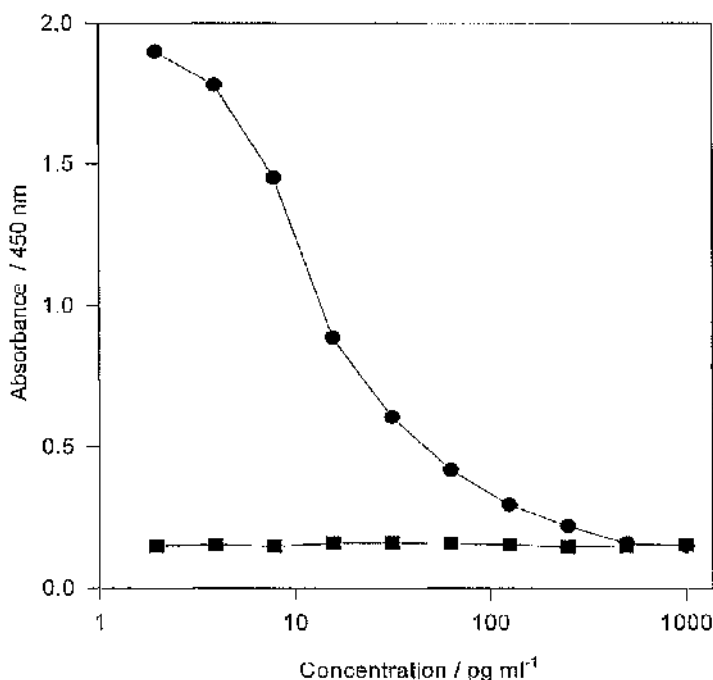
Figure 5.11 – A plot showing the change in optical density across a streptavidinated 96 well microtitre plate as a function of the concentration of free biotin. As the amount of free biotin increases, so less biotinylated horseradish peroxidase HRP can bind. The reaction mixture added to each well contained a 1μg ml^{-1} of biotinylated HRP with increasing concentrations of free biotin from 0 - 1000 pg ml^{-1} (●). A similar change in optical density was not observed when the reaction mixture only contained 0 - 1000 pg ml^{-1} free biotin (■).

The absorbence is seen to decrease with an increasing amount of free biotin included in the reaction solution. In cases where either HRP (unbiotinylated) or only free biotin are used instead of biotinylated HRP, the absorbence is no greater than background (0.15) and a similar change in absorbance is not observed.

The change in absorbence is, therefore, as a direct consequence of the increased competition between biotinylated protein and free biotin in solution, resulting in fewer HRP molecules becoming tethered to the microtitre plate via the biotin/streptavidin interaction.

A 2 μg ml^{-1} biotinylated HRP solution was considered optimal as at this concentration the maximal absorbence observed was within the dynamic range of the spectrophotometer. Concentrations between 1 and 5 μg ml^{-1} are also commonly acknowledged to give good binding to surfaces[172].

The biotin-streptavidin system, as with the biotin-avidin system, has characteristics that make it ideal for use in a diverse range of applications, with particular relevance to immobilisation and sensing systems[173,174]. For example, Streptavidin has the ability to bind the vitamin biotin **Figure 5.12** with an unusually high affinity **Figure 5.13**. This very specific non-covalent interaction has an affinity constant of *ca.* 10^{15} M^{-1} = 80 KJ mol^{-1}, close to a covalent bond, which is in general 10^3-10^6 times greater than those of antibodies for their particular ligands[175] (N.B. This figure is for the solution phase and may be less for unfolded protein close to the surface). This strong bond ensures that the complex is stable despite large environmental changes (e.g. pH, temperature). The specificity also ensures a low degree of cross-reactivity.

Streptavidin is tetramic and as a result possesses four biotin binding sites. This allows for a high degree of amplification to be built into sensing systems that are based on biotin/avidin interactions. This tetramic nature also allows the streptavidin moiety of a streptavidin/biotin sensing system, to undergo immobilisation procedures, without a concurrent loss of biotin binding capability[175].

Biotin is a small molecule (244.31 Da) **Figure 5.12** and can be bound to macromolecules such as proteins having little or no effect on their biological activity[175].
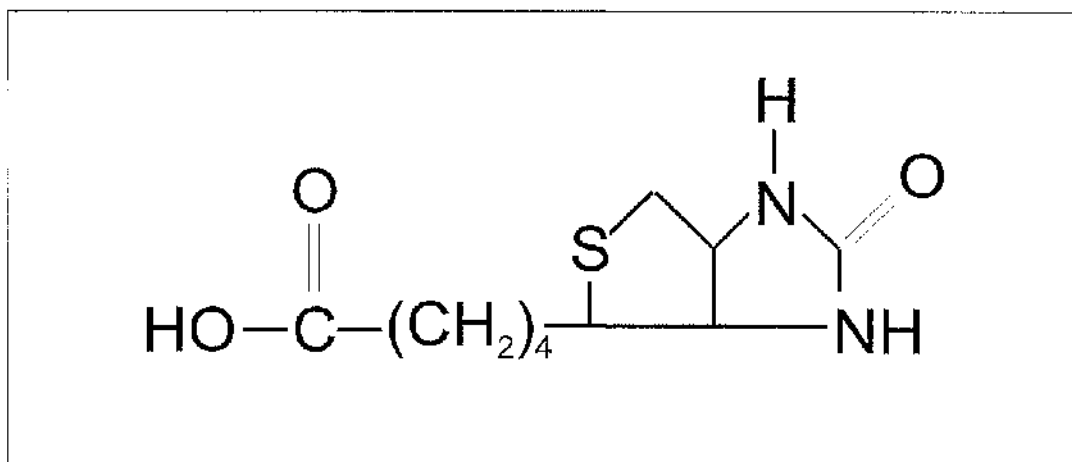
Figure 5.12 - Biotin.

Although avidin also possesses the same properties described above, streptavidin is often used in preference, especially for sensor applications, as a result of its ability to produce a surface which is not susceptible to NSB from other proteins. The susceptibility of avidin to non-specific adsorption is a consequence of both its high pI value (ca. 10) and its glycosylation (avidin contains both mannose and N-actylglucoseamine)[173].

In a streptavidin/biotin based system, a wide range of molecules can be biotinylated including, proteins, nucleic acids and polysaccharides. For each class of compounds, a variety of procedures has been developed[176]. In the case of proteins, the vast majority of proteins can be biotinylated via N-hrdoxy-succinimide ester linkages to the ε-amino groups of lysines within the protein. Gradients made using the streptavidin/biotin relationship, are very stable and also have the capability to be used in a wide variety of circumstances linking with a number of different binding and immobilisation strategies, as illustrated in the following sections.
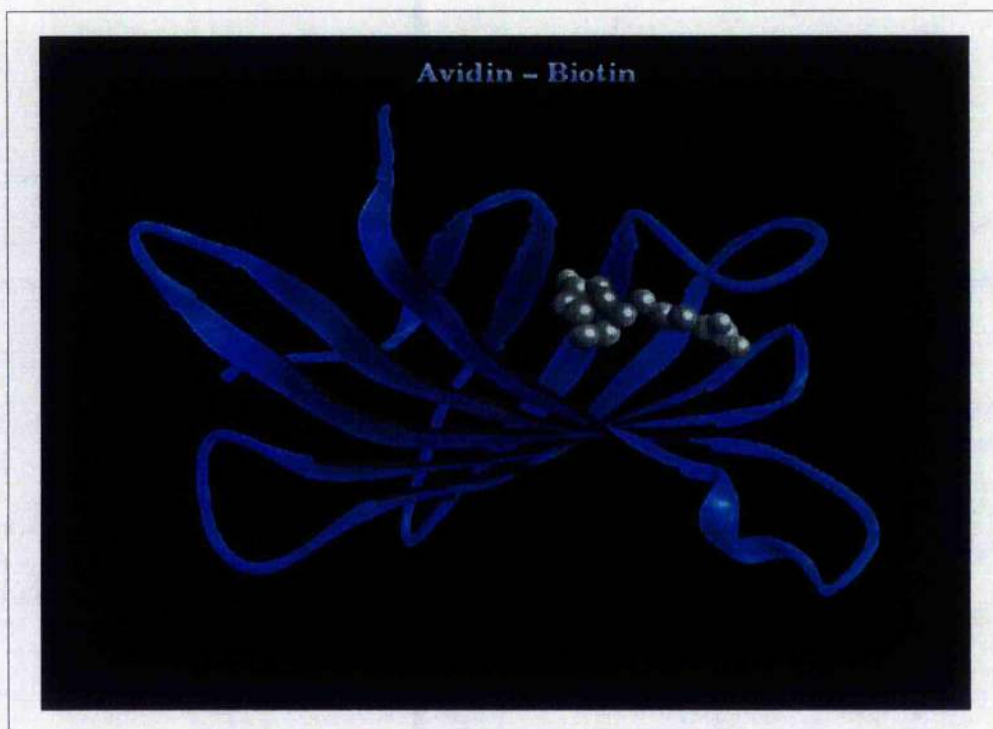
Figure 5.13 - Structural diagram showing an avidin sub-unit binding biotin.

5.3.3.1 Streptavidin Gradients for Immunosensing.

Streptavidinated plates were used in a protocol similar to that described above in order to control the immobilisation of antibody in a manner suitable for the production of gradients. **Figure 5.14** shows the change in optical density observed when varying concentrations of biotinylated antibody are incubated with increasing concentrations of free biotin.

114
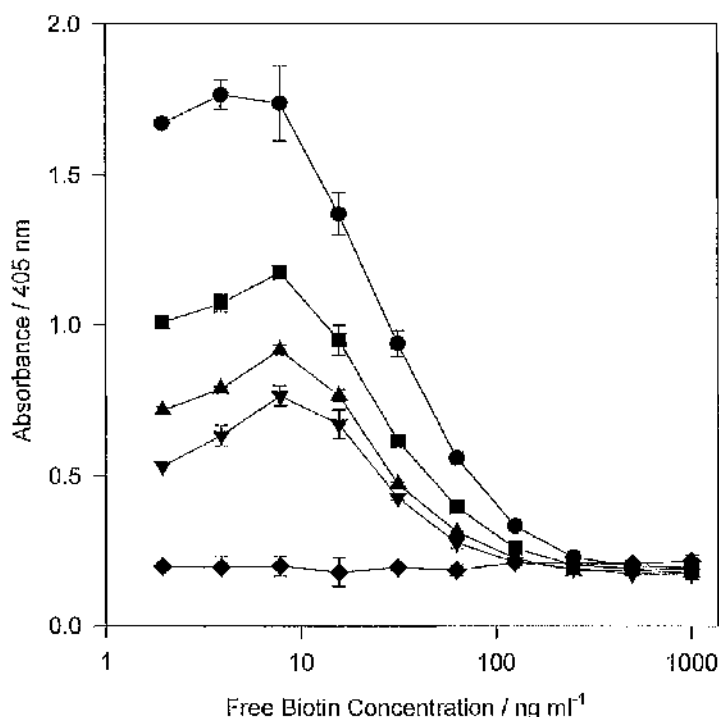
Figure 5.14 – Shows a plot of the change in the optical density across a streptavidinated 96 well microtitre plate as the concentration of free biotin increases resulting in the binding of less biotinylated antibody. Biotinylated goat IgG dilutions 1/1000 (●), 1/2000 (■), 1/4000 (▲), and 1/8000 (▼) of a 50 μg ml^{-1} stock solution. A similar change in optical density was not observed when the reaction mixture contained 0 - 1000 pg ml^{-1} free biotin (◆) and unbiotinylated IgG. To each well 100μl of a 1/1000 dilution of 50 μgml^{-1} phosphatase labelled rabbit anti-goat IgG was added.

It is interesting to note that, for those gradients shown in **Figure 5.14**, the absorbence measured initially rises on addition of free biotin, before dropping off to background levels. This is probably due to steric hinderance preventing binding of the secondary antibody to the primary body as illustrated schematically in **Figure 5.15**. As the free biotin competes for some of the binding sites, the primary antibody is no longer sterically inhibited and is able to bind to the secondary antibody, leading to an initial increase in binding, results which concur with similar observations of others[42,43,48].

115
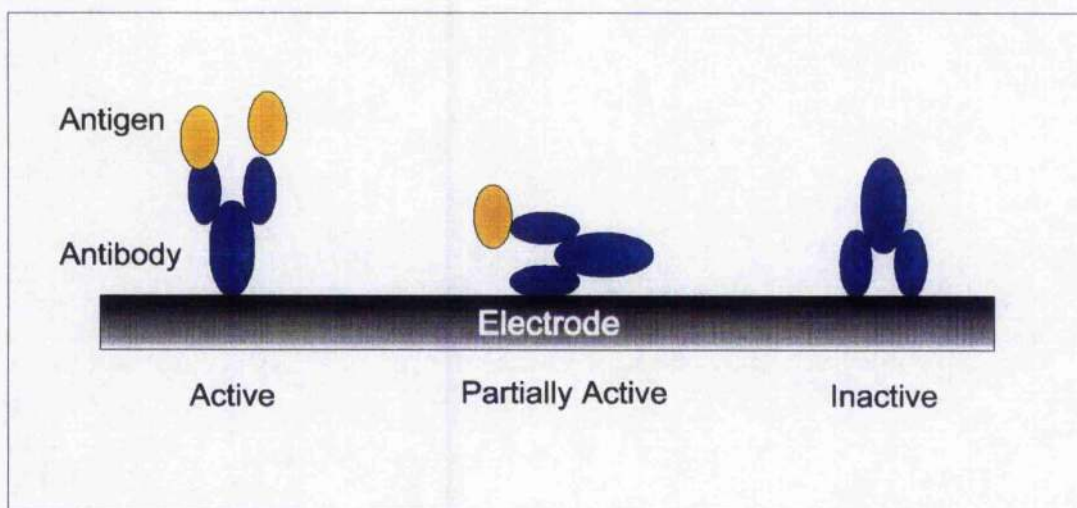
Figure 5.15 - The effect of orientation on antibody activity. For an protein to be active once bound to a surface, the antigen/substrate binding sites must be accessible to the solution phase.

The method of detection involved the addition of a secondary sensing antibody which was coupled to the reporter enzyme alkaline phosphatase. as illustrated in **Figure 5.8(3)**. The optimal concentration of this secondary antibody was found to be a 1 in 8000 dilution of the supplied solution. **Figure 5.16** shows how higher concentrations yielded absorbencies greater than 2, which was considered beyond the (linear) dynamic range of the spectrophotometer.
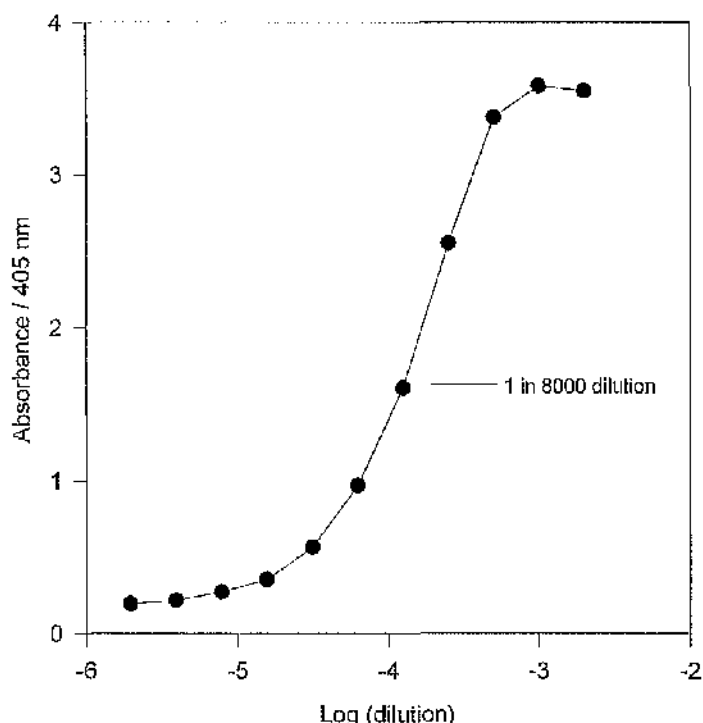
Figure 5.16 - Optimisation of detection antibody dilution for biotinylated-IgG immobilised at streptavinated microtitre plates. 1 in 1000 dilution of a 50 µg ml^{-1} biotinylated IgG incubated for two hours at room temperature. A 1 in 8000 dilution of detection antibody is seen to give optimal absorbence after colour development in pNPP liquid substrate system for 30 minutes prior to addition of stop solution and absorbence measured at 405 nm.

The use of the competition between biotin and biotinylated proteins for streptavidin can therefore be used as a means of controlling immobilisation at a surface in such a manner as to be appropriate for protein gradients. The use of this system does pose one further possible advantage of offering some control over the orientation of the proteins concerned. The loss of biological activity which is often associated with antibody immobilisation is believed to be attributed to the random orientation of antibodies at the surface[167]. It may, therefore, be possible to immobilise antibodies at a surface, controlling the proteins orientation, without the concurrent loss of activity usually observed, due to steric hindrance.

117

5.3.3.2 HRP Gradients Prepared for Electrochemical Detection

By controlling the composition of the alkanethiol monolayer to which a protein is tethered, and also the manipulation of the competition for streptavidin binding sites, we have shown that it is possible to create protein gradients on gold (Section 5.3.1 and 5.3.2). Combining these two methods we are able to demonstrate a possible secondary level of control over the immobilisation of proteins to gold surfaces.

Initially, by cross-linking a streptavidin monolayer to a SAM of amine terminated thiols on gold, we created a surface at which biotin and biotinylated proteins would be bound (by the streptavidin). The manipulation of the ratio of free biotin to biotin-HRP in the reaction mixture (in which the streptavidinated gold working electrodes were immersed), allowed control over the amount of HRP immobilised.
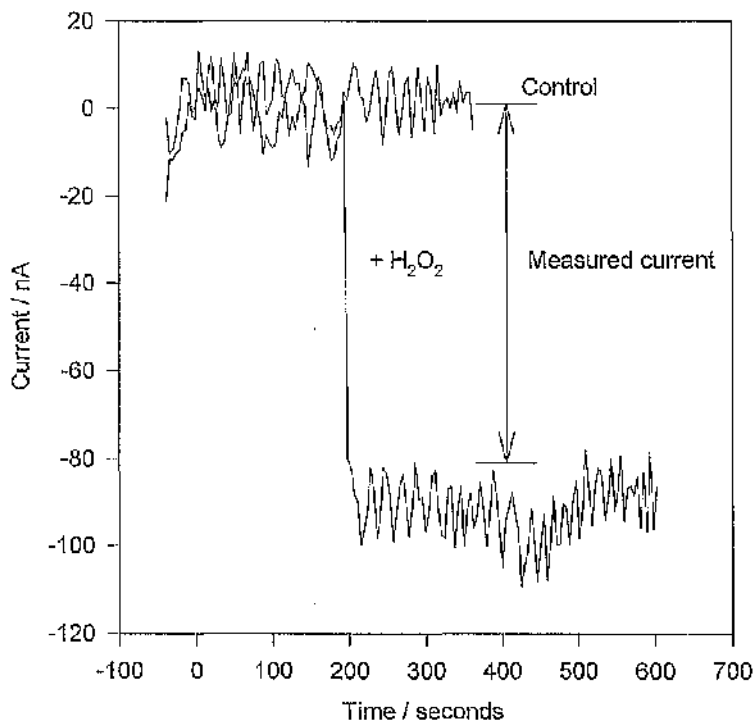
Figure 5.17 – Shows a plot of i-t measurements taken at gold electrodes modified with biotinylated HRP, bound through avidin covalently attached to thiol SAM. The electrode was poised at 0 mV versus a Ag|AgCl reference electrode. The control measurement shows the current measured on the addition of H_2O_2 when only unbiotinylated HRP is included in modifying solution containing free biotin. In those cases where biotinylated HRP is included a corresponding increase in current is observed, when a steady state was achieved the difference between the control measurement and this increase was recorded.

The change in current observed at these electrodes was recorded upon the addition of 10 mM H_2O_2 in the presence of 0.5 mM ferrocene (held at 0 V vs Ag|AgCl reference)

Figure 5.17. These conditions were optimised by varying the concentrations of both hydrogen peroxide and ferrocene independently of each other.

As the free biotin in solution increases, the measured current on the addition of H_2O_2 was shown to decrease **Figure5.18.** Although an increase in acidity is known to disrupt the avidin biotin bond, the buffer used is considered to quench the local changes in pH produced by the oxidation of hydrogen peroxide[105]. In addition, this change is in accordance with those observed in colourimetric studies, and is most probably as a consequence of the decrease in bound protein as competition for binding increases with addition of free biotin.
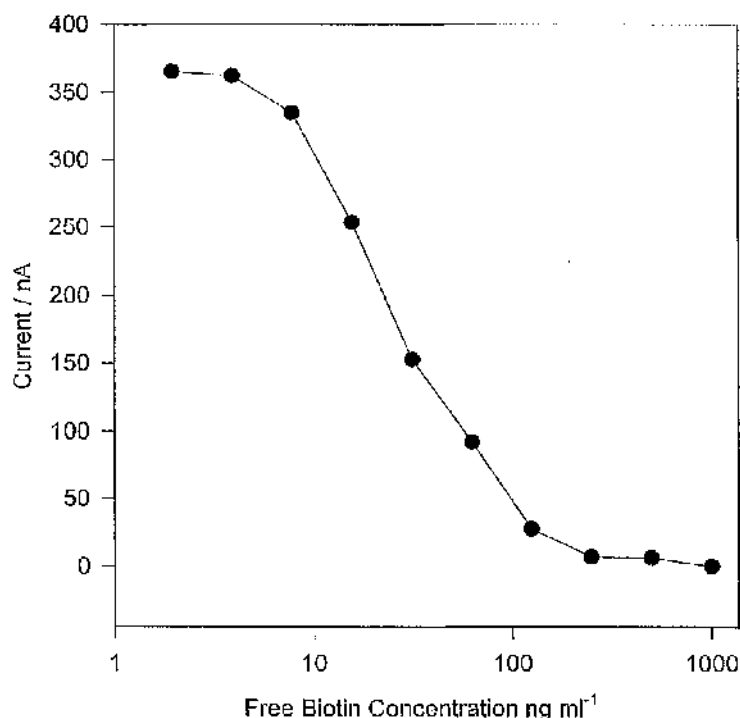
Figure 5.18 – Shows a plot of the change in steady state current measured at gold electrodes previously modified with avidin immobilised to an alkanethiol SAM, after incubation in solutions containing constant biotinylated HRP concentrations (1 μg ml⁻¹) and increasing free biotin concentration. Current was measured by recording i-t curves on the addition of 10 mM hydrogen peroxide. The working electrode was held at 0 mV vs. Ag|AgCl reference electrode, in the presence of 0.5 mM FMCA in PBS.

119

5.4 Conclusions

We have presented four methods of controlling the immobilisation of proteins at electrode surfaces. These methods are all appropriate for creating gradients with respect to time and space over micron scale distances. These gradients as well as being suitable for on sensor calibration applications are also appropriate for investigations into cellular behaviour at bio-material surfaces.

By combining the control at the primary level, i.e. that of an alkanethiol SAM, with control through avidin immobilised at this layer, we have demonstrated how to manipulate the molecular architecture in a multi-layer system.

There has recently been an increased scientific interest in the miniaturisation of devices, as a consequence of the given analytical advantages. With miniaturisation, however, any loss of protein activity can have more extreme effects than those in macro scale devices. Methods such as these, where the nature of immobilisation and the local environment can be manipulated to give optimal conditions will therefore become more important.

CHAPTER 6: MICROFABRICATED ELECTRODE ARRAYS FOR IMMUNOASSAY APPLICATIONS

6.1 Introduction

Recently the number of chemical compounds held in the 'libraries' of both companies and research laboratories has increased dramatically lately, most probably as a direct result of advances in the methods for purification of compounds from natural products and the novel chemical synthesis of compounds. For example, using combinatorial chemistry[14,177-180], a single chemist can synthesise a library in excess of 50,000 compounds in a single day **Figure 6.1**.

High-throughput screening (HTS) is the automated testing of these large numbers of library compounds for their activity as inhibitors (antagonists) or activators (agonists) of a particular biological target, such as a cell-surface receptor or a metabolic enzyme[15,16,181]. With such large libraries to test, advances in screening technologies are paramount. In conjunction with developments in robotic screening, gains in throughput have been achieved by way of the miniaturisation of assay systems[14]. As well as enhancing throughput, miniaturisation may also has the simultaneous benefit of reducing cost. As a consequence, there have been intensive efforts to produce arrays of miniaturised sensing devices which are suitable for high-throughput screening applications, particularly for optical assays. Concurrently, the use of microfabricated devices to perform electrochemical measurements has also attracted much attention in the last decade. In one area of particular interest, micro-sensors have been employed to perform both cell based and enzyme based electrochemical assays[59,61,62,182]. Most devices fabricated at present have consisted of systems designed with a single sensing area, and, as a result are not directly applicable to HTS. However, the production of arrays of micro-sensor systems would have potential applications to HTS.
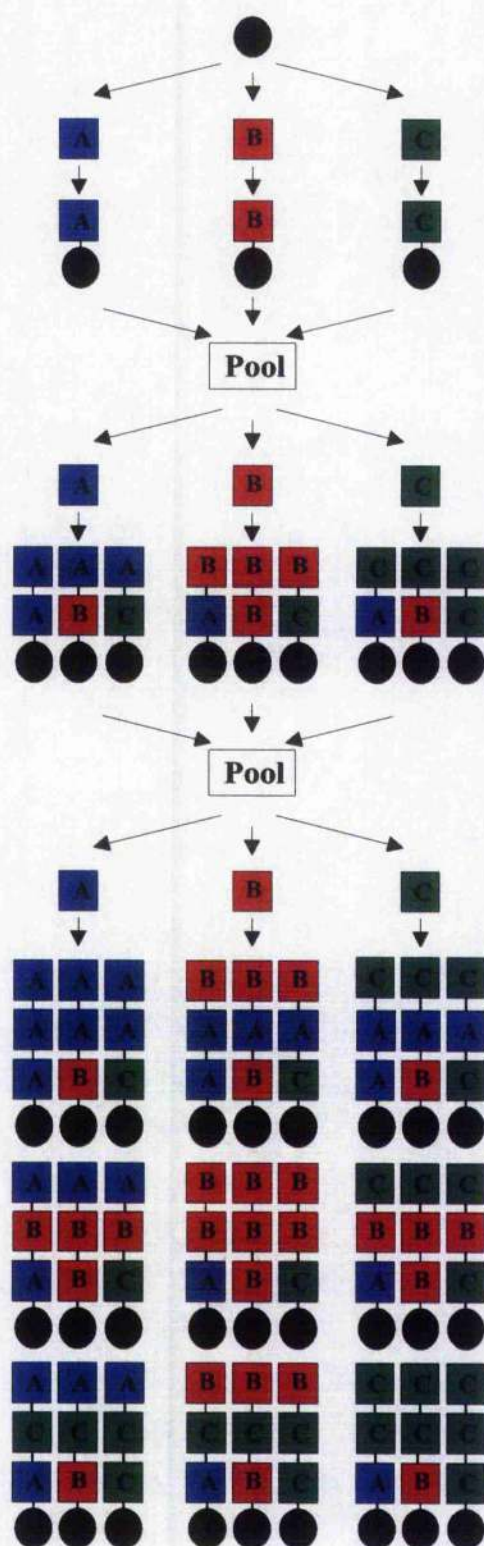
Figure 6.1 - Combinatorial chemistry on solid supports using the split resin method, first described by Furka *et al.*, whereby the peptide synthesis beads are divided for chemical coupling steps, then combined, mixed to homogeneity and subdivided for subsequent reactions.

The use of electrode arrays to perform electrochemical assays has several likely advantages over optical systems. Fluorophores are, by their nature, environmentally sensitive[183,184] and their activity changes easily, for example with pH. Moreover, as electrochemical assays are not dependant on either transmitted or absorbed light they are suitable for use on turbid or opaque solutions such as cell culture or whole blood, offering a system which is less prone to error resulting from 'cross talk' between samples. Electrochemical assays do however have the disadvantage that they have to be 'read' serially and not in parallel as is possible for optical assays[93].

Although a great deal of work has been focused on the fabrication of micro-electrode arrays[96-101], few examples use arrays of individually addressable electrodes. Some electrochemical array systems have been developed consisting of a microplate reader equipped with a single electrode probe which is placed, in turn, into each well. These systems primarily utilise Enzyme Linked Immuno-Sorbent Assay (ELISA) systems carried out in standard sized microwells[106]. The potential advantages of these assay systems have not, however, been realised due to passivation of the working electrode surface after successive visits to microtitre chambers. Such passivation is caused by a combination of various factors, such as deposition of impurities and the formation of insoluble films, oxides, and protein adsorption, resulting in a short working lifetime of the electrode[106].

In this chapter we describe a model micro-array system for the fabrication of disposable arrays of 8μl wells, each well possessing its own planar electrode configuration, thereby negating the problem of passivation. The device consists of a glass slide photo-lithographically patterned with a planar array of metallic electrodes, with dimensions equivilent to that for an 864 well format (864 wells in a 10 x 10 cm area), if extended over a suitable area. A plastic template, consisting of machined plate with 2mm diameter holes, is chemically bonded to the patterned glass slide. The resulting arrays of wells all possess individually addressable working electrodes and common counter and reference electrodes **Figure 6.2**.

The feasibility of creating micro-chamber arrays made wholly of plastic with photolithographically defined gold electrodes has also been investigated, as well as a third fabrication protocol, making such wells by a non-photolithographical method. All devices have been characterised through the analysis of the electrochemical behaviour of the model redox compound, ferrocene mono-carboxylic acid (FMCA), at the working electrode. FMCA has traditionally been used as a standard for such studies not only because it is electrochemically well behaved in aqueous solutions (such as biological buffers), but because it has received much attention for its role as an electron-transfer mediator for many redox enzymes[73].

As stated, the size of wells fabricated by 'machining' are comparable to those in use at present by international pharmaceutical companies in an 864 well format[14]. The use of photolithographic patterning also offers the potential for significant reduction in device proportions (i.e. "1536" format). In order to demonstrate the applicability of such devices to biological assays systems, microwells were used to perform simple enzymatic electrochemical assays using horseradish peroxidase, HRP, as a model detection method, thereby enabling direct comparisons with a commercially available HRP based enzyme linked immuno-sorbent assay.
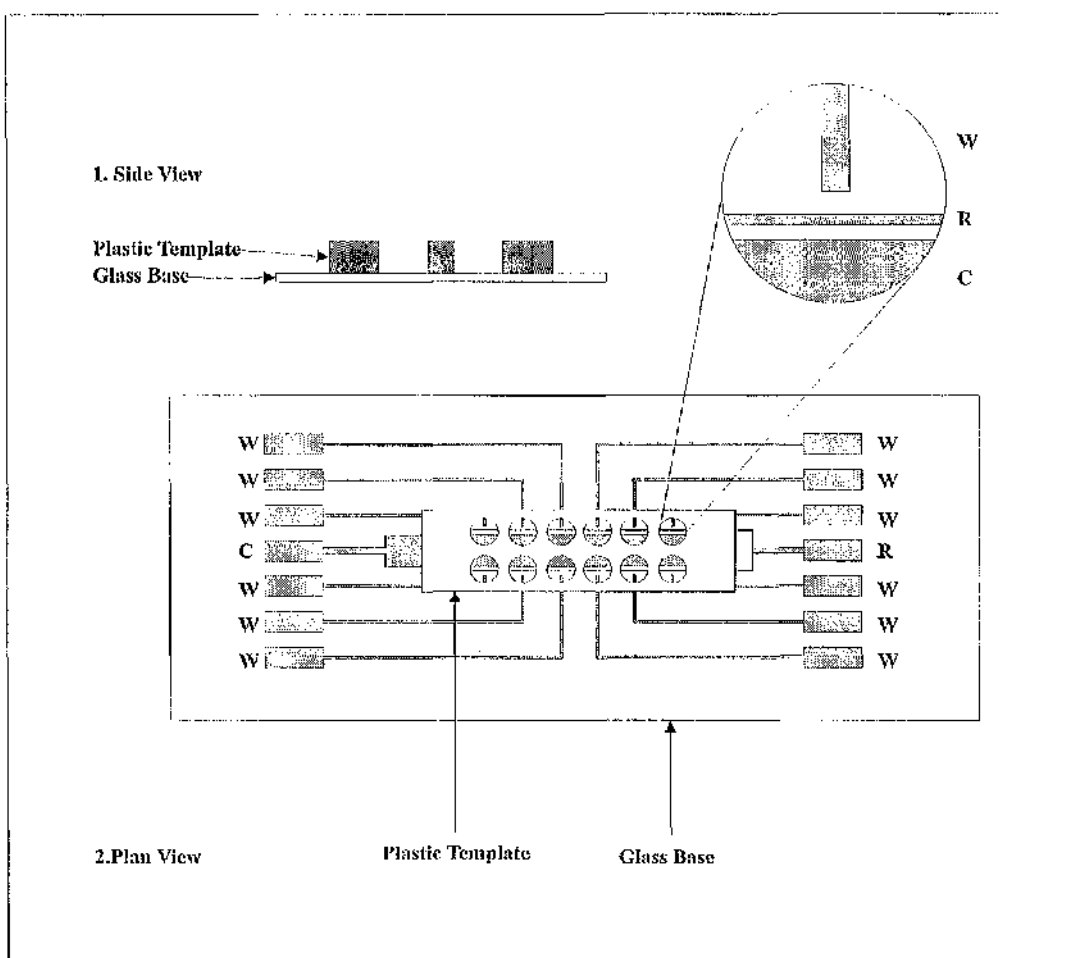
Figure 6.2 - Diagram to represent the electrode layout of a 12 well (864 format) electrode array fabricated using plastic/glass hybrid structures. In the case represented the device is fabricated from a glass/plastic composite - the plastic template defining the wells. Each well has a diameter of 2mm and a 1mm thickness containing a three electrode configuration, consisting of a common reference **R** and counter electrode **C**, with an individually addressable working electrode **W**.

6.2 Experimental Section

6.2.1 Materials

Unless otherwise stated all chemicals and solvents were purchased from Sigma (Poole UK) and used without any further purification. Phosphate buffered saline PBS solutions (10 mM potassium phosphate buffer, 2.7 mM potassium chloride and 137 mM sodium chloride) were also purchased in 'tablet form' from Sigma (Poole, UK) and made up to the appropriate volume by the addition of reverse

125

osmosis (RO) ultrapure water (Millipore, UK). Marco sized gold electrodes were fabricated using standard photolithographic procedures, as described in section 6.2.2. The materials used, titanium (Ti), palladium (Pd) and gold (Au) were purchased, from Goodfellows (Cambridge, UK), as were all other metals and plastics used. In addition, a Ag|AgCl reference electrode (MF-2063) was obtained from BioAnalytical Systems (Luton, UK). Horseradish peroxide HRP type IV (Sigma, UK) was reconstituted to 500 μg ml^{-1} in PBS (pH 7.4) and stored in 100 μl aliquots at -20°C. Ferrocene monocarboxylic acid FMCA 0.5mM was prepared immediately prior to use by dissolving 5.75mg FMCA in 2 ml methanol and making up to 50 ml by the addition of 20mM phosphate buffer pH7 (containing 100mM sodium perchlorate as the supporting electrolyte).

6.2.2 Microfabrication

Photolithography, described in detail in **Section 4.2** and illustrated in **Figure 6.3**, was used to fabricate both 2mm macro electrodes, which were used in reference electrode tests as well as the miniaturised bio-analytical assays.

6.2.2.1 Substrate Cleaning

Cleaning of the samples prior to photolithography was carried out in a manner dependant upon the specific fabrication process:

1. Glass samples were cleaned by sonication for 5 minutes in each of the following cleaning agents: Opticlear™ (G&S Inc.); acetone; methanol; and finally reverse osmosis (RO) water.
2. Due to the susceptibility of polystyrene to dissolution in acetone an alternative method of cleaning was used, where samples were sonicated for 20 minutes in a 1:1 mixture of Decon 90 (Decon Labs Ltd.) and RO water.

After either of the two routines described, the samples were dried in a stream of nitrogen, and then baked for 10 minutes at 50°C, in order to ensure removal of any remaining residual water.

126
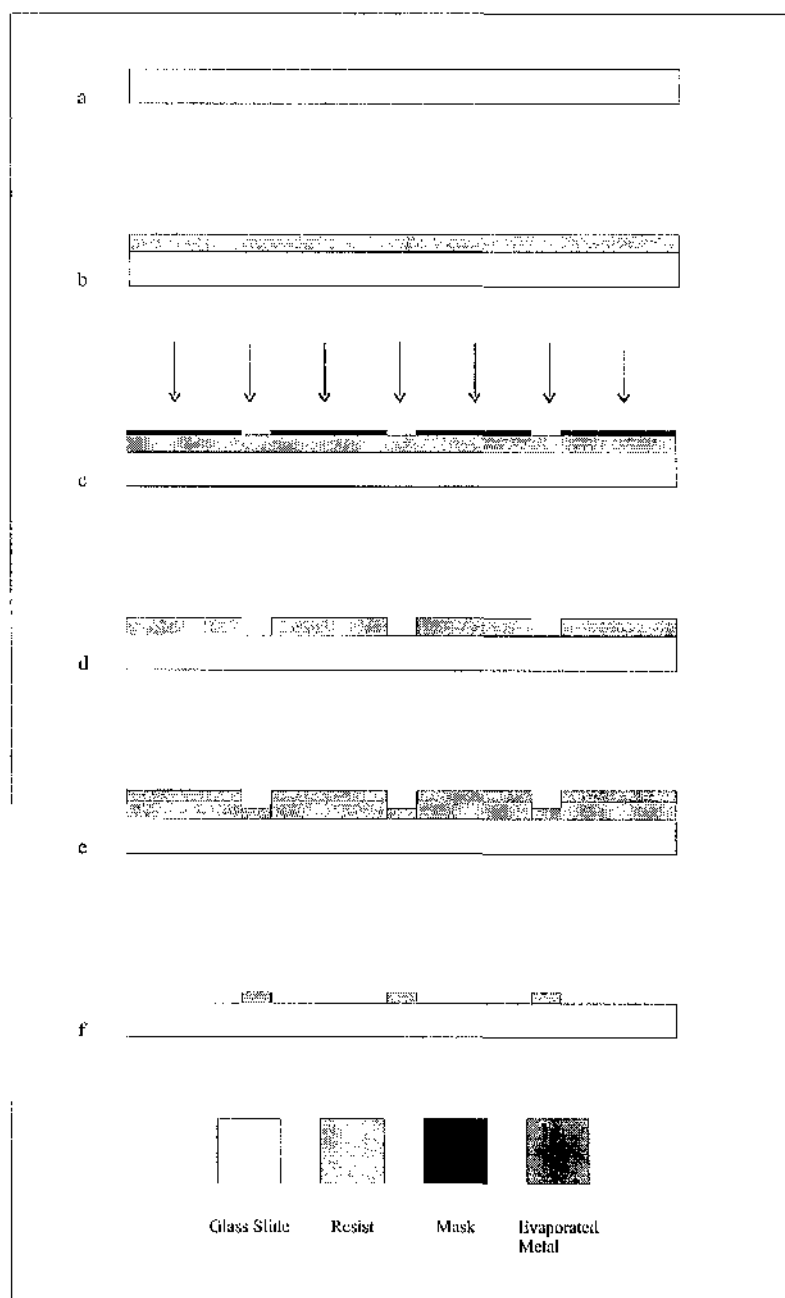
Figure 6.3 - Gold electrodes were prepared by photolithography followed by electron-beam evaporation of a Ti/Pd/Au (10/10/100 nm) multi-layer structure. A clean glass (or plastic) substrate **A** was coated by a 1.8 μm layer of S1818 resist (Shipley, UK) by spinning for 30 seconds at 4000 rpm, **B**. The required electrode pattern was transferred to the resist, by UV exposure through a ferric oxide mask (14 seconds, Hybrid Technology mask aligner, 32J cm^{-2}, 364nm), **C**. After developing for approximately 80 seconds in Microposit developer (1:1 mix with RO water) **D**, the multilayer metal structure was deposited by e-beam evaporation using a Plasyss QD1 automated e-beam evaporation system **E**, performing 'lift-off' by dissolving the resist in acetone the metal remaining defined the electrodes **F**.

6.2.2.2 Photolithography

In brief samples were spin-coated (at 4000 rpm) with S1818 resist (Shipley Inc.), which had been pre-filtered using a 0.25μm particle filter. In order to define metallic electrodes with clean, sharp edges, after fifteen minutes baking time at 90°C, glass samples where soaked for 10 minutes in chlorobenzene, prior to a further fifteen minutes bake, also at 90°C. Since polystyrene is also soluble in chlorobenzene these samples were baked at 90°C for 30 minutes (but omitting the chlorobenzene soak). Patterning of the photoresist was achieved by UV exposure through a purpose made ferric oxide photomask, for 14s on a Hybrid Technology mask aligner, (photon flux = 32J cm^{-2}, λ = 364nm). The pattern was developed by the immersion of the sample, for approximatly 80 seconds, in Microposit developer (Shipley Inc.) mixed 1:1 with RO water. Samples were finally dried in a stream of nitrogen and then baked for 10 minutes at 50°C to remove any residual water.

6.2.2.3 Metal Evaporation and Lift-off

Metals were deposited by electron beam evaporation (Plassys QD1 automated e-beam evaporation system), as a Ti/Pd/Au (10:10:100nm) multi-layer structure. This well established recipe provides excellent adhesion of the electrode to the underlying substrate and gives good electrochemical stability at high oxidative potentials. A 30 nm layer of nickel - chromium (60:40) (NiChrome) was also evaporated on to the electrode structure, which could be removed by etching with a standard nichrome etch (3.5 ml glacial acetic acid and 20 g ammonium ceric nitrate dissolved in 100 ml of RO water). This final evaporated layer served as a sacrificial protective coating and enabled electrodes to be produced which were "clean" (i.e. free from particulate contamination). Following electron beam evaporation of metals, the electrode patterning was finally achieved by the 'lift-off' of the remaining photoresist. For those samples patterned on glass, an acetone 'lift-off' incubation was used, otherwise plastic samples were placed in propan-2-ol. In either case the 'lift-off' procedure was continued until the

electrode pattern had been clearly developed. Finally it was necessary to take the sample from the 'lift-off' solution whilst under a flow of RO water, in order to ensure that none of the metal particles re-adhere to the sample.

6.2.2.4 Silicon Nitride Deposition

In order to define the electrode area when a glass substrate was used, a 500nm layer of insulating silicon nitride was deposited over the whole sample by plasma enhanced chemical vapour deposition using an Oxford Plasma Technology μP-80 (deposition rate *ca.* 10 nm min^{-1}). This layer of nitride was photo-patterned as described in section 6.2.2.3 (*In brief: spinning of a photoresist layer, prior to UV exposure through ferric oxide mask and finally development in Microposit developer*). The unwanted nitride removed by reactive ion etching in C_2F_6 with a standard etch rate of 50 nm min^{-1} at 100W (Oxford Plasma Technology BP-80, 30sccm flow rate, 10 mT). Finally before an RO water wash and dry as described previously (section 6.2.2.1) any residual resist was removed by soaking in acetone.

Note: The nitride deposition temperature occurs in excess of 300°C, and as such it was not possible to define the electrode areas in this manner for those devices made using a plastic base. In such cases electrode areas were calculated and normalised with ferrocene monocarboxylic acid using standard electrochemical techniques described later.
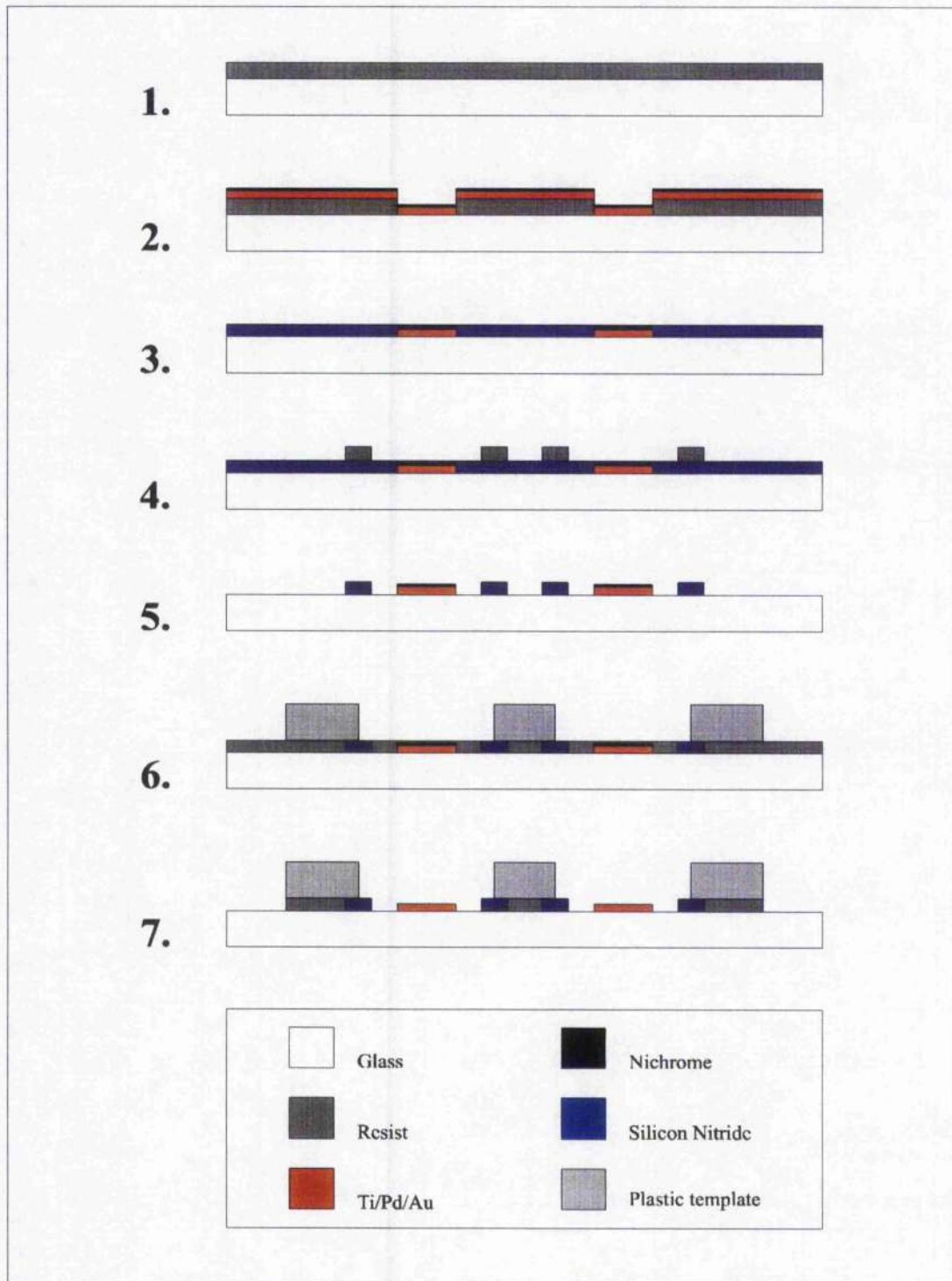
Figure 6.4 - The steps in the fabrication process for glass/plastic electrode arrays. Initially a layer of photo resist is spun onto a glass substrate prior to patterning and metallisation **1** + **2** (see Figure 6). The surface is then covered by a 500 nm layer of silicon nitride by plasma enhanced chemical vapour deposition **3**, which is photolithographically patterned **4** to define the working electrodes areas before dry etching **5**. Finally a further layer of photoresist is spun in order to act as an adhesive layer for the plastic template **6**. Sacrificial nichrome layer is removed by wet etching prior to use **7**.

6.2.3 Microchamber Formation

Micro-chambers and micro-chamber arrays were formed by machine drilling 2mm diameter holes in 1mm thick polystyrene and poly-methylmethacrylate PMMA. In those cases where micro-chamber arrays were formed the holes had a 3mm pitch (centre-centre).
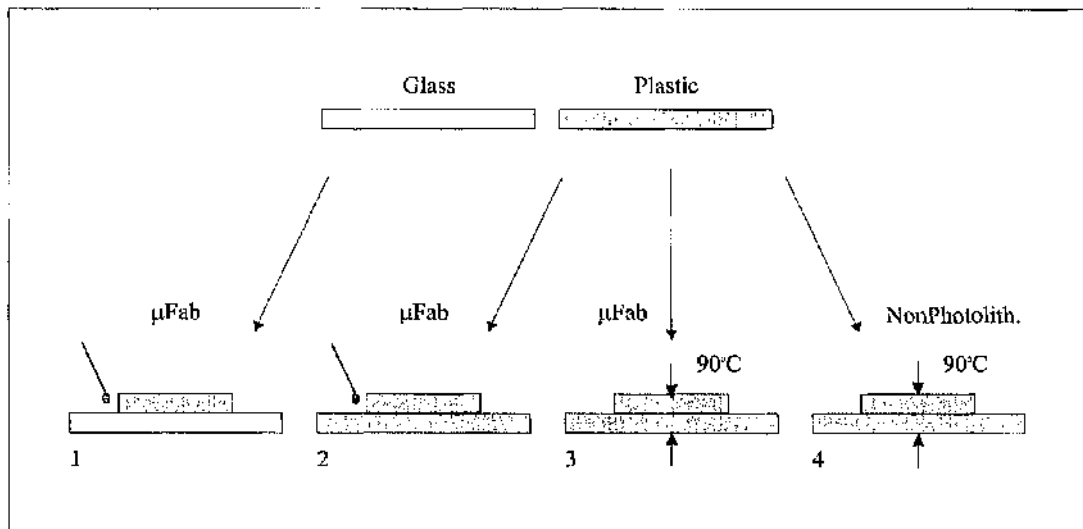
Figure 6.5 - Diagrammatic representation of the different fabrication methods used. Electrodes were incorporated onto a glass or plastic base using microfabrication (μFab) or non-photolithographic methods. A plastic template defining the wells was then attached by either chemical or thermal adhesion. The resulting devices were as follows:
1. A glass base, with microfabricated electrodes and a chemically attached plastic template;
2. A plastic base, with microfabricated electrodes and a chemically attached plastic template;
3. A plastic base, with microfabricated electrodes and a thermally attached plastic template;
4. A plastic base, with non-photolithographically defined electrodes and a thermally attached plastic template.

6.2.3.1 Glass/Plastic devices.

Shipley S1818 resist was spun onto the patterned electrode sample to act as an adhesive layer. After baking for 30 minutes at 90°C, the machined PMMA micro-chambers were carefully aligned over the silicon nitride insulating pattern, clamped and 20μl of chloroform was applied to the plastic/glass interface. Capillary forces drive the chloroform across the electrode array, bonding the two layers together. After approximately 2 hours any remaining resist was removed

by thorough rinsing in propan-2-ol, prior to the removal of the sacrificial Nichrome layer before use (see section 6.2.2.3). The method is represented schematically in **Figure 6.5**.

6.2.3.2 Plastic/Plastic Chambers

In cases where the electrodes had been patterned onto a polystyrene substrate, the wells were defined by bonding a machine drilled polystyrene template, using either a chemical or thermal method of adhesion. Chemical adhesion was achieved by clamping the two layers together and the application of a drop of cyclohexane at the plastic/plastic interface in a similar fashion to that for the glass/plastic device. Alternatively the clamped pieces could be heated to 95°C for 30 minutes in order to thermally bond the two samples **Figure 6.6**.

In either case the protective sacrificial Nichrome layer was removed as described above, prior to the further use of the devices. The inclusion of membranes into this fabrication process was also investigated by incorporating a small piece of poly-acetate membrane into the sandwich prior to thermal adhesion.
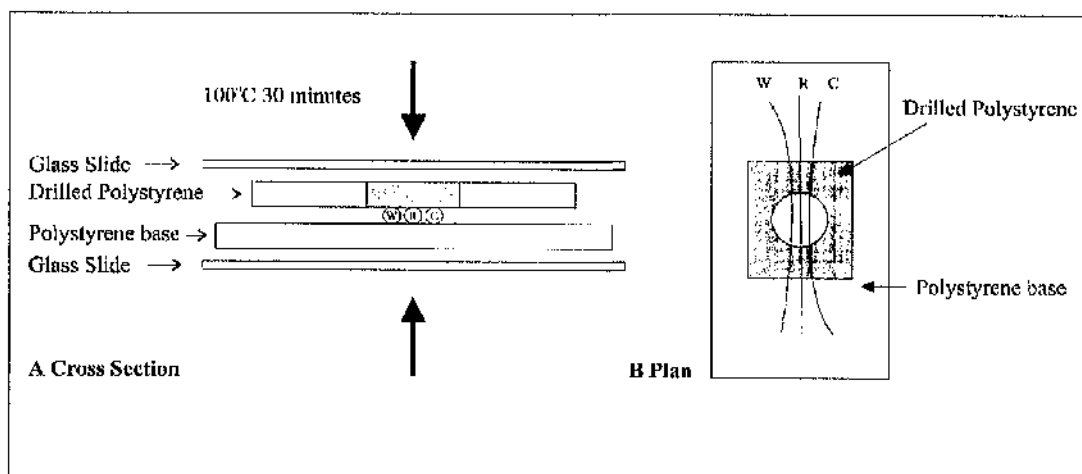
Figure 6.6 - Production of non-microfabricated device. The polystyrene sandwich is clamped and heated at 100°C for 30 minutes. The electrodes are formed by metal wires held within the plastic sandwich - W a working electrode (consisting of 250μm diameter gold wire),R a reference electrode (consisting of 250μm diameter silver wire) andC a (consisting of 250μm diameter platinum wire).

6.2.4 Fabrication of Non-Lithographic Microwell.

A silver, gold and platinum wire each 250μm diameter where carefully positioned on a small piece of polystyrene. On to this a 2mm diameter machined hole in polystyrene was aligned and clamped. The whole device was heated for 30 minutes at 95°C, or until the two pieces were fully bonded **Figure 6.6**. The silver wire was converted into a pseudo-reference electrode by holding it at 0.1V for 30 seconds in a similar method to that described in **Section 6.2.7**. *A summary of all of the fabrication procedures described above is shown in* ***Figure 6.5***.

6.2.5 Storage of Microfabricated Devices

Where necessary, the finished devices were stored between electroanalytical tests, dry and covered, but were rinsed in RO water and blow dried in a stream of nitrogen before re-use. Connections to the reference, counter and working electrodes were made by the attachment of multicore wire to the bonding pads with silver paint (Agar Scientific Ltd, UK), and securely attached using silicon adhesive/sealant (Dow Corning Corp, USA).

6.2.6 Experimental Set-Up For Electrochemical Measurements

In all of the following experiments the electrochemical responses of electrodes were recorded using a low current potentiostat (BAS CV-37, Stockport, UK). Data was collected in an 'in-house' data acquisition interface comprising an PC30AT multi-function analogue and digital input/output board Amplicon (Brighton, UK), installed in an IBM compatible personal computer.

6.2.7 Reference Electrodes

6.2.7.1 Psuedo-Reference Electrode Preparation[76]

Psuedo-reference electrodes were prepared using both the photolithographically defined 2mm gold macro-electrodes gold electrodes, or as microfabricated electrodes as shown schematically in **Figure 6.3**. In both cases, the electrode to be modified was silver plated with approximately 100nm of silver (measured electrochemically and confirmed by Dek-Tak), by electro-deposition from an aqueous plating solution of 0.2M AgNO3 / 2M KI/ 0.5mM $Na_2S_2O_3$, (containing the complex ion $[AgI2]^- K^+$). Sodium thiosulphate served to reduce the size of nucleation of the deposited silver crystalites.
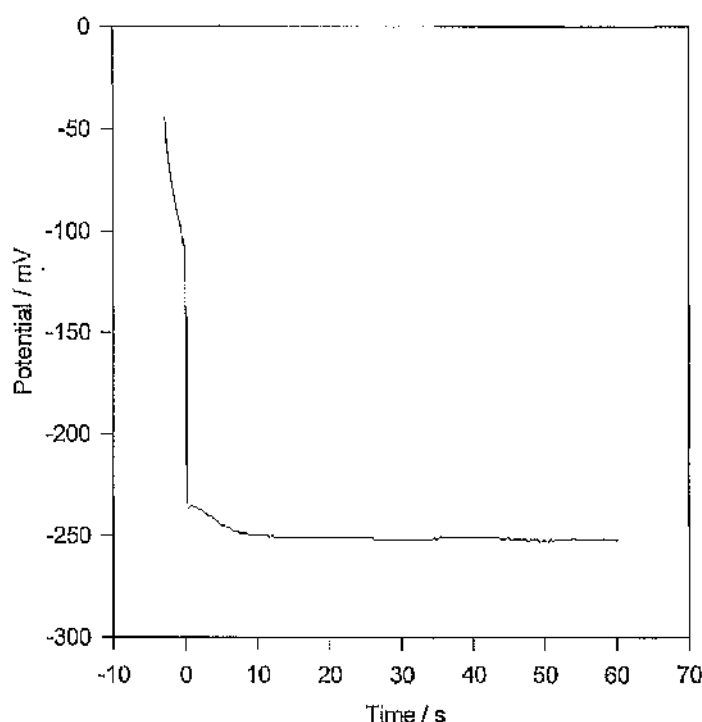
Figure 6.7 - Chronopotentiometry showing the plating of the common reference electrode with silver ions prior to oxidation in phosphate buffer in order to create a $Ag|AgPO_4$ pseudo-reference electrode in the microwell array. The electrode to be plated was set-up as the working electrode in a standard three electrode configuration with a standard $Ag|AgCl$ electrode as reference electrode and a platinum wire as counter electrode. -500μA were passed for 60 seconds in a plating solution containing 0.2M $AgNO_3$, 2M KI and 0.5mM $Na_2S_2O_3$.

A current of -500µA was passed for 1 minute using a standard three electrode configuration with the electrode to be plated acting as the working electrode, a platinum wire as a counter electrode and a Ag|AgCl reference electrode **Figure 6.8.**

As the thickness of the silver layer is unimportant (above a threshold of *ca.* 50 nm to ensure good coverage) the deposition time was not critical. However, in the case of microfabricated electrode arrays, care had to be taken not to pass too much charge in order to prevent the silver layer growing to such an extent that shorting could occur between either, or both of the counter and working electrodes.
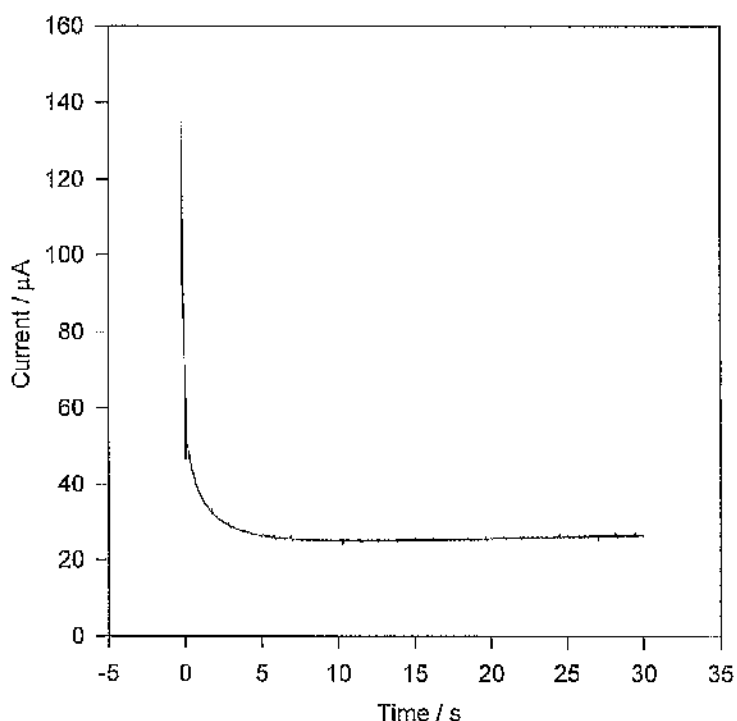
Figure 6.8 - Chronoamperommetry showing the formation of Ag|AgPO$_4$ pseudo-reference electrode following plating with silver. Again the electrode to be converted was configured as the working electrode against a Ag|AgCl$_2$ standard reference electrode and a platinum wire acting as thereference electrode. The working electrode was poised at 0.1V for 30 seconds in a pH 7, 20 mM potassium phosphate buffer.

Where macro-electrodes were used, the pseudo-reference electrode was completed by passing 500mA for 30 seconds in a solution of 0.1HCl or 0.1M potassium phosphate **Figure 6.8**. In the case of microfabricated arrays however, in order to prevent the contamination of the device by a process involving anodic stripping and precipitation of silver ions (discussed later) the pseudo-reference electrode was instead poised at 0.1V vs. Ag|AgCl standard reference electrode (BioAnalytical Systems Luton, UK) for 30 seconds.

6.2.7.2 Micro-Polarisation Tests

Each macro pseudo-reference electrodes was characterised by two methods:

1. By testing its ability to show good reversible ferrocene mono-carboxylic acid electrochemistry when used as the reference for a gold working electrode (2mm diameter photolithographically defined gold macro electrode), with a platinum counter electrode (for full experimental details please see section 6.2.8.1 below).

2. By testing the electrodes ability to maintain its reference potential using micropolarisation tests. In such circumstances, the electrode under test was cycled 20mV either side of its open circuit potential whilst connected as the working electrode in a standard three electrode configuration (standard Ag|AgCl reference electrode, platinum gauze counter electrode, in 20mM phosphate buffer pH7 containing 100mM sodium perchlorate as the supporting electrolyte) and the current-voltage profiles were collected.

6.2.8 Electrochemical Characterisation of Electrodes and Electrode Arrays.

6.2.8.1 Ferrocene Electrochemistry

The electrochemical performance of fabricated devices and reference electrodes was investigated using an aqueous solution of 0.5mM monocarboxylic acid

ferrocene mono-carboxylic acid. Immediately prior to each experiment, an appropriate amount of ferrocene mono-carboxylic acid was dissolved in 3% methanol before being diluted to 0.5mM using 20mM phosphate buffer pH7 (containing 100mM sodium perchlorate as the supporting electrolyte). A drop of 0.5 mM FMCA was placed in the well under study and the device was tested with one of two reference electrode configurations comprising: either an external Ag|AgCl standard reference electrode (BioAnalytical Sciences) inserted into a large droplet (volume = 100 μl) placed on the device or an internal pseudo-reference electrode. The working electrode was scanned between -300 mV and +300 mV, and scan rates (v) were varied between 10 and 100 mVs^{-1}.

6.2.8.2 Chronoamperometry of Horseradish Peroxidase (HRP)

Horseradish Peroxidase, HRP, at concentrations of 0 - 250 μg ml^{-1} and hydrogen peroxide, at concentrations of 0 - 400 μM, were made up separately as stock solutions at the twice the required concentration (see results) using 20mM phosphate buffer pH 7.0 (containing 0.5 mM FMCA and 100mM sodium perchlorate as the supporting electrolyte). The concentration of H_2O_2 in a 30% solution (as supplied) is inherently unstable even when stored at 4°C. Consequently the actual concentration was confirmed by measuring the absorption at 240 nm (molar extinction coefficient = 43.6 M^{-1} cm^{-1}) using a Hitachi S2000 spectrometer. i.e. 8 mM H_2O_2 (0.025%) has an optical density of 0.35(optical pathway of 1 cm). The two solutions were mixed immediately prior to their addition to the electrochemical microwell, and current-time measurements carried out with the working electrodes poised at 0mV, versus an in-situ pseudo-reference electrode.

6.3 Results and Discussion

6.3.1 Reference Electrodes
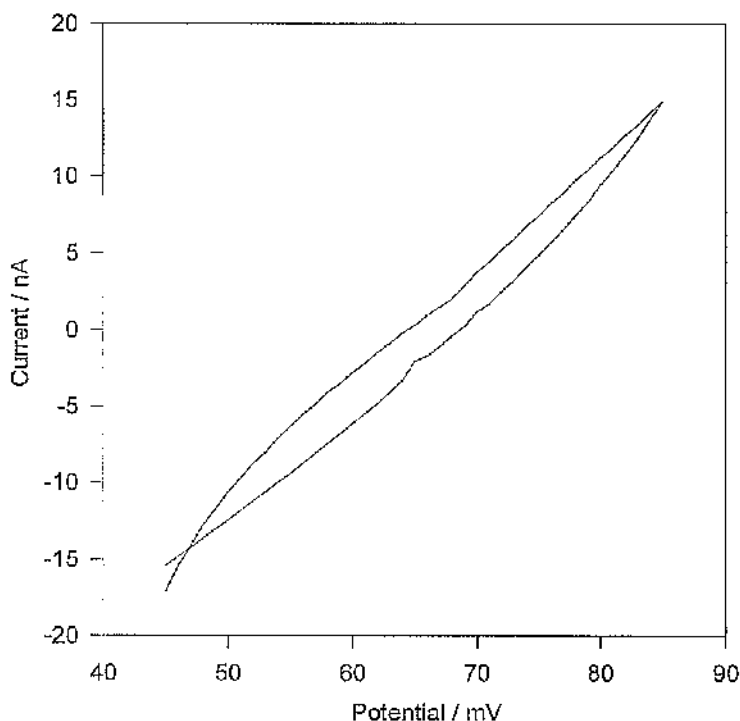
Figure 6.9 - Micropolarisation test of a Ag|AgPO$_4$ pseudo-reference electrode formed on 2mm diameter gold disk. In a standard three electrode configuration, the pseudo electrode is used as the working electrode and is cycled within a few millivolts of its open circuit potential (65mV). The experiment was conducted in 20 mM sodium phosphate buffer pH 7.0 with reference to a standard Ag|AgCl reference electrode (BioAnalytical Systems, Luton, UK.), at a scan rate of 5mVs^{-1}.

In previous studies[76] one of the three microfabricated gold electrodes has been used as a pseudo- Ag|AgCl reference electrodes by plating with silver, followed by oxidation in HCl. Such reference electrodes are sensitive to changes in the concentration of chloride ions in the assay solution, with the consequence of causing shifts in the applied potential. A typical buffer, such as PBS, has only 137 mM chloride ions, a concentration which is changed significantly by the addition of any other solutions. This problem is accentuated when operating in small volumes, as the absolute amount of material present is small, evaporation may contribute to changes. As an alternative, the use of an Ag|Ag$_2$PO$_4$ pseudo-

reference was investigated. Phosphate ions are present in significantly higher proportions in the buffers used and also has a notably lower solubility ($K_{sp} \approx 9 \times 10^{-17}$) than AgCl ($K_{sp} \approx 2 \times 10^{-10}$), over-coming solubility problems that are previously documented[76].
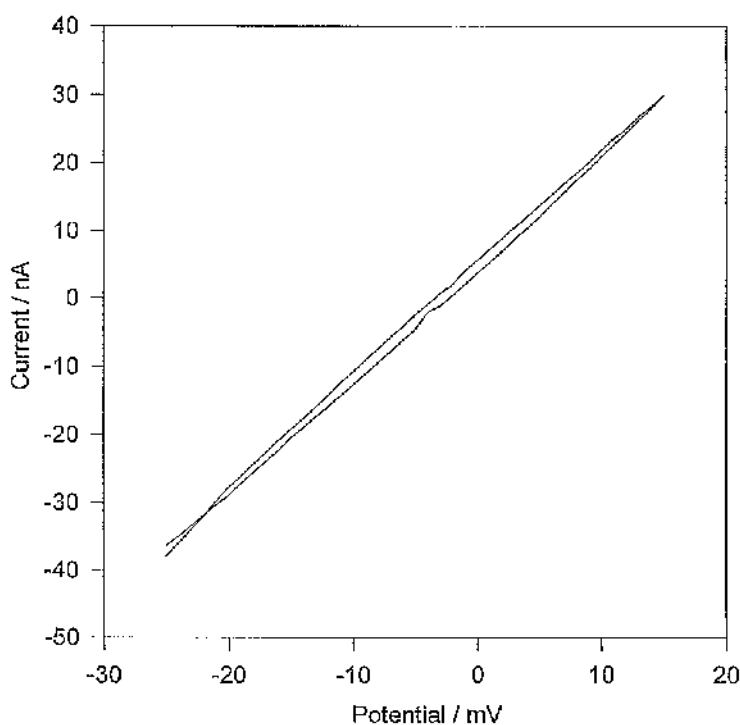
Figure 6.10 - Micropolarisation test of a standard Ag|AgCl reference electrode, cycled in 20 mM sodium phosphate buffer pH7 a few mV either side of its open circuit potential ~0.5mV with reference to another standard Ag AgCl reference electrode. Scan rate 5mVs^{-1}.

Prior to exploring results using micro-fabricated structures, reference electrodes were initially made using macro sized gold electrodes (dia. 2mm). The role of a reference electrode is to provide a fixed potential that does not vary during the experiment, whilst isolating the working electrode, as the electrochemical system under study. In practice, the reference has to draw some current and, therefore, it is essential that a good reference electrode maintains its reference potential, even if a few microamperes pass through it (a criterion which is dependent upon a reversible reaction occurring at the reference electrode[111]). The behaviour of a reference electrode can best be characterised using micropolarisation tests[111].

139

The reference electrode under examination is cycled, as the working electrode in a standard three electrode configuration, within a few millivolts of its open circuit potential. Any hysterisis present in the curves is indicative of irreversibility and error in the reference potential when current is forced to pass through the electrode. The pseudo Ag|AgPO$_4$ electrode **Figure 6.9** gave comparable results to those obtained for a standard Ag|AgCl reference electrode **Figure 6.10**, and a pseudo Ag|AgCl reference electrode **Figure 6.11**.
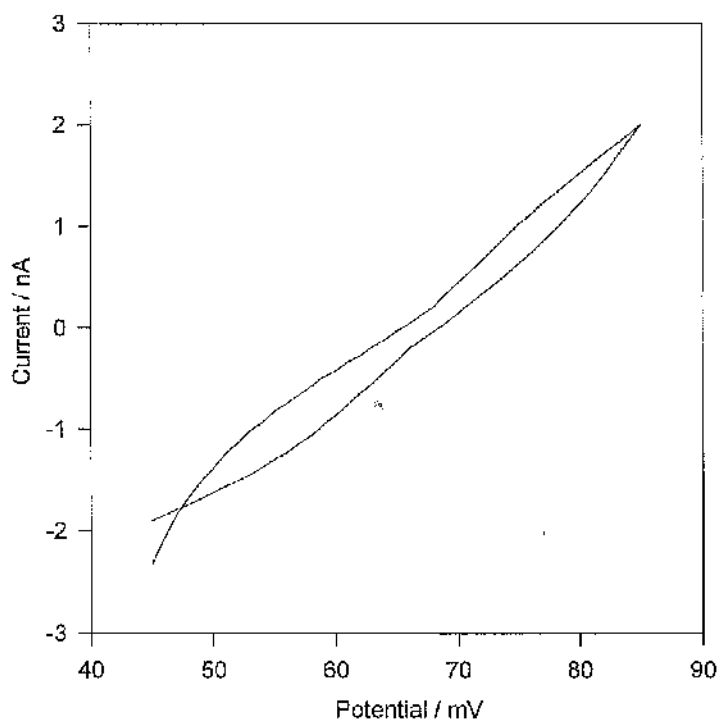
Figure 6.11 - Micropolarisation test on Ag|AgCl pseudo-reference electrode (E° = 65mV) vs Ag|AgCl standard (BioAnalytical Systems), at a scan rate 5mVs^{-1} in electrolyte containing 20mM sodium phosphate buffer pH7.0.

The same macro sized electrodes were also characterised electrochemically using FMCA as a model redox compound. The results shown demonstrate that the Ag|AgPO$_4$ pseudo-reference **Figure 6.12a** again gave results comparable to both the standard reference electrode **Figure 6.12b** and the Ag|AgCl pseudo-reference **Figure 6.12c**, the only difference being a slight shift in the measured E$_{1/2}$.
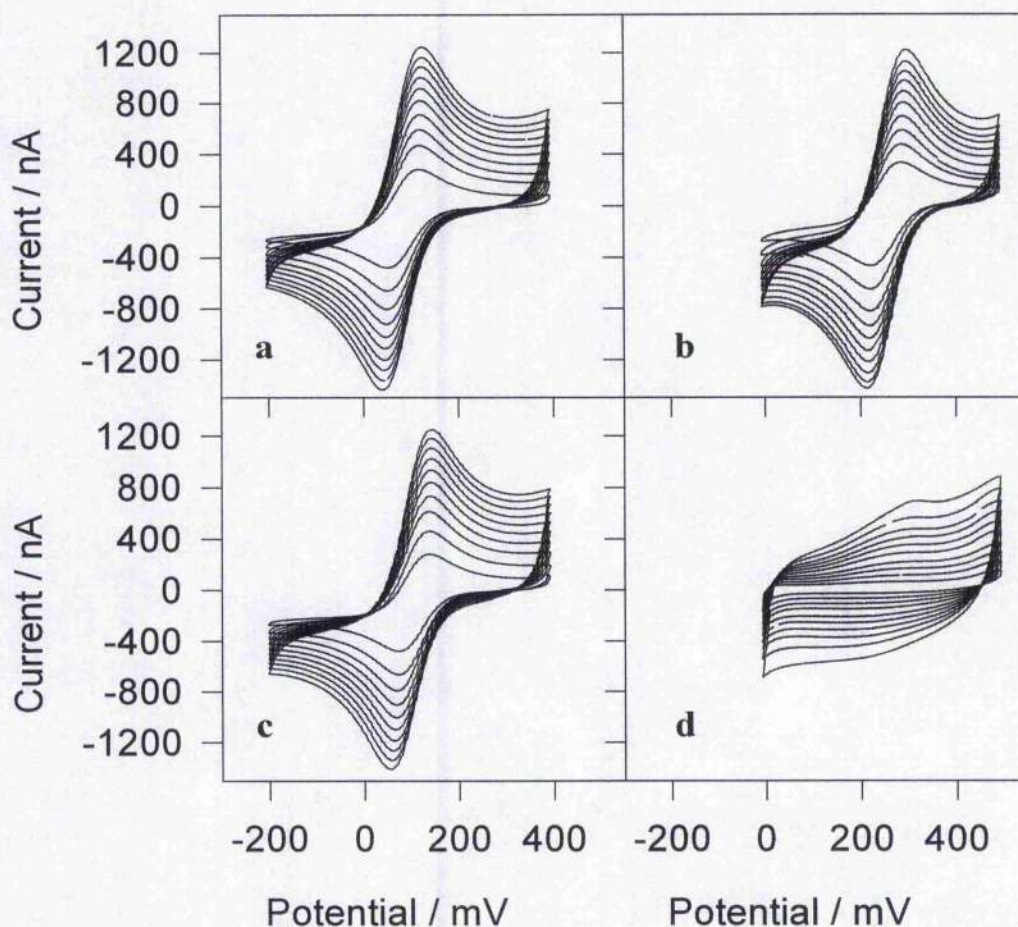
Figure 6.12 - Cyclic voltammograms of 0.5mM FMCA in 20mM sodium phosphate buffer pH 7at a plain gold (2mm Dia.) working electrode versus an $Ag|AgPO_4$ pseudo-reference electrode **A**, a $Ag|AgCl_4$ standard reference electrode (BioAnalytical Sciences) **B**, a $Ag|AgCl_4$ pseudo-reference electrode **C**, and a 2mm diameter plain gold electrode **D**. Scan rates 10 - 100 mVs^{-1} (at 10 mVs^{-1} intervals).

Each reference shows a reversible one electron transfer as would be expected for the cyclic voltammetry of 0.5 mM FMCA at a gold electrode as indicated by linearity in the plot of the peak current versus square root (scan rate) proportionality **Figure 6.13**. The use of a good reference electrode is illustrated by the results shown in **Figure 6.12d**, where a plain gold electrode is used as a pseudo-reference electrode. As a result of the good performance and decreased solubility, pseudo-$Ag|AgPO_4$ reference electrodes where chosen for use in all further experiments.
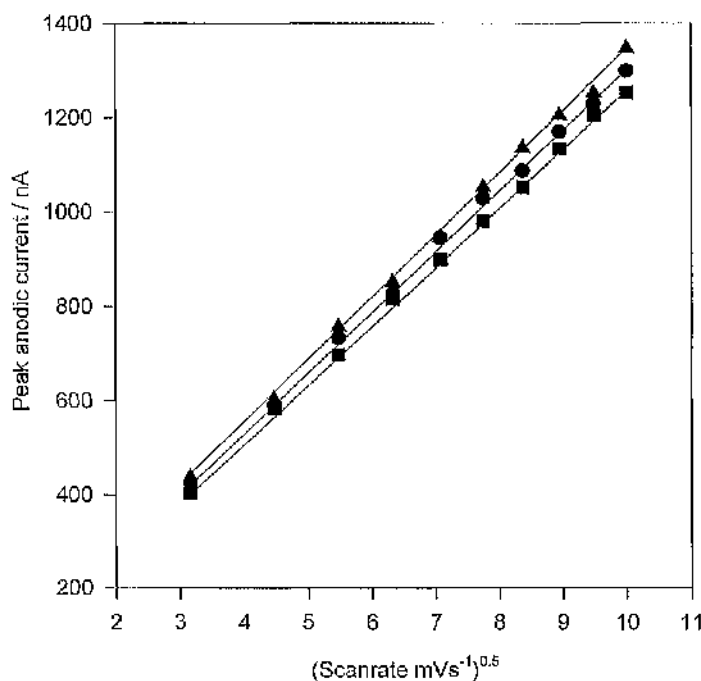
Figure 6.13 Anodic peak current against (scanrate)$^{0.5}$ from cyclic voltammograms shown in figure 14(a,b, and c). ● - Ag|AgPO$_4$ pseudo-reference (figure 14a), ■ - Ag|AgCl$_2$ standard reference (figure 14b), ♦ - Ag|AgCl$_2$ pseudo-reference (figure 14c). Conditions as for figure 14.

It was observed that the control of the voltage during oxidation for the formation of the pseudo-reference electrode was critical when using microelectrodes. If the voltage at the working electrode was allowed to exceed 0.3V, the stripping of silver from the working electrode occurred and the resulting silver phosphate precipitation caused irreversible damage to the device as the precipitate was difficult to remove and silver peaks were observed in any future voltammograms **Figure 6.14.**
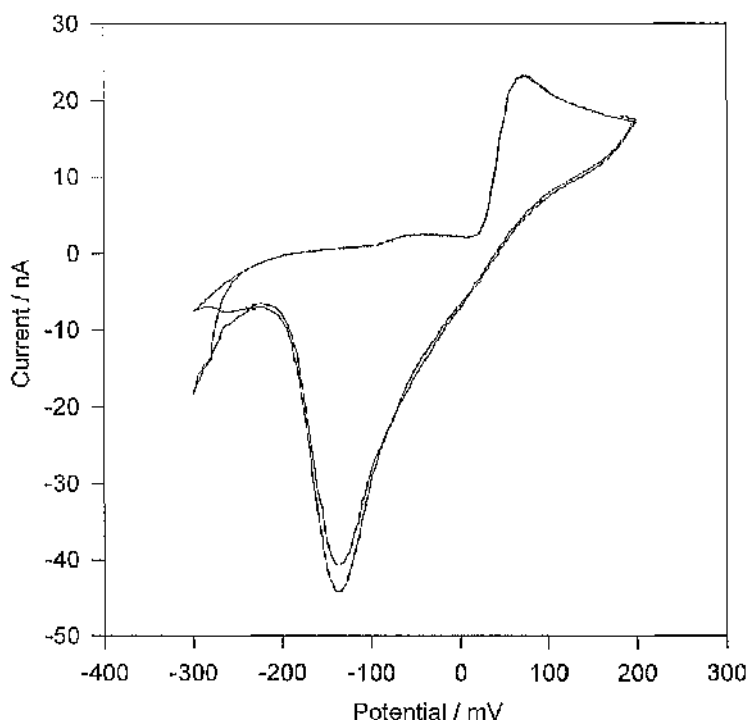
Figure 6.14 - Cyclic voltammogram recorded at the working electrode of a microwell, after modification of Ag|AgPO₄ pseudo-reference electrode by oxidation at 0.5V in a 20mM potassium phosphate buffer. Electrolyte (pH 7.0 20mM phosphate buffer) also containing 0.5mM FMCA, scan rate 50mVs⁻¹.

6.3.2 Glass/Plastic Micro-chamber Array

6.3.2.1 Fabrication

Using the method illustrated in **Figure 6.5i** it has been possible to reliably fabricate arrays of twelve, 8 µl electrochemical cells shown in **Figure 6.15** (*Photo/SEM not ready*). When made in batches of six, no significant inter- or intra-batch variations were detected for electrochemical measurements made with freshly cleaned devices (coefficient of variation ± 6%). Choice of the solvent used in fabrication process as well as the type of plastic, defining wells, was critical. For example, if chloroform was used to bond polystyrene, too much plastic became solvated and the pressure, due to the clamps, forced solvent and plastic over the microfabricated electrode areas. Another undesirable effect of an inappropriate bonding solvent, was the formation of 'bubbles' at the bonding

143

interface. Both polystyrene and PMMA were used to define the wells (bonded using cyclohexane and chloroform respectively). However, when bonding to glass, in this manner, PMMA proved preferable to polystyrene, which had a tendency to crack when under pressure. Although relatively strong, the adhesion was not permanent, and it was found that devices had an approximate life span of one month.

Figure 6.15 – Showing a 12 well microfabricated electrode array, after bonding of plastic template, and prior to electrode modification. (Device is 75 mm in length)

6.3.2.2 Electrochemical Characterisation

Characterisation was performed using 0.5 mM FMCA as a model redox compound. Both an external reference electrode and an internal psuedo-$Ag|AgPO_4$ reference electrode were used for characterisation of the microarray structures. The typical responses at a single micro-chamber working electrode are illustrated in **Figures 6.16 and 6.17** when using either an external or an internal reference electrode respectively.

The device showed appropriate $Fe^{2+}|Fe^{3+}$ redox behaviour - having an experimentally measured $E^O{}_{1/2}$ of 246 mV and good linearity of peak current versus square root of the scan rate. Deviation in peak current (coefficient of variation $\pm$ 3%) and standard electrode potential (coefficient of variation $\pm$ 5%) between chambers on the same device was minimal when using an internal reference, as indicated in **Figures 6.18 and 6.19**.
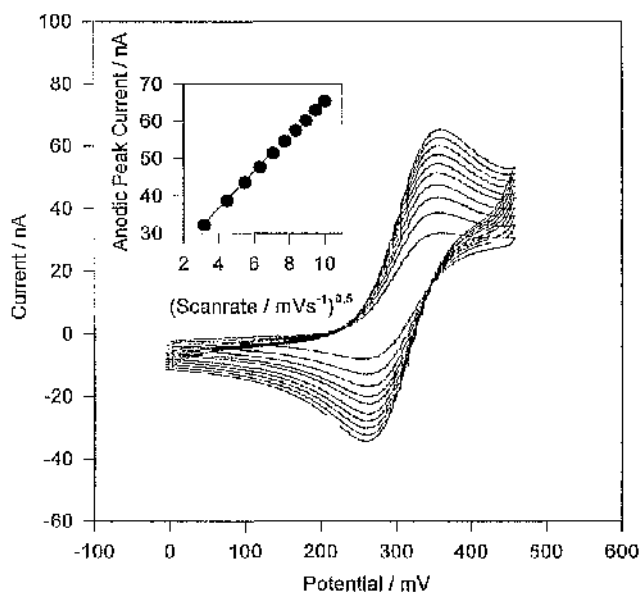
Figure 6.16 - Cyclic voltammogramms of 0.5mM FMCA recorded at the gold working electrode in a single well of a plastic/glass twelve well electrode array using a Ag|AgCl external standard reference electrode (BioAnalytical Systems). Background buffer was 20 mM sodium phosphate buffer pH 7.0, scan rates 10 - 100 mVs^{-1} at 10 mVs^{-1} intervals.
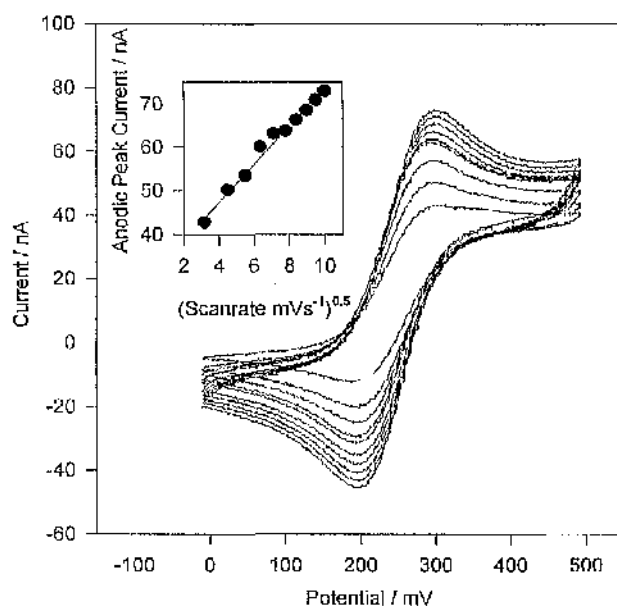
Figure 6.17 - Cyclic voltammogramms of 0.5mM FMCA recorded at the gold working electrode in a single well of a plastic/glass twelve well electrode array using a Ag|AgPO$_4$ internal pseudo-reference electrode. Background buffer was 20 mM sodium phosphate buffer pH 7.0, scan rates 10 - 100 mVs^{-1} at 10 mVs^{-1} intervals.
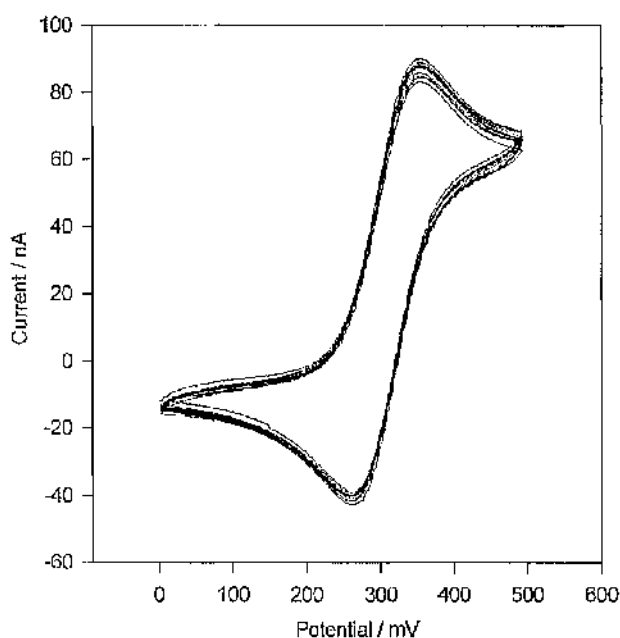
Figure 6.18 - Cyclic voltammograms of 0.5mM FMCA, collected at 12 individual working electrode on a plastic/glass 12 well electrochemical array, versus a standard Ag|AgCl external reference electrode. Scan rate 50 mVs^{-1}, background buffer 20 mM phosphate pH 7.0.
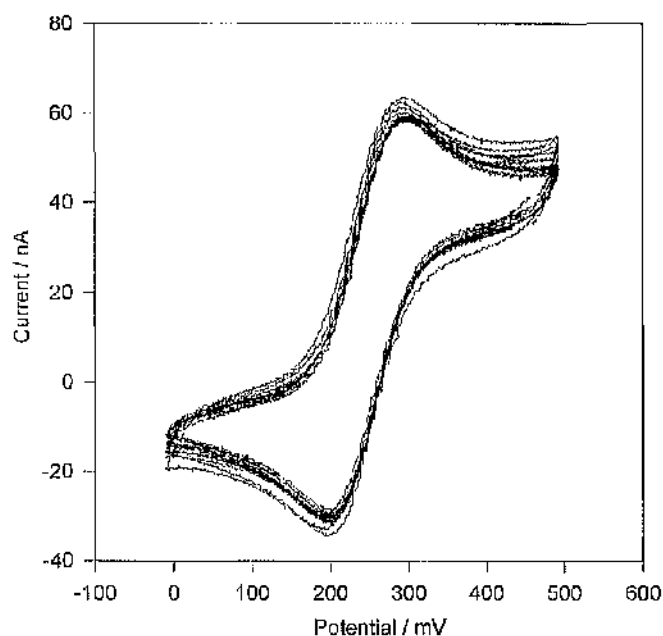
Figure 6.19 - Cyclic voltammograms of 0.5mM FMCA, collected at 12 individual working electrode on a plastic/glass 12 well electrochemical array, versus a Ag|AgPO$_4$ internal pseudo-reference electrode. Scan rate 50 mVs^{-1}, background buffer 20 mM phosphate pH7.0.

6.3.3 Plastic/Plastic Micro-chambers

Arrays of electrochemically addressable micro-wells were also fabricated by the bonding together of sandwiches of polystyrene, either by chemical or thermal adhesion. Single wells were tested and characterised using FMCA as described above and, again, showed acceptable redox behaviour for the $Fe^{2+}|Fe^{3+}$ couple with good reversibility **Figure 6.20.**
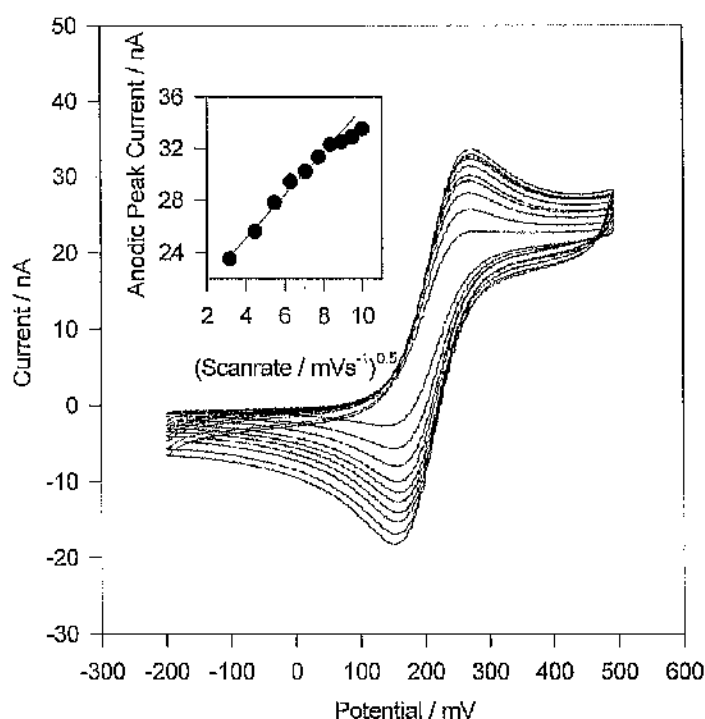
Figure 6.20 – Cyclic voltammograms of 0.5mM FMCA recorded at the gold working electrode in a single well of a 12 well array microfabricated plastic device. The background electrolyte consisted of 20mM phosphate buffer pH 7.0, Ag|AgPO$_4$ pseudo-reference electrode. Scan rates 10 - 100 mVs^{-1} (10 mVs^{-1} increments).

Defining the electrode areas using plasma enhanced chemical vapour silicon nitride deposition was not possible, as the deposition process takes place at temperatures in excess of 300°C and, as a result, there was a large degree of variation in working electrode surface area between wells on the same device (as described previously). As a consequence the coefficient of variation was

147

dependant upon the precision of alignment between the template for the wells and the microelectrode array base, leading to values which were typically in the region of 16%. However, with calibration and normalisation of assay signals, to the electrode area calculated from FMCA scans it would be possible to use such arrays to perform multiple assays.

6.3.4 Non-Photolithographically Fabricated Micro-chambers

6.3.4.1 Fabrication

The possibility of producing micro-chambers without using photolithographic methods was also investigated. Following the procedures illustrated in **Figure 6.6** and described in **Section 6.2.4** - it was possible to produce single electrochemically addressable micro-wells with a diameter between 2 mm and 5 mm. Wells with a diameter smaller than 2 mm proved difficult to manufacture in this manner as the thermal bonding of the plastic was incomplete and capillary action allowed solutions to pass from the well along the wires.
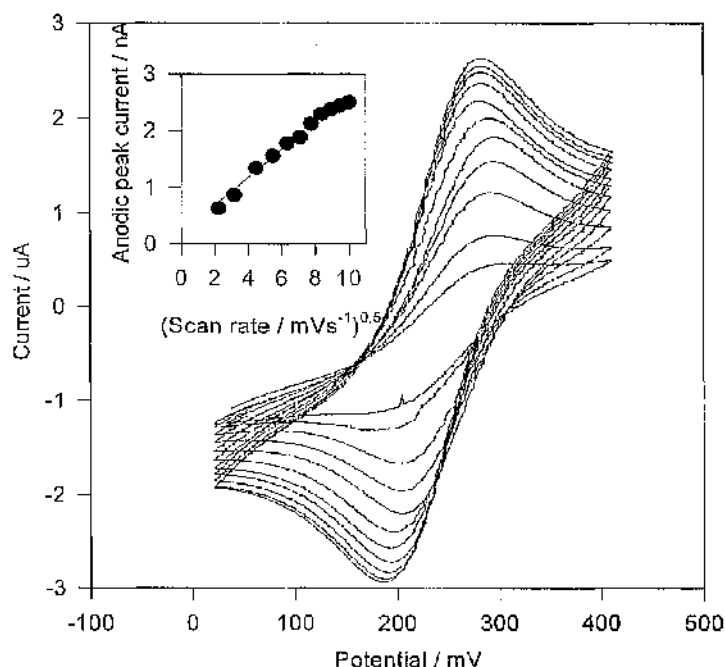
Figure 6.21 - Cyclic voltammograms of 0.5mM FMCA recorded at the gold working electrode of a single well in a 12 well array plastic device fabricated non-photolithographically. A 20mM phosphate buffer pH 7.0 for the background electrolyte, and reference provided by a Ag|AgPO$_4$ pseudo-reference electrode. Scan rates 10 - 100 mVs^{-1} (10 mVs^{-1} increments).

6.3.4.2 Electrochemical Characterisation

Devices were again characterised by following the electrochemistry of FMCA at the gold wire - having oxidised the silver wire in phosphate to create a pseudo Ag|AgPO$_4$ reference electrode as before **Figure 6.21**. Due to the nature of fabrication, the surface area, of each working electrode could not easily be tightly controlled and as a result there was a large degree of variation between devices (coefficient of variation > 20%).

6.3.5 Effect of Evaporation From Microwells.

Evaporation of supporting solvent is an increased problem when conducting experiments in miniaturised microwells. This is clearly demonstrated in **Figure 6.22** where the peak anodic current (I$_{pa}$) increases over a period of time as a result of the increased concentration of FMCA due to water loss by evaporation. It can be seen that within as little as 5 minutes, a five percent increase of peak current occurs, prior to catostrophic drying out.
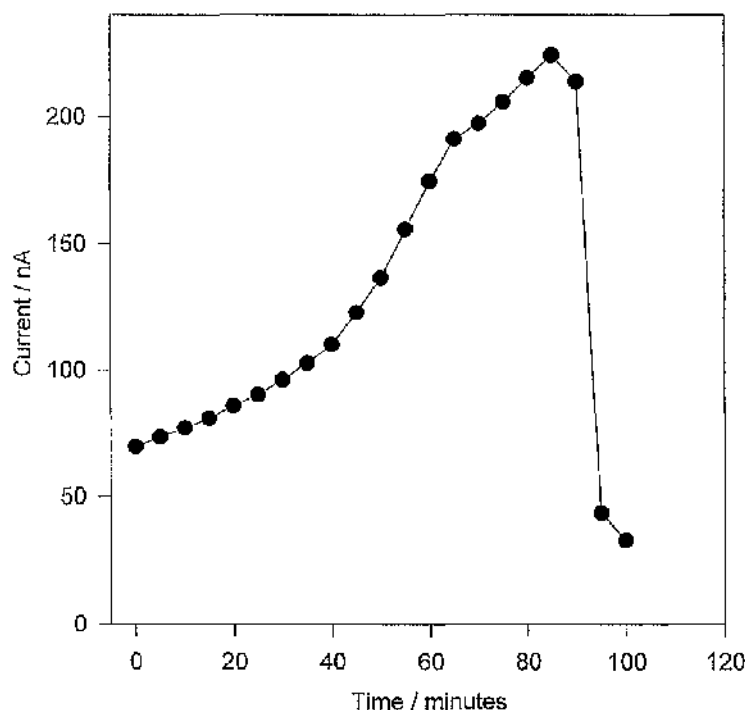
Figure 6.22 - The peak current from the cyclic voltammogram of FMCA recorded at the working electrode of a 5μl microwell increases over time as a result of fluid loss by evaporation. Scan rate 50 mVs^{-1} background electrolyte 20 mM phosphate buffer pH7.0.

149

It is therefore important, where possible, to conduct experiments in as short a time scale as possible whilst attempting to minimise evaporation. When similar experiments are conducted on a macro scale, the peak current stays within the expected error range for a much longer period of time (typically hours, rather than minutes).

6.3.6 Biological Measurements
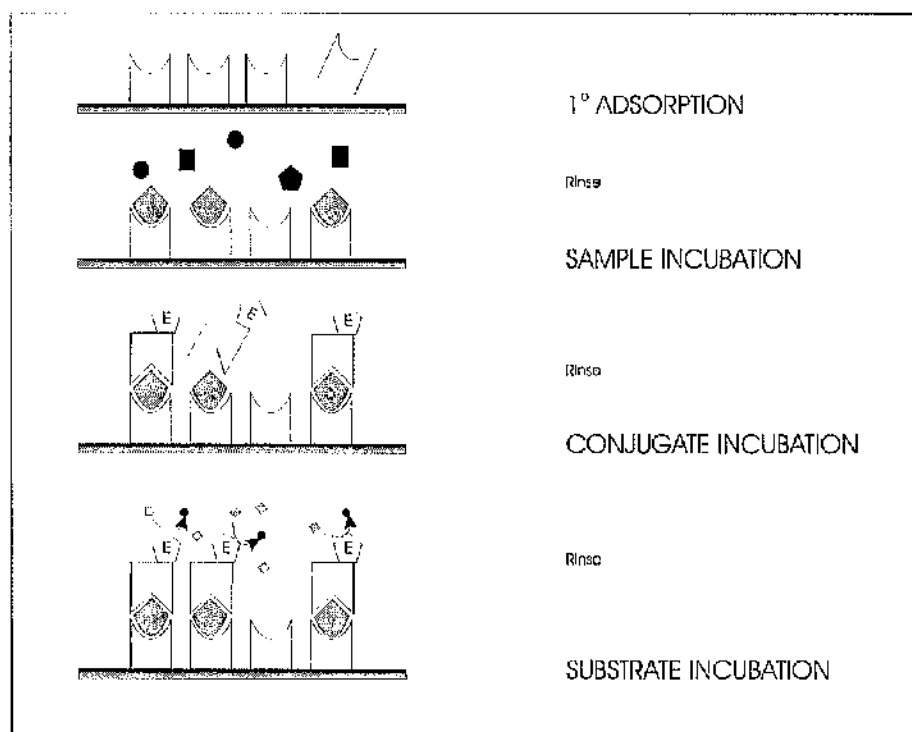
Figure 6.23 - Shows a schematic representation of typical protocol for a sandwich ELISA. The first step binds a primary antibody (often described as the capture antibody) to the solid-phase. After blocking and rinsing steps, the sample is added and incubated. If the sample contains the target analyte, it will be bound by the primary antibody. Further rinsing steps precede the addition of the conjugate (or detection) antibody, which binds to the primary antibody/target analyte complex. The enzyme conjugated to the detection antibody on addition of a suitable substrate will initiate a detectable change, for example, a change in colour. In an electrochemical immunoassay the enzyme produces a change which can be measured via electrodes in close proximity to the antibody/antigen complex.

Horseradish peroxidase (HRP) is an enzyme that is commonly used in many biological assays. For example, **Figure 6.23** shows how enzymes are used as

reporters of ligand binding in an enzyme linked immunosorbet assays (ELISAs). In order to investigate the potential use of the microfabricated electrode well arrays for similar assays using electrochemical detection (as opposed to colorimetric detection), simple electrochemical assays were performed using both HRP and GLOX as electrochemical reporter enzymes.

After initial optimisation of the electrochemical HRP assay (in which the protein and substrate concentrations were altered independently) the device could be used to detect HRP within the range of 0 - 100 μg ml^{-1} with a detection limit, under these conditions, of 1 μg ml^{-1} HRP (approximately 1ng, or a few femtomoles, of protein) **Figure 6.24.** When using the optimum HRP concentration (100μgml^{-1}) an assay for H_2O_2 could be performed with a detection range 0 - 100 μM **Figure 6.25.**
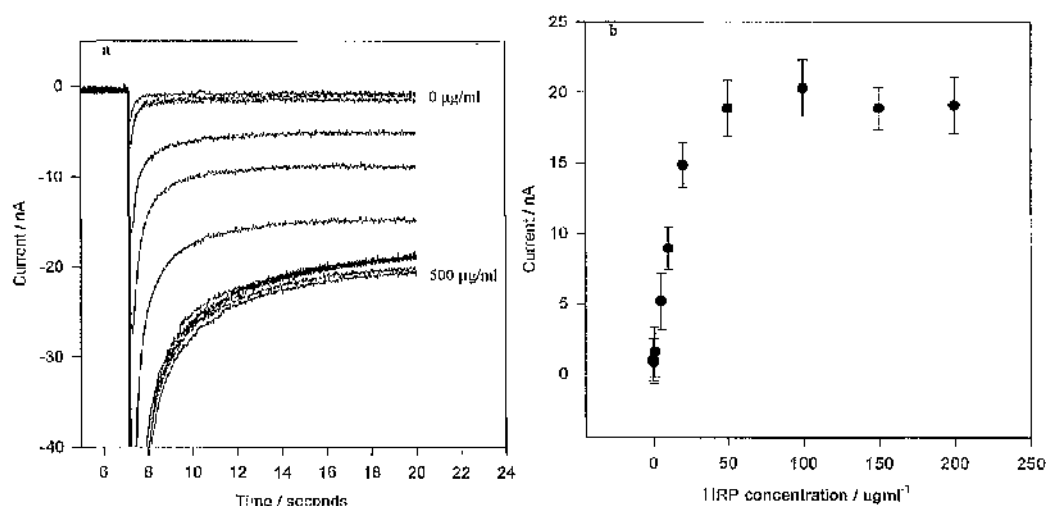
Figure 6.24 – Current-time recordings of a solution of 0 - 500μg/ml HRP in pH 7.0 phosphate buffer (containing 0.5mM FMCA, 100mM sodium perchlorate and 100μM hydrogen peroxide) recorded at gold working electrodes, poised at 0mV versus internal psuedo-Ag|AgPO$_4$ reference electrode. Each reading was measured in a different well on the same electrochemical microwell array. The response is seen to plateau beyond 100 μg/ml and as a result this concentration was chosen as the optimum HRP concentration for further experiments.

In immunosensor applications it can be observed that the detection limits required are usually in the nanomolar range[185]. Significant enhancement of the

electrochemical device should, however, be obtained by the immobilisation of the sensing proteins close to the working electrode providing a diffusional enhancement of the signal.
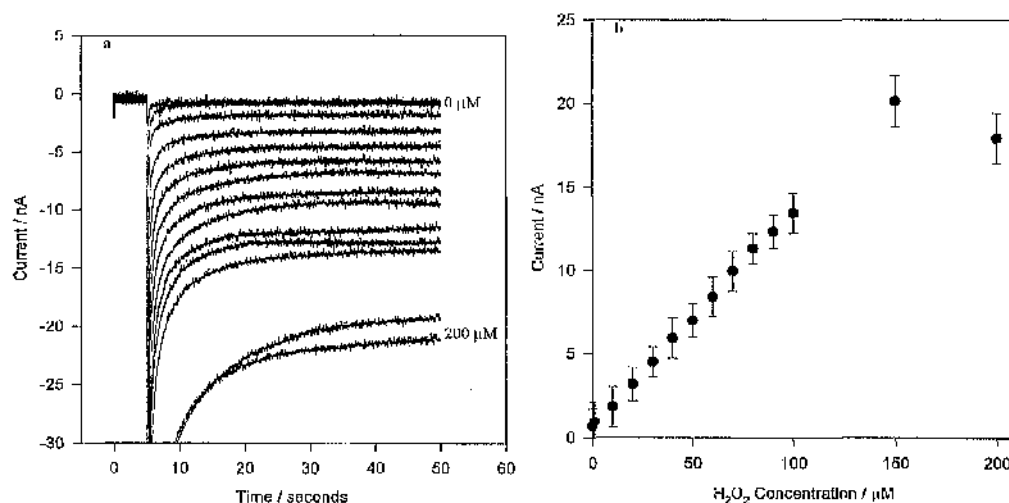
Figure 6.26 - Chronoamperometry of a solution of 100µg/ml HRP in pH 7.0 phosphate buffer (containing 0.5mM FMCA, 100mM sodium perchlorate and 0-200µM hydrogen peroxide) recorded at a gold working electrodes poised at 0mV versus internal psuedo-Ag|AgPO₄ reference electrode. Each reading recorded in a different well on the same electrochemical microwell array.

Commercially available immunosensing assays often take several hours to prepare and complete, it would therefore be essential to monitor the evaporation from the electrochemical devices, to prevent protein denaturation, and/or the passivation of the electrodes.

6.4 Conclusions

We have demonstrated that, by the use of a 'sandwich' method of construction, we can fabricate arrays of electrodes, both wholly in plastic or of a plastic/glass composite, either with individually addressable working electrodes. Although it is only possible to define the electrode area when using the plastic/glass composite devices, by normalising electrode response to calculated electrode area it will be possible to use wholly plastic arrays to perform electrochemical enzyme assays. This sandwich method of construction, also allows for the inclusion of a membrane in the fabrication method such that future devices may be used with samples, which at present would cause electrode passivation, such as whole blood samples or cell culture supernatants. Indeed, early results (not shown) have demonstrated that it is possible to introduce a cellulose acetate membrane above the electrode of plastic only devices.

Our use of $Ag|AgPO_4$ pseudo-reference electrodes has been useful to solve solubility problems which were previously encountered by Bratten *et al*[76]. However, further study should investigate the long-term functionality of such electrodes.

Finally our ability to fabricate single electrode wells without the use of expensive microfabrication techniques could widen the number and range of potential users of low volume micro-electrochemical assays. However, one problem to be overcome is the decrease of variation between devices.

CHAPTER 7: CONCLUSIONS

The work presented here investigates a number of the issues relating to biosensor technology, in particular the design of interfaces showing controlled biomolecular composition. Initially the use of mixed monolayers of alkanethiols on gold to control the immobilisation of proteins at gold interfaces was investigated, with the eventual aim of applying the techniques within miniaturised amperometric assay systems.

Using high resolution X-ray photoelectron spectroscopy, we have demonstrated that the degree of head group functionality in a SAM on gold can be altered in a time dependant fashion through the displacement of an adsorbed alkanethiol by a second thiol bearing an alternative head group. Through the measurements by XPS we showed that the method of displacement was not via an initial dissociative step (the N1s signal does not diminish after immersion of a mercaptoethylamine monolayer in reverse osmosis water for extended periods of time). A method of displacement involving a disulphide transition state was proposed although further investigation would be required to confirm if this is the case. It was also interesting to note that the use of mercaptopropanol as a modifier resulted in significant reduction in the amount of physisorbed contamination often observed in thin film XPS experiments. Control over the head group composition of a SAM on gold in this manner, in turn, enabled the regulation of biomolecular recognition at biosensor interfaces in a number of different ways.

Initially we investigated the use of short chain thiols to control the electrochemistry of the metalloprotein of cytochrome c at a gold electrode. The use of short chain molecules with an 'open molecular architecture' had the advantage that they do not present a diffusional barrier to electron transfer. This is in contrast to the loss of sensitivity that is observed for long chained, highly ordered alkanethiol SAMs[141]. We showed that by using a combination of alkanethiols, where one species bears a head group that promotes cyctochrome c electrochemistry, and the other does not, we are able to control the degree of molecular recognition. We noted that in order to

transform the interfacial properties of the gold surfaces with respect to cyctochrome *c* electrochemistry, it was not necessary to produce a homogeneous surface coating. For example, under the electrochemical conditions employed, cytochrome *c* redox currents similar to those on suitable homogenous SAMs are obtained even when the mixed SAM surface contains a significant proportion (40%) of 'non-promoter functionality's as indicated by XPS measurements.

We also demonstrated that the displacement reactions by solution phase thiols, are not necessarily reversible, over the moderately long time scales used. Thus exposure of a gold electrode surface to a binary thiol solution may not lead to a mixed monolayer SAM of the same relative composition as the solution. Interestingly, we demonstrated the use of a number of different combinations of thiols to determine a hierarchy corresponding to the ability of a solution thiol to displace a surface species. Thus it may be possible to readily create surfaces containing controlled quantities of multiple functionalities.

To further investigate the ability of mercaptopropanol to prevent the phyisorbtion of proteins at surfaces, we used FT-iR to demonstrate the use of SAMs of alkanethiols on gold to regulate molecular recognition in this manner. We showed how both SAMs of mercaptoethyalamine and mercaptopropanol led to significant reductions in the non-specific adsorption of proteins, 38% and 72% respectively compared to an untreated gold surface. Although neither competed with a standard detergent such as Tween 60, where protein adsorption was reduced close to 95%, mercaptopropanol monolayers would offer an alternative in situations where the use Tween 60 would not be appropriate.

Finally we demonstrated the use of mixed monolayers on gold formed by displacement to control the covalent immobilisation of proteins at surfaces, allowing the manipulation of the density of protein immobilised at the surface, in a manner such that protein gradients can be created. These gradients, as well as being suitable for on sensor calibration applications, are also appropriate for investigations into cellular behaviour at bio-material surfaces. By combining the control at the level of

an alkanethiol SAM, with control through avidin immobilised at this layer, we have shown how control over the molecular architecture could be achieved in a multi-layer system.

We have, therefore, shown that mixed SAMs formed by displacement, can be used as a method for controlling the interactions of proteins with engineered devices. The possible applications covering reduction/oxidation reactions, directed protein immobilisation, the reduction of non-specific protein adsorption as well as possible cellular engineering applications (directing cell growth through gradients). These results demonstrate the wide range of applications that SAMs of alkanethiols on gold can be used for. With such a variety of both alkanethiols and bi-functional cross-linking agents available to be exploited in this manner, the formation of mixed monolayers by displacement could be used as a tool to enable a very high degree of control over the molecular architecture of gold surfaces used both in biosensor and bioengineering fields.

In acknowledgement of the recent increased scientific interest in the miniaturisation of devices, with the increased implications of activity loss through in appropriate immobilisation, in the final section we fabricated arrays of micro-amperometric devices in which our methods of control could be further investigated, such that the nature of immobilisation and the immobilisation environment could be manipulated to give optimal sensor performance.

By using a 'sandwich' method of construction for bonding plastics, it was possible to fabricate arrays of electrodes both wholly in plastic and in plastic/glass composites, with individually addressable working electrodes, and common reference and counter electrodes. Devices fabricated in this way were characterised using the redox behaviour of FMCA and were used to demonstrate their applicability to biological assay systems using horseradish peroxidase. However, the reduced geometries have been shown to create problems as a consequence of evaporation from the device, thus, quick measurement times are essential. In addition the use of $Ag|AgPO_4$

pseudo-reference electrodes, as opposed to Ag|AgCl has been useful to overcome solubility problems previously encountered by Bratten *et al*[76].

This method of construction also allows the possibility to include a membrane within the fabrication procedure such that future devices maybe used with samples which at present would cause electrode passivation, e.g. whole blood samples or cell culture supernatants. Early results have shown that it is indeed possible to introduce a cellulose acetate membrane above the electrode of plastic only devices.

Finally, the ability to fabricate single electrode wells without the use of expensive microfabrication techniques confers the ability to perform small volume electrochemistry to research groups where access to microfabrication equipment is not available.

7.1 Suggestions for further work:

As a result of the breadth of this project, there are a number of opportunities for further work. The fabrication of glass/plastic composite microelectrode arrays will allow the development of numerous assay systems which are applicable to HTS. In one area that already shows promise, we intend to use the electrode arrays to investigate glutamate production from rat brain neural cell samples[186]. It would also be useful to investigate the ability to perform electrochemical immunoassays with the electrode arrays. The use of SAMs and avidin/biotin, to control the immobilisation of the appropriate immunoglobulins within the devices could then be studied. The extension of the arrays in to 864 well format, presents the challenge of creating a suitable measurement system for multiple assays, as a consequence the efficient multiplexing of the devices and quick measurement from each well would become essential.

The possibility of including membranes within the devices requires further investigation. Although the feasibility has been proven, measurements with appropriate solutions (blood or cell culture supernatants) is necessary.

With the possibility of further decreasing the sizes of the electrodes, other methods of defining the wells could be investigated by the use of embossing or dry etching, however, the effects of evaporation will become more important to control with increased miniaturisation of the devices.

Finally the use of displacement of SAMs to fabricate mixed monolayer surfaces presents the possibility to investigate the interactions of cells with surfaces, from directing cell movement (along cytokine gradients), to preventing cells and proteins binding at implanted materials.

7.2 Publications and Conference Contributions Arising from this Work

- 'Dynamics of the Formation of Mixed Alkanethiol Monolayers: Applications in Structuring BioInterfacial Monolayers' Cotton, C.M., Glidle, A., & Cooper, J.M. *Langmuir,* volume 14 pg. 5139-5146, 1998.

- 'XPS investigation of mixed alkanethiol monolayers on gold' Cotton, C.M., Glidle, A., & Cooper, J.M., Poster presentation at Artificial Biosensor Interfaces, European Union Network Conference, Sitges, Barcelona, Spain 23 -25th October 1997.

- 'Control of Molecular Recognition at gold surfaces' Cotton, C.M., Glidle, A., & Cooper, J.M., Poster presentation at Electrochem '96 Conference: Bath, England 14 - 17th September 1996.

REFERENCES

1.   Bronzino, J.E., *The biomedical Engineering Handbook.* 1995: Boca Raton.

2.   Kasemo, B., *Biological Surface Science.* Current Opinion in Solid State and Materials Science, 1998. **3**: p. 451-459.

3.   Sethi, R.S., *Transducer Aspects Of Biosensors.* GEC Journal Of Reseach, 1991. **9**(2): p. 81-95.

4.   Collings, A.F. and F. Caruso, *Biosensors: Recent Advances.* Reports on Progress in Physics, 1997. **60**: p. 1397-1445.

5.   Braguglia, C.M., *Biosensors: An Outline of General Principles and Application.* Chemical and Biochemical Engineering Quarterly, 1998. **12**(4): p. 183-190.

6.   Hall, E.A.H., *Biosensors*, in *Biosensors.* 1990, Open University Press: Milton Keynes.

7.   Hoffman, A.S., *Biomaterials: Interfacial Phenomena and Applications*, ed. S.L. Cooper and M.A. Peppas. 1982, Washington, DC: American Chemical Society.

8.   Geckeler, K.E., F. Rupp, and J. Geis-Gerstorfer, *Interfaces and Interphases of (Bio)materials: Definitions, Structures, and Dynamics.* Advanced Materials, 1997. **9**(6): p. 513-518.

9.   Lambrechts, M. and W. Sansen, *Biosensors: Microelectrochemical Devices.* Sensors, ed. B.E. Jones. 1992, Bristol, UK: IOP Publishing.

10.   Fujimasa, I., *Micromachining Technology and Biomedical Engineering.* Applied Biochemistry and Biotechnology, 1993. **38**: p. 233-242.

11.   Ramsey, D., S.C. Jacobson, and M.R. Knapp, *Microfabricated Chemical Measurement Systems.* Nature Medicine, 1995. **1**: p. 1093-1096.

12.   Chung-Chiun, L. and J. Zhihong, *Applications of Microfabrication and Micromachinig Techniques to Biotechnology.* Trends in Biotechnology, 1997. **15**: p. 213-216.

13. Heinze, J., *Ultramicroelectrodes in Electrochemistry.* Angewandte Chemie - International Edition in English, 1993. **32**: p. 1268-1288.

14. GlaxoWellcome, *Redesigning Drug Discovery.* Nature, 1996. **384 Supplement**: p. 1-5.

15. Silverman, L., R. Campbell, and J.R. Broach, *New Assay Technologies for High-thoughput Screening.* Current Opinion in Chemical Biology, 1998. **2**: p. 397-403.

16. Major, J., *Challenges and Opportunities in High Throughput Screening: Implications for New Technolgies.* Journal of Biomolecular Screening, 1998. **3**(1): p. 13-17.

17. Clark, L.C. and C. Lyons, *Electrode systems for continuous monitoring in cardiovascular surgery.* Annals of the New York Academy of Science, 1962. **102**(1): p. 29-45.

18. Charles, M., R.W. Coughlin, E.K. Paruchuri, B.R. Allen, and F.X. Hasselberger, *Enzymes immobilised on alumina and stainless steel supports.* Biotechnology and Bioengineering, 1975. **17**: p. 203-210.

19. Nakabayashi, I., T. Tomida, and K. Kawashiro, *Modification of titanium electrodes for detection of biological substances.* Journal of the electrochemical Society, 1985. **132**(11): p. 2911-2613.

20. Morrissey, B.W. and C.C. Han, *The conformation of gamma gobulin adsorbed on polystyrene lattices determined by quasielectric light scattering.* Journal of colloid and interface science, 1978. **65**(3): p. 423-431.

21. Ulbrich, R., R. Golbik, and A. Schellenberger, *Protein adsorption and leakage in carrier-enzyme systems.* Biotechnology and Bioengineering, 1991. **37**: p. 280-287.

22. Bartlett, P.N. and J.M. Cooper, *A review of the immobilisation of enzymes in electropolymerrised films.* Journal of Electroanalytical Chemistry, 1993. **362**(1-2): p. 1-12.

23. Rechnitz, G.A., *The development of biocatalytic memebrane electrodes.* Analytica Chimica Acta, 1986. **180**: p. 281-287.

24. Scouten, W.H., J.H.T. Luong, and R.S. Brown, *Enzyme or protein immobilization techniques for applications in biosensor design.* Trends in Biotechnology, 1995. **13**: p. 178-185.

25. Williams, R.A. and H.W. Blanch, *Covalent Immobilization of Protein Monolayers For Biosensor Applications.* Biosensors and Bioelectronics, 1994. **9**: p. 159-167.

26. Leckband, D. and R. Langer, *An approach for the stable immobilisation of proteins.* Biotechnology and Bioengineering, 1991. **37**: p. 227-237.

27. Rao, S.V., K.W. Anderson, and K. Bachas, *Orientated immobilisation of proteins.* Mikrochimica Acta, 1998. **128**: p. 127-143.

28. Mrksich, M. and G.M. Whitesides, *Patterning self-assembled monolayers using microcontact printing: a new technology for biosensors?* Trends in Biotechnology, 1995. **13**(June): p. 228-235.

29. Nuzzo, R.G. and D.L. Allara, *Adsorption of bifunctional organic disulphides on gold surfaces.* Journal of the American Chemical Society, 1983. **105**: p. 4481-4483.

30. Bain, C.D. and S.D. Evans, *Laying it on thin.* Chemistry in Britain, 1995. **January**: p. 46-48.

31. Ulman, A., *An Introduction to Ultrathin Organic Films.* 1991, Boston, MA: Academic Press.

32. Ulman, A., *Formation and Structure of Self Assembled Monolayers.* Chem. Rev., 1996. **96**: p. 1533-1554.

33. Chailapakul, O., L. Sun, C. Xu, and M. Crooks, *Interactions between organized, surface-confined monolayers and vapor-phase probe molecules .7. comparison of self-assembling n-Alkanethiol monolayers deposited on gold from liquid and vapor-phases.* Journal of the American Chemical Society, 1993. **115**: p. 12495

34. Xu, J. and H.L. Li, *The Chemistry of Self-Assembled Long-Chain Alkanethiol Monolayers on Gold.* Journal of Colloid and Interface Science, 1995. **176**: p. 138-149.

35. Dubois, L.H. and R.G. Nuzzo, *Synthesis, structure and properties of model organic-surfaces.* Annual Review of Physics and Chemistry, 1992. **43**: p. 437-463.

36. Ulman, A., *Modelling organic thin films.* Chemical Review, 1996. **1**: p. 127-126.

37. Piehler, J., A. Brecht, K.E. Geckeler, and G. Gauglitz, *Surface modification for direct immunoprobes.* Biosensors and Bioelectronics, 1996. **11**(6/7): p. 579-590.

38. Lotzbeyer, T., W. Schuhmann, E. Katz, J. Falter, and H.-L. Schmidt, *Direct electron transfer between the covalently immobilized enzyme microperoxidase MP-11 and a cystamine-modified gold electrode.* Journal of Electroanalytical Chemistry, 1994. **377**: p. 291-294.

39. Allen, P.M., H.A.O. Hill, and N.J. Walton, *Surface Modifiers for the Promotion of direct Electrochemistry of Cytochrome c.* Journal of Electroanalytical Chemistry, 1984. **178**: p. 69-86.

40. Mrksich, M., C. Chen, Y. Xia, L.E. Dike, D.E. Ingber, and G.M. Whitesides, *Controlling cell attachment on contoured surfaces with self-assembled monolayers of alkanethiolates on gold.* Proceedings of the National Academy of Science USA, 1996. **93**: p. 10775-10778.

41. Delamarche, E., G. Sundarababu, H. Biebuyck, B. Michel, C. Gerber, H. Sigrist, H. Wolf, H. Ringsdorf, N. Xanthopoulos, and H.J. Mathieu, *Immobilization of Antibodies on a Photoactive Self-Assembled Monolayer on Gold.* Langmuir, 1996. **12**: p. 1997-2006.

42. Schramm, W. and S.-H. Paek, *Antibody - Antigen Complex Formation with Immobilised Immunoglobulins.* Analytical Biochemistry, 1992. **205**: p. 47-56.

43. Wimalasena, R.L. and G.S. Wilson, *Factors affecting the specific activity of immobilised antibodies and their biologically active fragments.* Journal of Chromatography, 1991. **572**: p. 85-102.

44. Bain, C.D. and G.M. Whitesides, *Formation of monolayers by the coadsorption of thiols on gold - variation in the length of the alkyl group.* Journal of the American Chemical Society, 1989. **111**: p. 7164-7175.

45.   Bain, C.D., J. Evall, and G.M. Whitesides, *Formation of monolayers by the coadsorption of thiols on gold - variation in the head group, tail group and solvent.* Journal of the American Chemical Society, 1989. **111**: p. 7155-7164.

46.   Bain, C.D., H.A. Biebuyck, and G.M. Whitesides, *Comparison of self-assembled monolayers on gold - coadsorption of thiols and disulphides.* Langmuir, 1989. **5**: p. 723-727.

47.   Haussling, L., H. Ringsdorf, F.-J. Schmitt, and W. Knoll, *Biotin-Functionalised self-assembled monolayers on gold - Surface plansmon optical studies of specific recognition reactions.* Langmuir, 1991. **7**: p. 1837-1840.

48.   Rickert, J., W. Gopel, W. Beck, G. Jung, and P. Heiduschka, *A 'mixed' self-assembled monolayer for an impedimetric immunosensor.* Biosensors and Bioelectronics, 1996. **11**(8): p. 757-768.

49.   Takami, T., E. Delmarche, B. Michel, C. Gerber, H. Wolf, and H. Ringsdorf, *Recognition of Individual Tail Groups in Self - Assembled Monolayers.* Langmuir, 1995. **11**(10): p. 3876-3881.

50.   Hill, H.A.O., D.J. Page, and N.J. Walton, *Surface Substitution Reactions at Modified Gold Electrodes and their effect on the Electrochemistry of Horse Heart Cytochrome C.* Journal of Electroanalytical Chemistry, 1987. **217**: p. 141-158.

51.   Bertilsson, L. and B. Liedberg, *Infrared study of Thiol monolayer assemblies on gold: Preparation, characterization, and functionalization of mixed monolayers.* Langmuir, 1993. **9**(1): p. 141-149.

52.   Parikh, A.N., B. Liedberg, S.V. Atre, M. Ho, and D.L. Allara, *Correlation of Molecular Organization and Substrate Wettability in the Self-Assembly of n-Alkylsiloxane Monolayers.* Journal of Physical Chemistry, 1995. **99**: p. 9996-10008.

53.   Rubin, S., J.T. Chow, J.P. Ferraris, and T.A. Zawodzinski, *Electrical Communication between Components of Self-Assembled Mixed Monolayers.* Langmuir, 1996. **12**: p. 363-370.

54. Sato, Y. and F. Mizutani, *Electrochemical respones of Cytochromec on gold electrode modified with Bis (4-pyridyl) disulphide / in-n alkanethiol mixed monolayers.* Denki Kagaku, 1995. **63**(12): p. 1173-1178.

55. Prime, K.L. and G.M. Whitesides, *Self-assembled organic monolayers: Model Systems for studying adsorption of proteins at surfaces.* Science, 1991. **252**: p. 1164-1167.

56. Cooper, E. and G.J. Legget, *Static secondary ion mass spectrometry studies of self-assembled monolayers: influence of adsorbate chain length and terminal functional group on rates of photooxidation of alkanethiols on gold.* Langmuir, 1998. **14**: p. 4795-4801.

57. Arnold, A., Z.Q. Feng, T. Kakiuchi, W. Knoll, and K. Niki, *Investigation of the electrode reaction of cytochrome c through mixed monolayers of alkanethiols on gold surfaces.* Journal of Electroanalytical Chemistry, 1997. **438**: p. 91-97.

58. Schlenoff, J.B., M. Li, and H. Ly, *Stability and Self-Exchange in Alkanethiol Monolayers.* Journal of the American Chemical Society, 1995. **117**(50): p. 12528-12536.

59. Frew, J.E. and H.A.O. Hill, *Electrochemical Biosensors.* Analytical Chemistry, 1987. **59**(15): p. 933A-944A.

60. Sethi, R.S., *Transducer aspects of biosensors.* Biosensors and Bioelectronics, 1994. **9**(3): p. 243-264.

61. Wang, J., *Amperometric biosensors for clinical and therapeutic drug monitoring: a review.* Journal of Pharmaceutical and Biomedical Analysis, 1999. **19**: p. 47-53.

62. Heller, A., *Amperometric biosensors.* Current Opinion in Biotechnology, 1996. **7**: p. 50-54.

63. Kauffmann, J.-M. and G.G. Guilbault, *Enzyme Electrode Biosensors: Theory and Applications*, in *Bioanalytical Applications of Enzymes Volume 36*, C.H. Suelter, Editor. 1992, John Wiley and Sons, Inc. p. 63-113.

64. Davis, G., *Electrochemical Techniques for the Development of Amperometric Biosensors.* Biosensors, 1985. **1**: p. 161-178.

65.   Carr, P.W. and L.D. Bowers, *Immobilised enzymes in analytical and clinical chemistry,*. 1980, Wiley: New York. p. 197.

66.   Stryer, L., *Biochemistry*. 1 ed. ed. 1988, New York: W. H. Freeman and Company. 1065.

67.   Cooper, J.M. and C.J. McNeil, *Biosensors*, in *The encylopeadia of advanced materials*, D. Bloor and e. al., Editors. 1994, Pergamon. p. 257-264.

68.   Bott, A.W., *Electrochemical methods for the determination of glucose.* Current Separations, 1998. **17**(1): p. 25-31.

69.   Pickup, J.C., G.C. Shaw, and D.J. Claremont, *Implantable glucoe sensors: Choosing the appropriate sensing strategy.* Biosensors, 1988. **3**: p. 335-346.

70.   Svorc, J. and e. al., *Composite Transducers for Amperometric Biosensors. The Glucose Sensor.* Analytical Chemistry, 1997. **69**(11): p. 2086-2090.

71.   Scheller, F.W., F. Schubert, R. Renneberg, H.-G. Muller, M. Janchen, and H. Weise, *Biosensors: Trends and Commercialisations.* Biosensors, 1985. **1**: p. 135-160.

72.   Lobo, M., A. Miranda, and P. Tunon, *Amperometric Biosensors Based on NAD(P) - Dependent dehydrogenase enzymes.* Electroanalysis, 1997. **9**(3): p. 191-202.

73.   DeAngelis, T.P. and W.R. Heineman, Journal of Chemical Education, 1976. **53**: p. 594.

74.   Cass, A.E.G., G. Davis, G.D. Francis, H.A.O. Hill, W.J. Aston, I.J. Higgins, E.V. Plotkin, L.D.L. Scott, and A.P.F. Turner, *Ferrocene-mediated enzyme electrode for amperometric determination of glucose.* Analytical Chemistry, 1984. **56**: p. 667-671.

75.   Frew, J.E., M.A. Harmer, H.A.O. Hill, and S.I. Libor, *A method for estimation of hydrogen-peroxide based on mediated electron transfer reactions of peroxidases at electrodes.* Journal of Electroanalytical Chemistry, 1986. **201**: p. 1-10.

76.   Bratten, C.D.T., P.H. Cobbold, and J.M. Cooper, *Micromachining Sensors For Electrochemical Measurement in Subnanoliter Volumes.* Analytical Chemistry, 1997. **69**(1): p. 253-258.

77. Clark, R.A., P.B. Hietpas, and A.G. Ewing, *Electrochemical analysis in picolitre microvials.* Analytical Chemistry, 1997. **69**: p. 259-263.

78. Angell, J.B., S.C. Terry, and P.W. Barth, *Silicon Micromechanical Devices.* Scietific American, 1983: p. 36-47.

79. Frazier, A.B., R.O. Warrington, and C. Friedrich, *The miniaturisation technologies: Past, present and future.* IEEE Transactions on Industrial Electronics, 1995. **42**(5): p. 423-429.

80. Kovacs, G.T.A., K. Petersen, and M. Albin, *Silicon Micromachining - Sensors to Systems.* Analytical Chemistry, 1996. **368**: p. 407A-412A.

81. Wise, K.D. and K. Najafi, *Microfabrication Techniques for Integrated Sensors and Microsystems.* Science, 1991(29 November): p. 1335-1342.

82. Murphy, J., B. Carr, and T. Atkinson, *Nanotechnology in medicine and the biosciences.* Trends in Biotechnology, 1994. **12**: p. 289-290.

83. Hadd, A.G., D.E. Raymond, J.W. Halliwell, S.C. Jacobson, and J.M. Ramsey, *Microchip device for performing enzyme assays.* Analytical Chemistry, 1997. **69**: p. 3407-3412.

84. Connolly, P., *Bioelctric interfacing: micro- and nanofabrication techniques for generating predetermined molecular arrays.* Trends in Biotechnology, 1994. **12**: p. 123-127.

85. Li, P.C.H. and J. Harrison, *Transport, manipulation, and reaction of biological cells on-chip using electrokinetic effects.* Analytical Chemistry, 1997. **69**(8): p. 1175-1178.

86. Burke, D.T., M.A. Burns, and C. Mastrangelo, *Microfabrication Technologies for Integrated Nucleic Acid Analysis.* Genome Research, 1997. **7**: p. 189-197.

87. Baranski, A.S. and H. Quon, *Potentiometric stripping determination of heavy-metals with carbon fibre and gold microelectrodes.* Analytical Chemistry, 1986. **58**: p. 407-412.

88. Baranski, A.S., *Rapid anodic-stripping analysis with ultramicroelectrodes.* Analytical Chemistry, 1987. **59**: p. 662-666.

89.   Cheng, J., L.J. Kricka, E.L. Sheldon, and P. Wilding, *Sample Preparation in Microstructured Devices.* Topics in Current Chemistry, 1998. **194**: p. 215-231.

90.   Wrightman, R.M. and D.O. Wipf, in *Electroanalytical Chemistry*, A.J. Bard, Editor. 1989, Marcel Dekker: New York. p. 267-353.

91.   Connolly, P., P. Clark, A.S.G. Curtis, J.A.T. Dow, and C.D.W. Wilkinson, *An extracellular microelectrode array for monitoring electrogenic cells in culture.* Biosensors and Bioelectronics, 1990. **5**(223-234).

92.   Israel, D.A., W.H. Barry, D.J. Edell, and R.G. Mark, *An array of microelectrodes to stimulate and record from cardiac-cells in culture.* American Journal of Physiology, 1984. **247**: p. H669-H674.

93.   Rohwedder, J.J.R. and C. Pasquini, *Multi-electrode detection in voltammetry Part 1. A versatile multi-channel voltammetric instrument.* Analyst, 1998. **123**: p. 1641-1648.

94.   Strohben, W.E., D.K. Smith, and D.H. Evans, *Characterization of arrays of microelectrodes for fast voltammetry.* Analytical Chemistry, 1990. **62**(15): p. 1709-1712.

95.   Caudill, W.L., J.O. Howell, and R.M. Wightman, *Flow-rate independent amperometric cell.* Analytical Chemistry, 1982. **54**(14): p. 2532-2535.

96.   Aoki, A., T. Matsue, and I. Uchida, *Multichannel electrochemical detection with a microelectrode array in flowing streams.* Analytical Chemistry, 1992. **64**(1): p. 44-49.

97.   Matsue, T., A. Aoki, E. Ando, and I. Uchida, *Multichannel electrochemical detection system for flow-analysis.* Analytical Chemistry, 1992. **62**: p. 407-409.

98.   Dees, D.W. and C.W. Tobias, *Experimental-observations of free-convection mass-transfer to a horizontal surface with a micromosaic electrode.* Journal of the Electrochemical Society, 1987. **134**(2): p. 369-377.

99.   Fielden, P.R. and T. McCreedy, *Voltammetric information from arrays of individually controlled electrodes - their potential for industrial process measurements.* Analytica Chimica Acta, 1993. **273**(1-2): p. 111-121.

100. Hoogvliet, J.C., J.M. Reijin, and W.P. van Bennekom, *Multichannel amperometric detection systems for liquid-chromatography and flow injection analysis.* Analytical Chemistry, 1991. **63**: p. 2418-2423.

101. Brearley, T.H., D.K. Smith, and D.H. Evans, Anal. Proc., 1989. **26**: p. 389

102. Hengsakul, M. and A.E.G. Cass, *Protein patterning with a Photoactivatable Derivative of Biotin.* Bioconjugate Chemistry, 1996. **7**: p. 249-254.

103. Morgan, H., D.J. Pritchard, and J.M. Cooper, *Photo-patterning of sensor surfaces with biomolecular structures: characterisation using AFM and fluorescence microscopy.* Biosensors and Bioelectronics, 1995. **10**: p. 841-846.

104. Pritchard, D.J., H. Morgan, and J.M. Cooper, *Micron-Scale Patterning of Biological Molecules.* Angewandte Chemie, 1995. **34**: p. 91-93.

105. Pritchard, D.J., H. Morgan, and J.M. Cooper, *Patterning and Regeneration of surfaces with Antibodies.* Analytical Chemistry, 1995. **67**(19): p. 3605-3607.

106. Aizawa, M., *Immunosensors for clinical analysis.* Advances in Clinical Chemistry, 1994. **31**: p. 247-275.

107. Schullek, J., J. Butler, Z. Ni, D. Chen, and Z. Yuan, *A high-density screening format for encoded combinatorial libraries: assay miniaturisation and its application to enzymatic reactions.* Analytical Biochemistry, 1997. **246**: p. 20-29.

108. You, A., R. Jackman, G. Whitesides, and S. Schrieber, *A miniaturised arrayed assay format for detecting small molecule-protein interactions in cells.* Chemical Biology, 1997. **4**: p. 969-975.

109. Faulkner, L.R., *Understanding Electrochemistry: Some Distinctive Concepts.* Journal of Chemical Education, 1983. **60**(4): p. 262-268.

110. Fisher, A.C., *Electrode Dynamics.* 1 ed, ed. S.G. Davis and e. al. 1996, Oxford: Oxford University Press. 703.

111. Bard, A.J. and L.R. Faulkner, *Electrochemical Methods. Fundamentals and Applications.* 1 ed. 1980, New York: John Wiley & Sons. 451.

112. Pletcher, D., *A First Course in Electrode Processes.* 1 ed. 1991, Alresford: Alresford Press Ltd.

113. van Benschoten, J.J., J.Y. Lewis, W.R. Heineman, D.A. Roston, and P.T. Kissenger, *Cyclic Voltammetry Experiment.* Journal of Chemical Education, 1983. **60**(9): p. 772-776.

114. Kissenger, P.T. and W.R. Heineman, *Cyclic Voltammetry.* Journal of Chemical Education, 1983. **60**(9): p. 702-706.

115. Vickerman, J.C. and e. al, *Surface Analysis: The Principle Techniques.* 1 ed. 1997, Chichester: Joh Wiley & Sons. 451.

116. Fitzgerald, S., *Analysis of thin films and surfaces.* Microscopy and Analysis, 1995. p. 5-7.

117. Willard, H.H., *Chemical Analysis of Surfaces*, in *Intrumental Methods of Analysis.* 1974, Van Nostrand: London. p. 379-402.

118. Berkowitz, J., *Photoabsorption, Photoionisation and Photoelectron Spectroscopy.* 1 ed. 1979, New York: Academic Press Inc. 465.

119. Briggs, D. and e. al, *Practical surface analysis by Auger and X-ray Photoelectron Spectroscopy.* 1 ed. 1983, Chichester: John Wiley & Sons Ltd. 527.

120. Carlson, T.A., *Photoelectron and Auger Spectroscopy.* 1 ed. Modern Analytical Chemistry, ed. D. Hercules. 1975, New York: Plenum Press. 411.

121. Ratner, B., *Advances in the analysis of surfaces of biomedical interest.* Surface and Interface Analysis, 1995. **23**: p. 521-528.

122. Moulder, J.F. and e. al, *Handbook of X-ray Photoelectron Spectroscopy.* 1992, Minnesota: Perking-Elmer Corp.

123. Siegbahn, K., *ESCA Atomic Molecular and Solid State Structure Studies by Means of Electron Spectroscopy.* 1967, Uppsala: Almquist and Wiksells.

124. Kemp, W., *Organic Spectroscopy.* 3 ed. 1991, London: MacMillan Education Ltd. 384.

125. Williams, H.D. and I. Fleming, *Infrared Spectra*, in *Spectroscopic Methods in Organic Chemistry.* 1980, Magraw-Hill: London. p. 29-62.

126. Allara, D.L., *A summary of critical issues for application of IR spectroscopy to characterisation of surface processing.* Critical Reviews in Surface Chemistry, 1993. **2**(1.2): p. 91-110.

127. Haris, P.I. and D. Chapman, *Does Fourier-transform infrared spectroscopy provide useful information on protein structures?* Trends in Biochemical Sciences, 1992. **17**(9): p. 328-333.

128. Porter, M.D., *IR external reflection spectroscopy: a probe for chemically modified surfaces.* Analytical Chemistry, 1988. **60**(20): p. 1143A-1155A.

129. van der Maas, J.H. and G. Dijkstra, *Basic Infrared Spectroscopy.* 1969, London: Heyden & Sons Ltd. 105.

130. Davies, M. and e. al, *Infra-red spectroscopy and molecular structure: An outline of the principles.* 1 ed. 1963, New York: Elsevier Publishing Company. 459.

131. Susi, H. and D.M. Byler, *Resolution-enhanced fourier transform infrared spectroscopy of enzymes.* Methods in Enzymology, 1986. **130**(13): p. 290-311.

132. Surewicz, W.K. and H.H. Mantsch, *New insight into protein secondary structure from resolution-enhanced infrared spectra.* Biochimica et Biophysica Acta, 1988. **952**(2): p. 115-130.

133. Guilbault, G.G., *Practical Fluorescence.* 1990: Marcel Dekker.

134. Zhong, C.J. and M.D. Porter, *Designing Interfaces at the Molecular Level.* Analytical Chemistry, 1995. **367**(December 1): p. 709A-715A.

135. Byfield, M.P. and R.A. Abuknesha, *Biochemical Aspects of Biosensors.* GEC Journal Of Reseach, 1991. **9**(2): p. 97-117.

136. Bartlett, P.N., *Modified Electrode Surface In Amperometric Biosensors.* Medical and Biological Engineering and Computing, 1990. **28**: p. B10-B17.

137. Allara, D.L., *Critical issues in applications of self assembled monolayers.* Biosensors and Bioelectronics, 1995. **10**: p. 771-783.

138. Bishop, A.R. and R.G. Nuzzo, *Self Assembled monolayers: recent developments and applications.* Experimental Self-Assembly, .

139. Jiang, L., C.J. McNeil, and J.M. Cooper, *Direct electron transfer reactions of glucose oxidase immobilised at a self-assembled monolayer.* Journal of the Chemical Society, 1995. **12**: p. 1293-1295.

140. Mandler, D. and I. Turyan, *Applications of self-assembled monolayers in electroanalytical chemistry.* Electroanalysis, 1996. **8**(3): p. 207-213.

141. Bartlett, P.N., P. Tebbut, and R.G. Whitaker, Progress in Reaction Kinetics, 1991. **16**: p. 55.

142. Turner, N.H. and J.A. Schreifels, *Surface Analysis: X-ray Photoelectron Spectroscopy and Auger Electron Spectroscopy.* Analytical Chemistry, 1998. **70**: p. 229R-250R.

143. Griffith, A.W., *Applications of microfabrication in biosensor technology*, in *Electronics and Electrical Engineering*. 1996, University of Glasgow: Glasgow. p. 134.

144. Hofmann, S., *Practical Surface Analysis*, ed. D. Briggs and M.P. Seah. 1993, Chichester, U.K.: John Wiley & Sons.

145. Griffith, A., A. Glidle, G. Beamson, and J.M. Cooper, *Determination of the biomolecular composition of an enzyme-polymer biosensor.* The Journal of Physical Chemistry B, 1997. **101**(11): p. 2092-2100.

146. Uvdal, K., P. Bodo, and B. Liedberg, *L-Cysteine adsorbed on gold and cooper - An X-Ray photoelectron study.* Journal of Colloid and Interface Science, 1992. **149**(1): p. 162-173.

147. Cooper, E. and G.J. Legget, *Influence of Tial-group Hydrogen bonding on the Stabilities of Self-assembled Monolayers of Alkylthiols on Gold.* Langmuir, 1999. **15**(4): p. 1024-1032.

148. Qu, X., T. Lu, S. Dong, C. Zhou, and T.M. Cotton, *Electrochemical reaction of cytochrome c at gold electrodes modified with thiophene containing one functional group.* Bioelectrochemistry and Bioenergetics, 1994. **34**: p. 153-156.

149. Albery, J.W., M.J. Eddowes, H. Allen, O. Hill, and R.A. Hillman, *Mechanism of the reduction and oxidation reaction of Cytochrome c at a modified gold electrode.* Journal of the American Chemical Society, 1981. **103**: p. 3904-3910.

150. Szucs, A. and M. Novak, *Stable and reversible electrochemistry of cytochrome c on bare electrodes Part 1. Effect of ionic strength.* Journal of Electroanalytical Chemistry, 1995(383): p. 75-84.

151. Szucs, A. and M. Novak, *Stable and Reversible electrochemistry of cytochrome c on bare electrodes. Part II: Effects of experimental conditions.* Journal of Electroanalytical Chemistry, 1995. **384**: p. 47-55.

152. Paeschke, M., R. Hintsche, U. Wollenberger, W. Jin, and F. Scheller, *Dynamic redox recycling of cytochrome c.* Journal of Electroanalytical Chemistry, 1995. **393**: p. 131-135.

153. Santucci, R., M. Brunori, L. Campanella, and G. Tranchida, *Electrochemical Behavior of horse heart cytochrome c and microperoxidase at a gold electrode chemically modified with sulphu-containing compounds.* Bioelectrochemistry and Bioenergetics, 1992. **29**: p. 177-184.

154. Hidalgo-Alvarez, R. and F. Galisteo-Gonzalez, *The adsorption characteristics of immunoglobulins.* Heterogeneous Chemistry Reviews, 1995. **2**: p. 249-268.

155. Kleijn, M. and W. Norde, *The adsorption of proteins from aqueos solution on solid surfaces.* Heterogeneous Chemistry Reviews, 1995. **2**: p. 157-172.

156. Hlady, V. and J. Buijs, *Protein adsorption on solid surfaces.* Analytical Biotechnology, 1996.

157. Wang, J.-H., L.W. Ruddock, and A.E.G. Cass, *Microscopic investigations of the interactions of proteins with surfaces.* Biosensors and Bioelectronics, 1994. **9**: p. 647-655.

158. Yang, Z., A. Gonzalez-Cortes, G. Jourquin, J.-C. Vire, and J.-M. Kauffmann, *Analytical application of self-assembled monolayers on gold electrodes: critical importance of surface pretreatment.* Biosensors and Bioelectronics, 1995. **10**: p. 789-795.

159. Goldstein, E.L. and M.R. van de Mark, *Electrode cleaning and anion effects on ks for k3Fe(CN)6 couple.* Bioelectrochimica Acta, 1982. **27**: p. 1079-1085.

160. Chialvo, A.C., W.E. Triaca, and A.J. Arvia, *Changes in the polycrystalline gold electrode surface produced by square wave potential perturbations.* Journal of Electroanalytical Chemistry, 1984. **171**: p. 303-316.

161. Weisshaar, D.E., M.M. Walczak, and M.D. Porter, *Electrochemically induced transformations of monolayers formed by the self-assembly of mercaptoethanol at gold.* Langmuir, 1993. **9**: p. 323-329.

162. Creager, S.E., L.A. Hockett, and G.K. Rowe, *Consequences of Microscopic Surface Roughness for Molecular Self-assembly.* Langmuir, 1992. **8**: p. 854-861.

163. Armstrong, F.A., H.A.O. Hill, and N.J. Walton, *Electron transfer reactions of redox proteins at electrodes.* Quarterly Review of Biophysics, 1986. **18**: p. 261-322.

164. Marcus, R.A. and N. Sutin, *Electron transfers in chemistry and biology.* Biochimica and Biophysica Acta, 1985. **811**: p. 265-322.

165. McLendon, G., *Long distance electron transfer in proteins and model systems.* Accademical Chemical Research, 1988. **21**: p. 160-167.

166. Lehninger, A.L., *Principles of Biochemistry.* 1 ed. 1982, New York: Worth Publishers Ltd. 983.

167. Srivatsa, V.R., K.W. Anderson, and L.G. Bachas, *Oriented Immobilisation of Proteins.* Mikrochimica Acta, 1998. **128**(127-143).

168. McLean, M.A., P.S. Stayton, and S.G. Sligar, *Engineering Protein Orientation at Surfaces to Control Macromolecular Recognition Events.* Analytical Chemistry, 1993. **65**: p. 2676-2678.

169. Britland, S., P. Clark, P. Connolly, and G. Moores, *Micropatterned substratum adhesiveness: A model for morphogenic cues controlling cell behavior.* Experimental Cell Research, 1992. **198**: p. 124-129.

170. Ruardy, T.G., H.E. Moorlag, J.M. Schakenraad, H.C. van der Mei, and H.J. Busscher, *Growth of Fibroblasts and Endothelial Cells on Wettability Gradient Surfaces.* Journal of Colloid and Interface Science, 1997. **188**: p. 209-217.

171. Walt, D.R. and V.I. Agayn, *The chemistry of enzyme and protein immobilisation with glutaraldehyde.* Trends in Analytical Chemistry, 1994. **13**(10): p. 425-430.

172. Tijssen, P., *Practice and Theory of Enzyme Immunoassays.* Laboratory Techniques in Biochemistry and Molecular Biology. Vol. 15. 1992, Amsterdam: Elsevier.

173. Diamandis, E.P. and T.K. Christopoulos, *The biotin-(strept)avidin system: Principles and applications in biotechnology.* Clinical Chemistry, 1991. **37**(5): p. 625-636.

174. Bayer, E.A. and M. Wilchek, *The avidin-biotin complex in bioanalytical applications.* Analytical Biochemistry, 1988. **171**: p. 1-32.

175. Wilchek, M. and E.A. Bayer, *Methods in Enzymology.* Vol. 184. 1990, New York: Academic Press.

176. Wilchek, M. and E.A. Bayer, *Biotin containing reagents.* Methods in Enzymology, 1990. **184**: p. 138-162.

177. Verdine, G.L., *The combinatorial chemistry of nature.* Nature, 1996. **384**(7 nov): p. 11-13.

178. Fodor, S.P.A., J.L. Read, M.C. Pirrung, L. Stryer, A.T. Lu, and D. Solas, *Light - Directed, Spatially Addressable Parallel Chemical Synthesis.* Science, 1991. **251**: p. 767-773.

179. Jacobs, J.W. and S.P.A. Fodor, *Cominatorial chemistry - applications of light directed chemical synthesis.* Trends in Biotechnology, 1994. **12**: p. 19-26.

180. Hogan Jr, J.C., *Directed combinatorial chemistry.* Nature, 1996. **384**(7 Nov): p. 17-19.

181. Broach, J.R. and J. Thorner, *High-throughput screening for drug discovery.* Nature, 1996. **384**(7 nov): p. 14-15.

182. Morgan, C.L., D.J. Newman, and C.D. Price, *Immunosensors: technology and opportunities in laboritory medicine.* Clinical Chemistry, 1996. **42**(2): p. 193-209.

183. Waggoner, A., R. DeBiasio, P. Conrad, G.R. Bright, L. Ernst, K. Ryan, M. Nederlof, and D. Taylor, *Multiple spectral parameter imaging.* Methods in Cell Biology, 1989. **30**: p. 449-478.

184. Chen, R.F. and C.H. Scott, *Atlas of flourescence spectra and lifetimes of dyes attached to proteins.* Analytical Letters, 1985. **18**(393-421).

185. Foulds, N.C., J.E. Frew, and M.J. Green, *Immunoelectrodes*, in *Biosensors: A Practical Approach*, A.E.G. Cass, Editor. 1990, Oxford University Press: Oxford. p. 97-124.

186.	Madaras, M.B., R.B. Spokane, J.M. Johnson, and J.R. Woodward, *Glutamine Biosensors for Biotechnology Applications, with Suppression of the Endogenous Glutamate Signal.* Analytical Chemistry, 1997. **69**: p. 3674-3678.